Ph.D. Thesis

Fabrication and Evaluation of Chemically Modified Chitosan and Silk Fibroin Derived Nanomaterials for Anti-Cancer Agents

A Dissertation
Submitted in Partial Fulfillment of the
Requirements for the Degree of
Doctor of Philosophy

by

Himali Horo

Centre for the Environment

Indian Institute of Technology Guwahati

Guwahati-781039

Assam

November 2020

Dedicated

to

My family

INDIAN INSTITUTE OF TECHNOLOGY GUWAHATI

Centre for the Environment

Guwahati- 781039

STATEMENT

I do hereby declare that the matter embodied in this thesis entitled **"Fabrication and Evaluation of Chemically Modified Chitosan and Silk Fibroin Derived Nanomaterials for Anti-Cancer Agents"** is a work of research and investigation carried out by me, under the supervision of Dr. Lal Mohan Kundu and Prof. Bishnupada Mandal at the Centre for the Environment, Indian Institute of Technology, Guwahati, Assam, India.

In keeping with the general practice of reporting scientific observations, due acknowledgments have been made wherever the work described is based on other investigators' findings. I further declare that this work has not been submitted anywhere else for any degree, diploma, associateship, membership, etc. of any Institute or University to the best of my knowledge.

November, 2020 Himali Horo
IIT Guwahati

INDIAN INSTITUTE OF TECHNOLOGY GUWAHATI

Centre for the Environment

Guwahati- 781039

Certificate

It is certified that the thesis entitled **"Fabrication and Evaluation of Chemically Modified Chitosan and Silk Fibroin Derived Nanomaterials for Anti-Cancer Agents"** being submitted to the Indian Institute of Technology Guwahati by Himali Horo (Roll. No. 156152006) for the award of the degree of Doctor of Philosophy in Centre for the Environment, is a bonafide record of research work carried out by her. The information and data reported by her are solely the results of her original findings. She has diligently carried out the investigations and followed the guidelines of the laboratory. This work has not been submitted elsewhere for any degree or diploma.

Dr. Lal Mohan Kundu
(Supervisor)
Associate Professor
Department of Chemistry,
IIT Guwahati
Guwahati-781039, Assam,
India.
Place: Guwahati, Assam

Prof. Bishnupada Mandal
(Co-Supervisor)
Professor
Department of Chemical Engineering,
IIT Guwahati
Guwahati-781039, Assam,
India.
Place: Guwahati, Assam

Acknowledgments

It gives me immense pleasure in thanking all the people who have contributed significantly throughout this incredible journey of my Ph.D. This thesis would not have been possible without their guidance, support, and encouragement, and I am genuinely obliged and grateful for their time and effort.

I want to extend my deepest and heartfelt gratitude towards my thesis supervisor ***Dr. Lal Mohan Kundu,*** for mentoring me throughout this research period and helping me explore and understand the fascinating field of science and technology with innovative ideas. His esteemed guidance, advice, and encouragement at every step have enabled me to propel my research in a fruitful direction. I would also like to thank him for providing a well-equipped laboratory, vast resources, and dedicated work culture that has enabled my working in his laboratory a pleasant experience. Above all these, he has always been an understanding, kind, and caring guardian to me on the campus. Thank you so much, Sir.

I want to express my gratefulness to my co-supervisor, ***Prof. Bishnupada Mandal,*** for his valuable guidance, care, and support. I would also like to extend my gratitude towards my doctoral committee members ***Prof. Bhubaneshwar Mandal***, ***Prof. Gopal Das***, and ***Prof. Ajaikumar B. Kunnumakkara,*** for their critical assessments and valuable suggestions that helped me to focus on the lacking portion of my research and polishing my thesis.

I gratefully acknowledge ***Prof. Ruchi Anand***, IIT Bombay, for providing me her guidance and conducting some part of my research in her lab. I am also thankful to ***Prof. Siddhartha S. Ghosh***, IIT Guwahati, for helping me in conducting the cancer cell studies of my compound in his lab and ***Prof. Vimal Katiyar***, IIT Guwahati, for providing equipment access in his lab.

During this period, I had a great time with my research group, who have helped me and gave me a pleasant lab environment. I want to give my heartfelt thanks to my fellow lab mates, ***Ms. Kamili Gogoi***, ***Dr. Soumi Das***, ***Ms. Nibedita Ghosh***, ***Mr. Gourav Bhattacharjee***, ***and Ms. Himadree Das***, for their constant support professionally and emotionally. I also thank ***Dr. Kamalesh Verma***, ***Mr. Rahul Verma*** and ***Ms. Komal Jain*** for their help and support. My special thanks will be to ***Ms. Sini Porathoor*** and ***Ms. Srirupa Bhattacharya*** for their help in the biological studies of my work. I also owe my deep sense of thanks to all the staff members of the Centre for the Environment, Department of Chemistry, and CIF, IIT Guwahati for their assistance and technical support.

My special thanks will be to ***IIT Guwahati*** for providing me the fellowship, and a healthy atmosphere. For all the instrumental facilities required for my research work, I am truly thankful to ***Cente for the Environment***, ***Department of Chemistry*** and ***CIF (IIT Guwahati)***.

I would also like to acknowledge some of my seniors ***Dr. Mothe Gopi Kiran***, ***Dr. Vicky Rajulapaty***, ***Dr. D. Narendra Naik***, ***Dr. Lalit Goswami***, ***Mr. Rajneesh Kumar*** and ***Mr. Ponnala Vimal Mosahari***, for their valuable suggestions and support.

I cannot find words to express my gratitude towards my friends ***Anupama***, ***Jagadish***, ***Ankur***, ***Jayakrishnan***, ***Arnab***, ***Sushmita***, ***Madonna***, ***Deepshikha***, ***Sounak da***, ***Tanushree***, ***Jinat***, ***Sayanti***, ***Polomi***, ***Smita***, and ***Naveen*** with whom I share the most precious moments in IIT Guwahati with lots of happiness, laughter, parties, and trips. They filled my heart with positivity and motivation during challenging phases. Thank you for making my life on the campus a memorable and enjoyable one. You all are connected to my heart.

At the very end, I would like to thank ***Papa***, ***Maa***, ***Monty***, ***Manna***, ***Aita***, ***Bebu***, ***Mainu***, ***Maami***, ***Okoni***, ***Pinki***, and ***The Holy Trinity prayer group*** for their endless love, prayer, and encouragement. This thesis would have remained a dream without their support. And above all, I thank God Almighty for everything.

Thank you all for sharing my journey.

Himali Horo

November 2020

Abstract

My thesis entitled **"Fabrication and evaluation of chemically modified chitosan and silk fibroin derived nanomaterials for anti-cancer agents"** is compiled into seven chapters, which comprises the introduction, review of literature, experimental findings during my Ph.D. tenure, a summary of the work and future prospects.

Chapter 1 presents a brief introduction to the design and development of anti-cancer drug delivery systems based on biopolymers and their modified materials. It also showcases a brief review of biopolymer derived structures, including covalently conjugated systems, nanoparticles, and microparticles.

Chapter 2 presents the development of a photocleavable nanocarrier system where 5-fluorouracil (5-FU) is covalently conjugated to low molecular weight chitosan (LMWC) *via* a photocleavable linker. The conjugate was designed to be cleaved explicitly under UV-A radiations of wavelength 365 nm and release the drug in a dose-dependent manner. The conjugate was found to form hydrogel and organogel. The modified biopolymer was also fabricated into nanoparticles by ionic gelation technique for better cell penetration. The drug release study from the nanoparticles was done by irradiating it under a light of wavelength 365 nm.

Chapter 3 presents a method for antiproliferation of the cancer cells using a combination of 5-fluorocytosine (5-FC) loaded silver nanoparticles (AgNPs) prodrug and a non-mammalian enzyme Cytosine Deaminase (CD). 5-FC and 5-FU loaded AgNPs were synthesized using a green synthesis protocol using LMWC as the reducing and the stabilizing agent, and nanoparticles with size less than 25 nm were formed. CD activity study showed, it effectively hydrolyzes prodrug 5-FC in 5-FC loaded nanoparticles into 5-FU (active drug) but was inert to blank nanoparticles and 5-FU loaded nanoparticles, thus proving its efficiency and specificity. The investigation in MDA-MB-468 cell lines manifested potent cytotoxicity for 5-FU nanoparticles compared to the 5-FC loaded nanoparticles without CD, thus showing the prodrug nature of 5-FC loaded nanoparticles.

Chapter 4 presents the synthesis of gold nanoparticles using LMWC, loaded with a model anti-cancer drug, doxorubicin (DOX), which was further coated with folic acid (FA) and fluorescein (FL) conjugated silk fibroin (SF). The SF coating helps in the sustained release of the drug and provides a binding domain for FA attachment to facilitate cell-targeting. The drug release from both the coated and uncoated nanoparticles was studied, where the coated one showed slow and sustained release compared to the uncoated ones. The cytotoxicity of coated nanoparticles in HeLa cell lines showed a maximum dose-dependent decrease in cell

viability than the uncoated ones. The cellular uptake of coated and uncoated nanoparticles, as studied by confocal microscopy, showed increased uptake efficacy of the coated nanoparticles by the cells.

Chapter 5 presents the formulation of microparticles/beads from the synthesized DOX loaded gold nanoparticles in the previous chapter. Here, the beads were coated with FL coated SF for sustained drug release. The beads were synthesized by the ionic gelation technique using TPP, as the cross-linking agent. The drug release study from the coated beads showed slow and sustained release compared to the uncoated ones.

Chapter 6 presents the synthesis of biotin conjugated LMWC-SF based carbon dots (CS-dots) for targeted delivery of anti-cancer drugs and cell imaging. 5-FU is loaded to the conjugate as the model anti-cancer drug. LMWC and SF based Cdots possess a large number of free amino groups that can be utilized for functionalizations. The LMWC-SF mixture based Cdots were 3±1.5 nm sized and showed increased fluorescence intensity and relative quantum yield compared to the pure LMWC and SF based Cdots. Biotin covalently conjugated to the free amino group of Cdots can provide target specificity to the nanocarrier.

Chapter 7 consists of the summary and the future prospects of the thesis work.

Contents

List of Abbreviations

WHO	World Health Organization
5-FU	5-fluorouracil
PTX	Paclitaxel
FdUMP	Fluorodeoxyuridine monophosphate
FdUTP	Fluorodeoxyuridine triphosphate
FUTP	Fluorouridine triphosphate
TS	Thymidylate synthase
dUMP	Deoxyuridine monophosphate
dTMP	Deoxythymidine monophosphate
CH_2THF	5,10-methylenetetrahydrofolate
dNTP	Deoxynucleotide
dUTP	Deoxyuridine triphosphate
DOX	Doxorubicin
5-FC	5-fluorocytosine
CD	Cytosine deaminase
DDS	Drug delivery system
PHA	Poly(hydroxy alkanoates)
PHB	Poly(hydroxybutyrate)
PLA	Poly(lactic acid)
PLGA	Poly(lactic-co-glycolic acid)
SF	Silk fibroin
PEG	Poly(ethylene glycol)
PEO	Poly(ethylene oxide)
RGD	Arginine-Glycine-Aspartic acid
FA	Folic acid
SEM	Scanning electron microscope
HPMC	Hydroxypropyl methylcellulose
PVP	Poly(vinylpyrrolidone)
PMAA	Poly(methacrylic acid)
prGO	Porous reduced graphene oxide
MWCNT	Multiwalled carbon nanotubes
NIR	Near-infrared

OEG	Oligo(ethylene glycol)
LCST	Lower critical solution temperature
PCL	Poly(ε-caprolactone)
MPS	Mononuclear phagocytic system
CMC	Carboxymethyl chitosan
PPGs	Photoliable protecting groups
ApDC	Aptamer drug conjugates
GSH	Glutathione
Cys	Cysteine
LA	Lipoic acid
CA	Cholic acid
LV	Leucovorin
GI	Gastrointestinal
SLNs	Solid lipid nanoparticles
Sa	Stearic acid
Cer	Ceramide
LMWC	Low molecular weight chitosan
M_v	Viscosity average molecular weight
MW	Molecular weight
FTIR	Fourier Transform Infrared Spectroscopy
KBr	Potassium Bromide
FESEM	Field Emission Scanning Electron Microscope
FETEM	Field Emission Transmission Electron Microscope
DLS	Dynamic Light Scattering
EDX	Energy Dispersive X-Ray Analysis
DD %	Percentage degree of deacetylation
EDC	1-Ethyl-3-(3-dimethylaminopropyl) carbodiimide
NHS	N-Hydroxysuccinimide
MES	2-(N-morpholino)ethanesulfonic acid
TPP	Sodium tripolyphosphate
BSA	Bis(trimethylsilyl)acetamide
TGA	Thermogravimetric analysis
XRD	X-Ray Diffraction
PDI	Polydispersity index

AgNp	Silver nanoparticle
SPR	Surface plasmon resonance
DMEM	Modified eagle medium
ECD	*E.coli* cytosine deaminase
FBS	Fetal bovine serum
MTT	3-(4,5-dimethylthiazol-2-yl)-2,5diphenyl tetrazolium bromide
IC_{50}	Half-maximal inhibitory concentration
E.Coli	Escherichia coli
FA	Folic acid
FL	Fluorescein
LB	Luria Bertani
Cdots	Carbon dots
DCC	N,N′-Dicyclohexylcarbodiimide

nm	Nanometer
mm	Millimeter
cm	Centimeter
cm^{-1}	Inverse centimeter
µl	Microlitre
ml	Millilitre
L	Litre
mg	Milligram
g	Gram
c	Concentration
nM	Nanomolar
µM	Micromolar
mM	Millimolar
mmol	Millimole
mg/ml	Milligram per milliliter
µg/ml	Microgram per milliliter
g/dl	Gram/deciliter
IU/ml	International units per milliliter
cm^3/g	Cubic centimeter per gram
w/w	Weight/weight
v/v	Volume/volume
wt%	Weight percent
v%	Volume percent
s	Seconds
min	Minutes
h	Hours
°C	Degree Celsius
°C/min	Degree Celsius per minute
A	Absorbance
% T	Transmittance
λ	Wavelength
Da	Dalton
kDa	Kilo Dalton

rpm	Rotation per minute
θ	Theta
W	Watt
η_r	Relative velocity
η_{inh}	Inherent viscosity
η	Intrinsic viscosity
t	Time of flow of solution
t_0	Time of flow of solvent
T_i	Temperature at the beginning of decomposition
T_i	Temperature at the maximum rate of mass loss
T_m	Temperature at the end of decomposition.
%	Percent
±	Plus-minus
×	Multiplication
φ	Relative fluorescence quantum yield
η	Refractive index
E	Integrated fluorescence intensity
Å	Angstrom

List of Tables

List of Figures

Chapter 1 Introduction and Literature Review

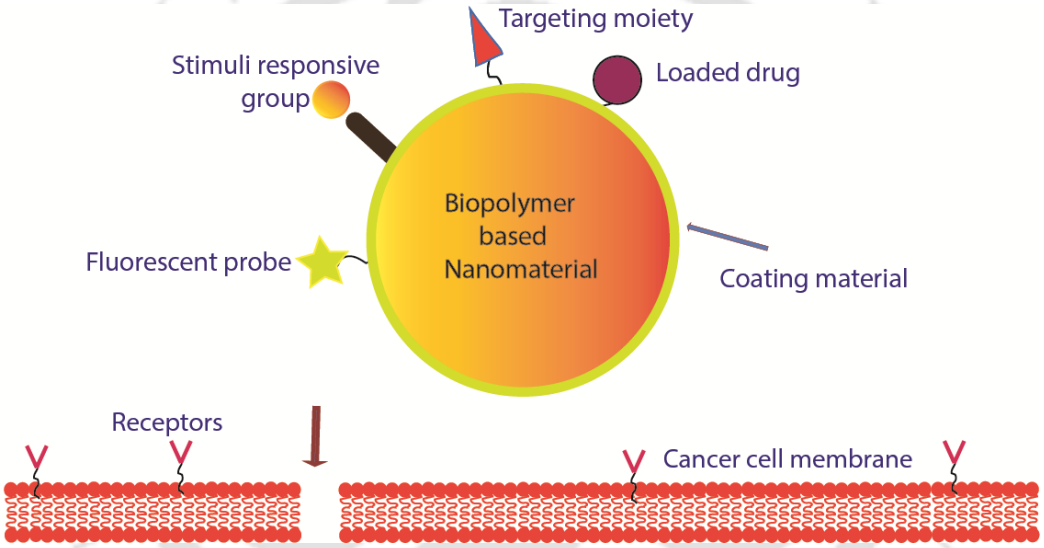

1.1. Cancer, anti-cancer agents and their mechanism

Cancer is a collection of diseases that is caused by the uncontrolled division of abnormal cells that can develop in any part of the body and possess the ability to spread to other parts. The normal cells divide in an orderly and controlled manner, and once they are worn out or damaged, they die and are replaced by new healthy cells. But in cancer, this process breaks down, and unhealthy cells start growing in an uncontrolled manner making new unhealthy cells that take over the normal cells. Benign is the type of non-cancerous tumor, while malignant are the cancerous tumors that have the potential to grow and spread by the process called metastasis. The cell division in normal and cancer cells is shown in **Figure 1.1**.

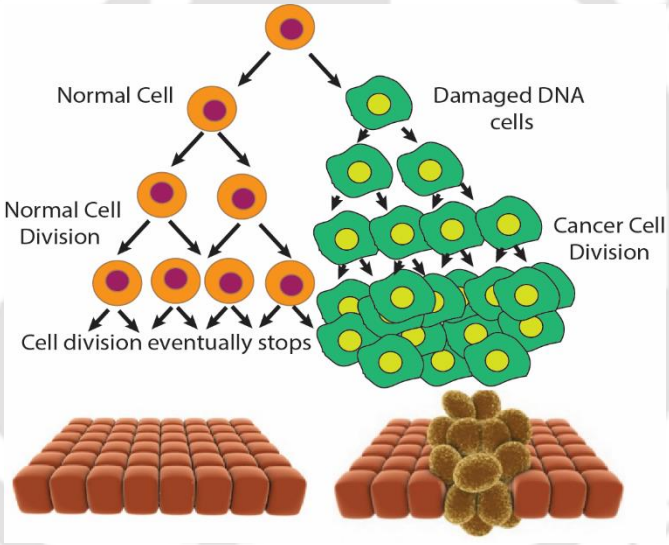

Figure 1.1 Cell division in normal and cancer cells.

Altogether, there are more than 200 different types of cancers, and the type of cancer is designated by the body part in which it originates. The type includes carcinoma (originate in the epithelial cells), sarcoma (originate from connective tissue), lymphoma and leukemia (originate from blood-making cells), germ cell tumor (derived from pluripotent cells of the testicle or the ovary), and blastoma (derived from embryonic tissue)[1].

Many factors can cause cancer, though most of them are still unknown. The most common causes are chemical carcinogens, biological carcinogens, and physical carcinogens. Many

other factors, such as hereditary, obesity, old age, are also responsible for causing cancers. The most common technique of cancer treatment includes surgery, chemotherapy, and radiation therapy. Surgery is generally done in earlier stages, while chemotherapy is useful for killing the spread cancer cells or retarding their growth. Radiation therapy is used to kill or slow down the growth of cancer cells, but it is generally given along with chemotherapy or surgery. Some other less used treatments are immunotherapy, hormone therapy, stem cell transplant, cryoablation, bone marrow transplant, etc. Even after the following treatments, the main target is to get rid of all the cancer cells from the body as even if a few of them remain, they can multiply again to produce a regeneration of the disease.

National Cancer Institute has listed more than 200 types of anti-cancer agents. The most well-known of them is 5-fluorouracil (5-FU), cyclophosphamide, doxorubicin (DOX), epirubicin, camptothecin, and paclitaxel (PTX). Their structures are shown in **Figure 1.2**. The anti-cancer agents can be broadly classified, as shown in **Table 1.1**.

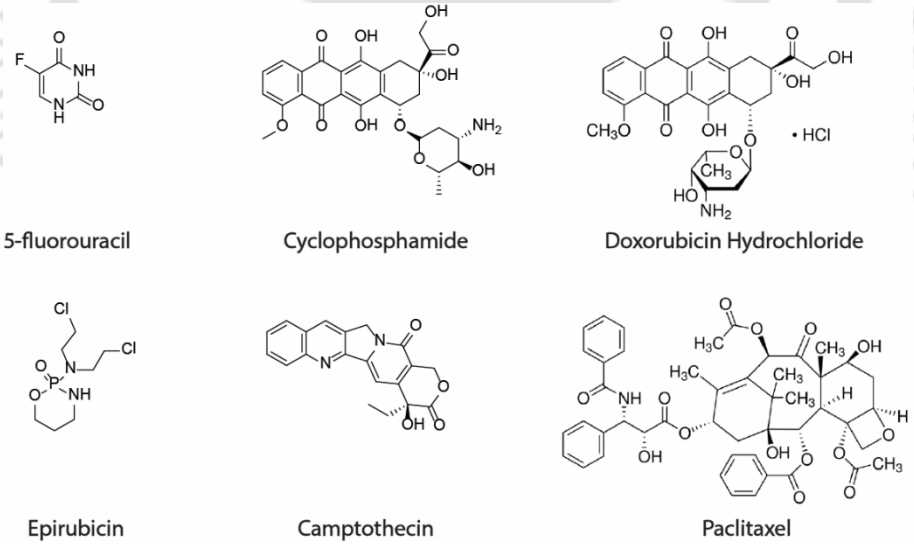

Figure 1.2 Chemical structures of some important anti-cancer agents.

Table 1.1 Classification of anti-cancer agents.

Type	Description	Example
Alkylating agents	Adds an alkyl group to guanine preventing linking of DNA helix.	Melphalan, Cyclophosphamide, Chlorambucil, Uramustine.
Plant alkaloids	Inhibits the polymerization of β-tubulin into microtubules, stopping spindle formation in cell division.	Paclitaxel, Docetaxel, Tenisopide.
Antitumor-antibiotics	Inhibit DNA replication by various means.	Doxorubicin, Daunorubicin, Mitomycin, Bleomycin.
Antimetabolites	Inhibits cells normal metabolic function by incorporation of chemically changed nucleotides or by reducing the deoxynucleotides supply.	5-fluorouracil,6-Mercaptopurine, Gemcitabine, Floxuridine.
Topoisomerase Inhibitors I and II	Blocks the action of topoisomerase(topoisomerase I and II), enzyme responsible for controlling the changes in DNA	Camptothecin, Diflomotecan, Doxorubicin, Daunorubicin.

Here, we have discussed some of the important anti-cancer agents and their mechanism of action inside the cell.

5-fluorouracil

It is an antimetabolite chemotherapeutic drug, an analog of uracil, substituting hydrogen with a fluorine atom at the C-5 position. It has shown promising effects in the treatment of various types of cancers such as colorectal cancer[2], skin cancer[3], stomach cancer[4], breast cancer[2], pancreatic cancer[5], to name a few. The mechanism of action of 5-FU is shown in **Figure 1.3**. In the cell, 5-FU gets converted to active metabolites: fluorodeoxyuridine monophosphate (FdUMP), fluorodeoxyuridine triphosphate (FdUTP), and fluorouridine triphosphate (FUTP),

which are responsible for its cytotoxic nature[2]. During DNA synthesis, deoxyuridine monophosphate (dUMP) gets transformed to deoxythymidine monophosphate (dTMP) by the transfer of methyl group, facilitated by 5,10-methylene tetrahydrofolate (CH_2THF) and catalyzed by Thymidylate Synthase (TS). 5-FU acts a competitive substrate for TS which inhibits the synthesis of dTMP and thereby stopping the synthesis of DNA in affected cells.

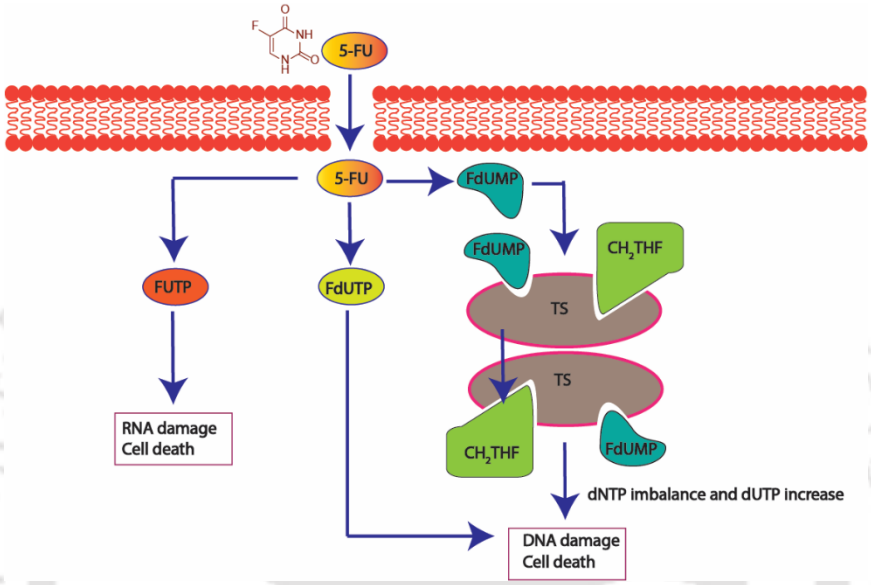

Figure 1.3 Mechanism of action of 5-FU inside a cell.

Doxorubicin

DOX is an anthracycline antibiotic chemotherapeutic drug. It's been used for treating different types of cancers like breast cancer[6], lung cancer[7], ovarian cancer[8], etc. There are several mechanisms of action that have been proposed for DOX, which includes (a) intercalation between DNA nucleotides; (b) inhibition of topoisomerase II enzyme by stabilizing it after it has broken DNA for replication, thus stopping resealing of DNA double helix and replication; (c) producing quinone type damaging free radicals, thus interrupting DNA replication and transcription leading to cell death[9–12].

5-fluorocytosine as a prodrug

5-FC is a fluoropyrimidine that is primarily used as an antifungal medicine to treat systemic mycoses and fungal infections that affect internal organs. But with the action of an enzyme,

cytosine deaminase, it gets hydrolyzed to 5-FU. It has been widely used as an enzyme-prodrug system for suicidal gene therapy for the treatment of cancer. CD is exclusively expressed only in certain types of fungi and bacteria and is absent in mammalian cells, and it encodes a protein that catalyzes the deamination of 5-FC to 5-FU. Thus, 5-FC acts as a prodrug that gets converted to 5-FU, an active antitumor agent upon the action of the gene, and causes cell death[13].

1.2. Drug delivery systems

A drug requires a suitable drug delivery system (DDS) for its safe, selective, and efficient administration into the cell for enhancing its bioavailability, target specificity, and cellular uptake. Designing a DDS requires careful observation and analysis in the following matters: type of drug, selecting drug carrier, designing the mechanism and kinetics of drug release, and finally, the drug administration pathway. A drug carrier carries the drug into the site of action and primarily controls its release into the systemic circulation. A carrier is also highly responsible for the pharmacodynamics and pharmacokinetics of the drug.

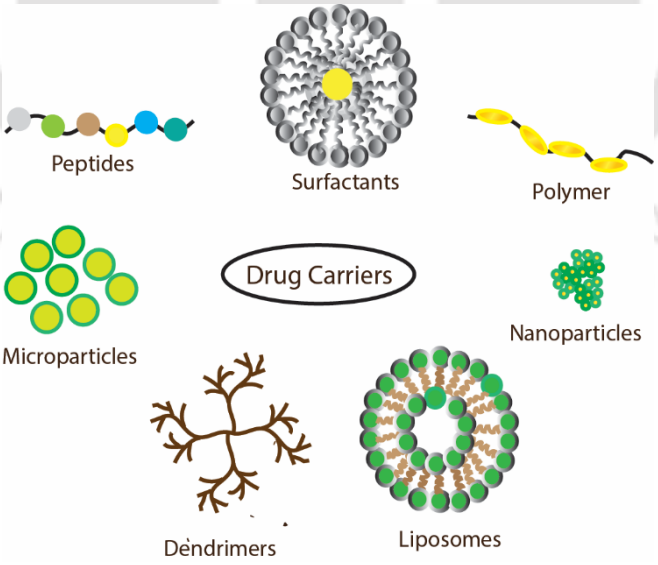

Figure 1.4 Various types of drug carriers used for chemotherapeutic drug administration.

Drugs are attached to the carriers in various ways like adsorption, encapsulation, covalent attachment, etc. Different types of drug carriers like polymers[14], microparticles[15,16], nanoparticles[17,18], peptides[19,20], liposomes[21], dendrimers[22], surfactants[23], etc., have been employed for the delivery of anti-cancer agents and are depicted in **Figure 1.4**. Among which, biopolymers have gained wide attention because of their extraordinary properties.

1.2.1. Biopolymers for chemotherapeutic drug delivery

Biopolymers such as proteins/peptides, carbohydrates, and their chemical modifications are very attractive as drug-delivery cargo, as many of them exhibit very low cytotoxicity in living cells. Such biopolymers also possess versatile functional groups and tunable physical properties. They are often found to be biodegradable as well, which can break down into natural by-products such as water, gases (CO_2, N_2), biomass, and inorganic salts, under the action of microorganisms and/or enzymes. Since they have less or no detrimental effect on the environment, they are in high demand to minimize the usage of non-renewable resources and synthetic materials that have an adverse environmental impact. The degradation may take hours, days, or even a few years, depending upon the polymer's molecular architecture. The use of naturally occurring biodegradable polymer dates back to almost 100 AD when *catgut sutures* were prepared using sheep intestine's collagen. Naturally available biodegradable polymers are mostly available in abundance, cost-effective, biocompatible, non-toxic, and environment friendly[24].

Most of the biodegradable polymers consist of amide, hydroxyl, ether, and ester functional groups. Based on structure and synthesis, they are classified into two broad groups, as shown in the chart in **Figure 1.5**.

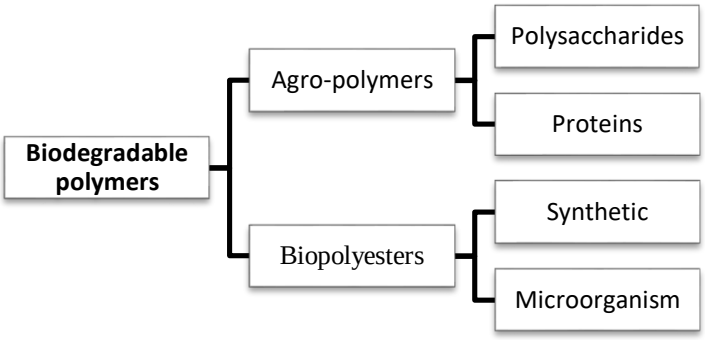

Figure 1.5 Classification of biodegradable polymers.

The agro-polymers are obtained from biomass and consist of polysaccharides like starch, chitin, pectin, etc., which contains glycosidic bonds; and proteins like corn protein, wheat gluten, casein, etc. which are made of amino acids. The biopolyesters are derived from microorganisms or synthetically prepared from natural and synthetic monomers. Some of the examples of biopolyester are poly (lactic acid) (PLA), poly (hydroxyalkanoates) (PHA), Poly (hydroxybutyrate) (PHB), and Poly (lactic-co-glycolic acid) (PLGA).

The use of biopolymers in drug delivery field has proved to be an effective and successful approach. Some of the most widely used biopolymers in drug delivery field are chitosan, silk fibroin (SF), gelatin, PLA, PLGA, hyaluronic acid, poly(L-lysine), poly(malic acid), poly(glutamic acid) (PGA), and poly(aspartame). They are used as it is or in various forms like nanoparticles, microparticles, and hydrogel.

We have used two types of biopolymers in our research, i.e., chitosan and silk fibroin. Therefore, we will be mainly focusing our further discussion on cancer drug delivery systems using biopolymers, especially chitosan and silk fibroin.

1.2.2. Chitosan and its chemical modification as drug delivery cargo

Among the natural polymers, polysaccharides have gained much attention nowadays due to their remarkable physical and biological properties. Chitosan is a natural linear bioaminopolysaccharide consisting of randomly distributed β-(1→4)-linked D-glucosamine

(deacetylated unit) and N-acetyl-D-glucosamine (acetylated unit). It is prepared by alkaline deacetylation of chitin, which is the second most abundant polymer after cellulose. Chitin is a specific component found in the cell walls of fungi, exoskeletons of insects and arthropods, beaks and internal shells of cephalopods, radulae of molluscs, and other soft tissues of fish as ordered crystalline microfibrils. Chitin is converted to chitosan to enhance its solubility, degradation and impart functionalization. The conversion can be done by chemical and enzymatic processes. Chemical deacetylation of chitin is done by the treatment of chitin with sodium hydroxide (NaOH) solution at elevated temperature, as shown in the reaction in **Figure 1.6**. The effect of various parameters, such as reaction times, NaOH concentration, and temperature, affect the degree of deacetylation (DDA) of the formed chitosan.

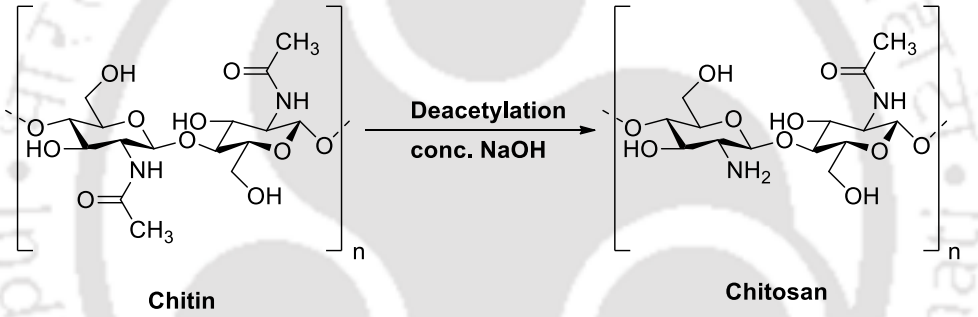

Figure 1.6 Deacetylation of chitin to chitosan.

The reaction of chitosan is significantly more versatile than cellulose and chitin because of the free amine and hydroxyl group in its backbone. Its properties can be played around by various chemical modifications leading to a wide range of derivatives. One of the major limiting factors of chitosan is its poor solubility as it is a weak base and is insoluble in water as well as in organic solvents. However, it is highly soluble in dilute aqueous acidic solution (pH<6.5) such as 1 v/v% of acetic acid, formic acid, hydrochloric acid, etc. converts the glucosamine units of chitosan into a miscible form $R\text{-}NH_3^+$.

Chitosan acquires wide applications in the biomedical field for its exceptional properties like excellent biocompatibility, non-toxicity, biodegradability, and the ability to get chemically modified by various functionalization because of the existence of free amino and hydroxyl

group in its backbone[25,26]. Moreover, it can be very easily formulated into hydrogels[27,28], nanoparticles[29–33], microparticles (beads)[34,35], films[36–41], nanofibres[42,43], and cross-linked compound[44–46]. It can also be used as the reducing agent for synthesizing various metal nanoparticles[26,47–50] and as a coating material[51,52].

1.2.3. Silk fibroin as a highly versatile biomaterial

SF is a protein that is one of the two components of raw silk, i.e., SF and sericin. The latter is the gummy part, which coats two singular filaments of the former. Silk is produced by larvae, hymenoptera, flies, beetles, arachnids, arthropods, and various other insects, but the best known SF is acquired from the cocoons of the mulberry silkworm *Bombyx mori* which is raised in sericulture[53,54].SF derived from *Bombyx mori* has shown various notable applications due to its high biocompatibility, tailorable degradation profile, ease in chemical modifications, aqueous processability, abundant availability, and excellent mechanical properties upon material fabrications[55–57]. It has an amino acid sequence dominated by repetitive Gly-Ala-Gly-Ala-Gly-Ser, as shown in **Figure 1.7**, with significant quantities of other amino acids such as aspartic acid, threonine, tyrosine, and glutamic acid, which are used for various modifications[56]. It has been used as sutures[58], in drug delivery[59], as coating materials[60], and in tissue engineering[61] for bones[62,63], cartilages[64,65], ligaments[66], skin[67,68], neural[69,70], etc.

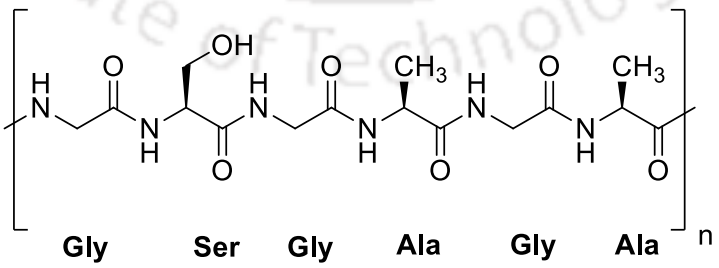

Figure 1.7 Structure of silk fibroin backbone

1.3. Controlled drug delivery systems

Before 1950, all types of drugs were delivered inside the body by formulating into pills and capsules, which releases the drug as it comes in contact with water. This technique does not offer any control over drug-releasing kinetics. By 1952, Smith Klein Beecham introduced the concept of a controlled drug delivery system in the form of a sustained drug-releasing formulation that can control the drug release kinetics and attain 12-hour efficacy[71].

It has been observed that despite the development of a large number of active therapeutic agents, only a few of them have been clinically successful. The poor activity of a drug inside the body is mostly due to its low bioavailability and the rate at which the drug is administered. This also results in improper drug dosage leading to various severe side effects. Controlled drug delivery is a technique that is designed in such a way that the drug is delivered into the site of interest in a controlled and pre-determined manner by maintaining a persistent concentration of the drug for a specified period, thereby regulating the bio-availability and minimizing side-effects of the drug[28]. Depending upon the type of carrier, formulation, and application of the delivery, delivery time may vary from a few hours to even years.

In controlled drug delivery systems, some external environment or stimuli control the kinetics of drug release. At least one of the carrier's parts responds to external physical stimuli like temperature, ultrasound, light, magnetic and electrical fields, or chemical stimuli like pH, redox potential, ionic strength, and chemical agents.

Various polymeric materials have been used as the stimuli response drug carriers. For example, many pH-responsive systems using polymer-based nanoparticles[72–74], micelles[75], hydrogels[76], and polymer-drug conjugates[77]; photoresponsive systems using copolymer[78] and nanocarrier[79]; ultrasound responsive systems using polymeric nanobubbles[80], microbubble[81], nanoparticles[82] and micelle[83] has been reported.

1.4. Targeted drug delivery systems

Most of the anti-cancer drug shows reduced efficacy due to the non-specificity of the drug toward cancer cells. Thus, a huge portion of the administered drug gets released into the normal cells, thereby decreasing the drug's bioavailability in the cancer cells and increasing side effects due to normal cell damage[84]. Cancer targeted drug delivery is a technique that specifically targets the cancer cells, sparing the healthy cells[22]. For designing cancer targeted drug delivery system, the difference in cellular micro-environment and cancer/normal cell composition like expression of surface receptors, the specific location of the diseased cells, etc., are studied.

The targeted delivery of drug can be attained by two modes of targeting: passive and active. Passive mode deals with the modification of the physical and chemical properties of the system to increase its circulation time inside the body and eventually combines with the tumor cells. For example, modification of the drug carriers with poly(ethylene glycol) (PEG) and poly(ethylene oxide) (PEO) improves drug solubility, circulation time and improvise specific cell targeting by better permeability and retention effect[85]. However, active targeting deals with employing cell-targeting moieties for site-specific delivery of anti-cancer drugs. So, a basic active targeting system consists of a targeting moiety, drug, and a carrier. The drugs and targeting moieties are attached to the carriers by various means like adsorption, encapsulation, and covalent attachment. The cell-targeting moiety is selected in such a way that it targets those receptors which are either overexpressed or exclusively present in the cancer cells. Various types of cell-targeting moieties like peptides, ligands, monoclonal antibodies, aptamer have been used. A schematic representation of typical targeted drug delivery systems is shown in **Figure 1.8**.

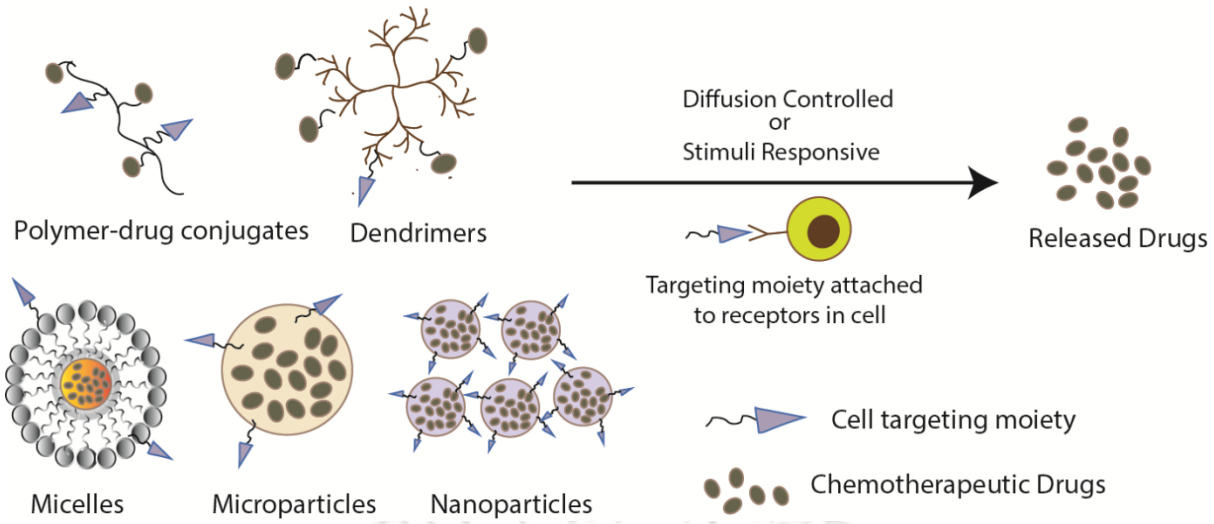

Figure 1.8 Schematic representations of targeted drug delivery systems

Various types of peptides have been found useful for cancer targeting, like Arginine-Glycine-Aspartic acid (RGD), which recognizes integrin, which is overexpressed in the cancer cells. It has been used along with nanoparticles[86],liposomes[87], etc. Antibodies are species that target antigens that are specifically present on affected cell membranes. Antigen-antibody interaction is a very specific chemical interaction as an antibody binds only to a particular antigen. Similarly, an aptamer is a single-stranded oligonucleotide that specifically recognizes their targets and binds with high affinity. Cell targeting aptamer can be produced by cell-SELEX (systematic evolution of ligands by exponential enrichment) process[88]. Ligands like folic acid (FA) and biotin have also been employed as cancer cell targeting moieties. Folate receptors are over-expressed in numerous kinds of cancer cells such as ovarian, breast, kidney, cervical, colorectal, lung, and brain tumors, which rapidly bind to FA and triggers cellular uptake *via* endocytosis[89]. Similarly, biotin receptors are even more overexpressed than folate receptors in some cancer cells like leukemia, ovarian, colon, mastocytoma, lung, renal, and breast[90].

1.5. Modifications of biopolymers for anti-cancer agents

Although numerous types of biopolymers are available, many of them lack significant physicochemical and biological properties, thus restraining them from using as an effective

drug delivery tool. For achieving the desirable properties, the development of a new polymer is a very tedious, expensive, and time-consuming process. However, modifying an existing polymer is the best way to overcome specific limitations and impart new physical, chemical, mechanical, and biological properties required for a particular application.

Various factors affect the selection of the parent polymers, their modifications, and optimization for effective drug delivery to get the required properties and architecture. Some of the factors are listed in **Table 1.2**[91].

Table 1.2 Factor determining the selection and modification of polymers for drug delivery application.

Polymer properties	Formulation	Delivery Paths	Delivery Techniques	Drug properties
Degradation profile Solubility Hydrophilicity Ionic nature Chemical Composition	Hydrogels Nanoparticles Microparticles Films Scaffolds Fibers Liposomes Micelles	Oral Intravenous Intradermal Subcutaneous, Ocular	Targeted Controlled	Stability Compatibility Solubility Dosage

The type of polymer modification done for drug delivery is broadly classified into two kinds:

(a) Physical modifications: blending and composite formation.

(b) Chemical modifications: copolymerization and surface functionalization

The techniques have been briefly discussed below, with some examples using biopolymers.

1.5.1. Biopolymer blends

Polymer blending is a technique by which more than one polymer is physically mixed to produce a new material with different physical properties. Various biopolymer blends using chitosan, PEG, PLGA, starch, silk fibroin, etc., have been developed and employed for anti-cancer agents. Chitosan/PEG-coated PLGA nanoparticles have been used for delivering curcumin[92] and paclitaxel[93]. This formulation could easily encapsulate hydrophobic drugs and increase blood circulation time and, thus, increase the drug's bioavailability by reducing the opsonization by blood protein, which helps avoid the phagocytic uptake. Chitosan/polycaprolactone blend nanofibres loaded with 5-FU were reported, which was prepared by electrospinning. Increasing chitosan content increased the fiber diameter and degradation rate. Nanofibres containing higher chitosan showed more drug loading efficiency and prolonged 5-FU release in neutral medium and faster release in an acidic medium because of acidic pH sensitivity[94]. Chitosan/starch blend film has been used for loading the anti-cancer drug hydroxyurea. It was observed from the scanning electron microscope (SEM) data that upon increasing the percentage of starch, the film roughness increased. The drug release from the blend was pH-dependent, which showed faster release in the acidic medium than in neutral medium (pH 7.4). Moreover, the release of drug at pH 7.4 and swelling percentage decreased with increasing chitosan percentage[95].

1.5.2. Biopolymer composites and nanocomposites

Polymer composites are made up of a combination of two or more polymers or polymers with other materials. Upon combining, it produces a new material having properties different from the individual components. However, the individual phases retain itself within the final structure, thus differentiating composites from mixtures and solid solutions. A composite consists of two phases: a discontinuous or reinforcing phase embedded in the continuous or matrix phase. Biopolymer based composites consist of a biopolymeric matrix reinforced by

organic or inorganic fillers. Similarly, Biopolymer based nanocomposites are multiphase materials where nanomaterial is embedded in a biopolymeric matrix. Various biopolymers like chitosan, PEG, PVP, PLGA have been used along with nanomaterials as polymer-nanocomposites for cancer therapy. For example, Nivethaa *et al.* have reported the synthesis of 5-FU loaded chitosan/ gold nanocomposite using a chemical method where the binding of gold to the free amine and hydroxyl group of chitosan was done and proved by XPS and FTIR data. The nanocomposite was cytotoxic toward carcinogenic MCF-7 cell lines while non-cytotoxic towards non-carcinogenic VERO cells[96]. They have also reported the synthesis of 5-FU loaded chitosan/silver and chitosan/silver/carboxylated multiwalled carbon nanotubes (MWCNT) nanocomposites. A sustained and prolonged release of drug was observed in the nanocomposite with MWCNT. It also showed better cytotoxicity towards MCF-7 cell lines as compared to the nanocomposite without MWCNT. Thus, the results showed that the use of MWCNT is fruitful in enhancing the release and cytotoxicity of the system[29].

Bothiraja *et al*. developed a layered nanocomposite system by intercalating PTX drug into the interlayer of Na^+-MMT by ion-exchange mechanism, which was further coated with chitosan. In vitro drug release study showed a controlled release of the drug, and studies in human colon cancer cell lines (COLO-205), showed superior anti-cancer activity of the nanocomposites as compared to blank PTX and blank MMT-chitosan nanocomposites[97].

Magnetic nanoparticles have been used to control the accumulation of the drug dose in the target of interest by means of a magnetic gradient. Synthesis of gemcitabine loaded magnetically responsive Fe_3O_4/chitosan nanocomposite was reported by Arias *et al*. The system also showed pH responsiveness, higher drug loading capacity, a slower drug release profile[98]. Synthesis of a core and shell material with chitosan-polymethacrylic acid (CTS-PMAA) shells and Fe_3O_4 cores was reported by Zarouni *et al*., which was loaded with DOX.

PMAA was used, as its high carboxyl content provides favorable electrostatic interactions, which lead to high drug encapsulation efficiency of about 98% and pH-dependent absorption and delivery of the drug. The system can halt the drug release at a neutral pH of 7.4; however, it permitted a fast release at acidic pH of 5.8[99]. Hazhir *et al*. has reported chitosan/ porous reduced graphene oxide (prGO) based nanocomposite loaded with DOX, which showed an effective drug loading efficiency compared to pure prGO due to the presence of free carboxyl and amino group of chitosan. The drug release was increased from 10% to 25% in 1 h, an acidic pH of 4.0 as compared to neutral[100]. Polypyrrole/chitosan-silver chloride core-shell nanocomposite was reported as a controlled release system for 3-amino-2-phenyl-4(3H)-quinazolinone (I). The products showed efficiency in antitumor activity against the EAC cell line and high antibacterial activity against gram-positive and gram-negative bacteria[101]. Synthesis of daunorubicin loaded nanofibres composite was reported, which was prepared by incorporating MWCNT/Fe_3O_4 into the electrospun PLA nanofibres. The diameter of the nanofibres is decreased by MWCNT/Fe_3O_4 incorporation. In the presence of a magnetic field, the encapsulation efficiency, drug release rate, and cell proliferation was amplified[102].

Synthesis of sodium alginate/chitosan/hydroxyapatite nanocomposite hydrogel was reported by varying the concentration of hydroxyapatite (0.6, 2.0, 3.5, and 5.0 % wt/v) and using gamma radiation as cross-linker for the oral delivery drug of DOX. The drug release was found to be pH-dependent, where 95% drug release was obtained at pH 5.0, and 60% release was obtained at pH 7.5, which is due to the carboxyl group in the polymer matrix[103].

1.5.3. Biopolymer based copolymers

By combining more than one dissimilar monomeric species/ repeating units, it is possible to get new and desirable properties. This linking of two or more monomers during polymerization is called copolymerization, and the polymer obtained is called a copolymer.

Along with the type and number of monomers, the spatial arrangement of the monomers is also an essential parameter in determining the properties. The possible classification of copolymers containing A and B repeating units are listed in **Figure 1.9**[104].

Figure 1.9 Classification of copolymers containing A and B repeating units

Copolymers have been used for the delivery of various types of drug due to their several advantages, as they have been found to control the solubility of multiple drugs, target the diseased tissues, and easily load biologically active molecules. Some of the biopolymers used mostly for this purpose are chitosan, hyaluronic acid, dextran, dextrin, poly(L-lysine), poly(glutamic acid), poly(malic acid), and poly(aspartame)[105]. Some of the examples of biopolymer-based copolymers used in cancer therapy have been discussed.

Wang *et al.* have used alternating copolymer-based pH-sensitive amphiphile for the delivery of DOX. It was synthesized by polycondensation of oligo (ethylene glycol) (OEG) with malic acid and DOX conjugation by benzoic imine linkages. The pH-responsiveness of the copolymer was due to the benzoic imine linkages, as shown in **Figure 1.10**. It showed a rapid release of DOX at pH 5 while slow release at neutral pH of 7.0. Moreover, a cell study on MCF-7 cell lines showed its cytotoxic nature, thus providing an efficient platform for cancer therapy[106].

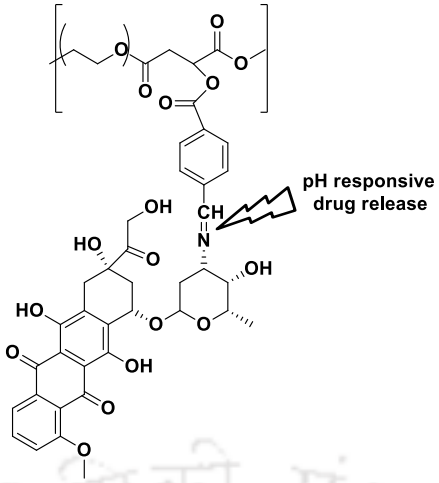

Figure 1.10 pH-mediated release mechanisms by benzoic imine linkage

Guragain *et al.* has reported the synthesis of nanoporous calcium carbonate ($CaCO_3$) sphere by chelating the self-assembling micelle of double hydrophilic block copolymer poly (acrylic acid-b-N-isopropylacrylamide) with calcium through mineralization activity. Due to the highly porous nature of the sphere, it could accommodate a large quantity of drugs (DOX). The drug release data showed that the release of DOX from the structure follows the Higuchi model[107].

Bio-copolymer based micro/nanoparticles have also been explored for cancer therapy, as reported by Savin *et al.*, where they have synthesized bevacizumab loaded micro/nanoparticles (MNP) from chitosan grafted poly(ethylene glycol) methacrylate by Michael addition reaction. The MNPs were double cross-linked by the ionic and covalent process in reverse emulsion, which offered mechanical stability. The material showed improved water solubility, pH sensitivity, and a controlled release of the drug for several days due to its swelling behavior in an aqueous medium. Moreover, the material without the drug was non-toxic to cells found by the cytotoxicity test on osteoblastic cell cultures[108].

1.5.4. Surface functionalization of biopolymers

In drug delivery, the surface functionalization of a polymer is done for several reasons:

(a) To protect the drug from degradation from drug stability affecting factors like temperature, oxidation, pH, light, and enzymatic reactions.

(b) Impart some desirable properties. E.g., improvement of hydrophilicity, biocompatibility, cellular uptake, cell imaging, etc.

(c) Conjugate targeting ligand for targeted drug release.

(d) Conjugate moieties that are responsive to a particular range of stimuli for controlled drug release.

A polymer's low hydrophilicity limits its use as an effective drug-carrying agent, especially for a hydrophobic drug, as a body treats a hydrophobic carrier as a foreign molecule. Moreover, a hydrophobic carrier can get surrounded by the mononuclear phagocytic system (MPS), which can absorb the drug carrier to the liver. Thus, the coating protects it from the MPS. PEG has been known to enhance the hydrophilicity of polymers upon conjugation. Cisplatin containing PLGA–mPEG nanoparticles were reported, which upon evaluation with water uptake or contact angle measurements, the hydrophilicity was found to increase with PEG content. The nanoparticles showed a rapid degradation and a sustained release of cisplatin. Moreover, upon administration of the nanoparticles intravenously into mice, a prolonged blood residence time was observed[109]. PEGylated chitosan is also being reported for gene delivery[110], paclitaxel delivery[93,111], targeted drug delivery using cell-targeting moieties[112]. While PEG attachment enhances the solubility and blood circulation time of chitosan, conjugation of targeting moieties along with it imparts cell-specific delivery property[113]. Chan *et al.* have developed a cell-specific gene delivery system with folate-PEG-grafted chitosan. The system showed improved water solubility and low cytotoxicity towards normal human embryonic kidney cell lines (HEK 293)[112]. Various water-soluble derivatives of chitosan like carboxymethyl chitosan (CMC), have also found wide application in the drug delivery field[114].

Targeting functionalization is done for imparting cell targeting properties to a polymer. As discussed in Section 1.4, various types of cell targeting moieties like peptides, ligands, monoclonal antibodies, aptamers are conjugated to the polymer. **Table 1.3** lists some examples of targeting functionalized biopolymers for cancer therapy.

Table 1.3 Cell targeting functionalization of biopolymers.

Targeting moiety	Biopolymer	Delivering molecule/drug	Ref.
Folic acid	Chitosan	Sirna, Ligustrazine, Gene, 5-FU, DOX, Ursolic acid.	33,112,115–118
	Silk Fibroin	DOX	119,120, 121
	PLGA-PEG	DOX	122
	Cellulose	DOX	123
	Carboxymethyl-cellulose	Curcumin, 5-FU	124,125
	PLA	Paclitaxel	126
Biotin	Chitosan	5-FU, Curcumin,Docetaxel, Bufalin.	127–130
	PLGA	BSA, SN38	131,132
	PLA-PEG	Paclitaxel	133
	PEG-PCL	Artemisinin	134
Aptamer	Chitosan	Docataxel, Epigallocatechin gallate,	135–137
	PLGA	Gefitinib,Nutlin-3a, Paclitaxel,	138, 139, 140
	PLGA-chitosan	Epirubicin	141
	PLGA-PEG	Gemcitabine, TFO, Docetaxel, P-gp siRNA, Cisplatin, DOX.	142, 143, 144, 145, 146, 147
	PAMAM-PEG	miR-15a & miR-16-1.	148
Antibody	Chitosan	DOX, α –hederin,	149–152
	PLGA	BSA, Docataxel,	153–155
	Silk fibroin	Dinutuximab	156

For obtaining stimuli-responsive behavior, drug carriers functionalized with stimuli-responsive linkers have been reported, connecting the drugs to the carriers. These linkers are chemical moieties designed so that they get altered upon exposure to a specific stimulus and release the drug into the target and provide control over the drug-releasing kinetics. For

example, photo liable linkers, also known as photolabile protecting groups (PPGs), can be decomposed by photoirradiation. The decomposition mostly occurs in mild conditions without the presence of any special chemical reagents. Derivatives of *o*-nitrobenzyl based, carbonyl based, and benzyl based showed photo responsiveness and have been used[157]. The *o*-nitrobenzyl groups can be activated by exposure to a light of wavelength 365 nm, which comes under UV-A radiations (long wavelength) and regards relatively safe for cells[158]. Wang *et al*. developed a cell targeting aptamer-drug conjugate (ApDC), where they have designed a phosphoramidite that contains 5-FU and a photocleavable linker of the *o*-nitrobenzyl derivative, as shown in **Figure 1.11**. This phosphoramidite moiety was conjugated to a DNA aptamer (sgc8) by an automated DNA synthesizer. The aptamer sgc8 was chosen as a model, and it can bind to target protein tyrosine kinase 7, which is overexpressed on target colon cancer cell lines (HCT116)[88].

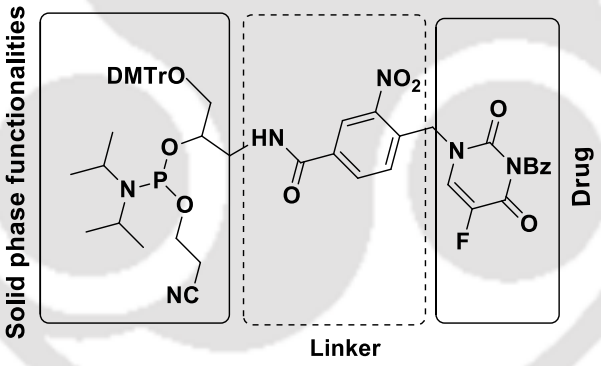

Figure 1.11 Structural features of the phosphoramidite.

Similarly, Zhang *et al.* has synthesized 5-FU attached to a tumor homing cyclic peptide Cys-Asn-Gly-Arg-Cys (CNGRC) *via* an *o*-nitrobenzyl derivative. CNGRC recognizes a cancer marker of specific amino peptidase N (APN/CD13) isoform, which is overexpressed on tumor blood vessels' surface[159].

Like photolabile linkers, various other types of linkers are available, sensitive to different types of stimuli like disulfide linkers, which are easy to conjugate and are susceptible to reducing agents like glutathione (GSH) or cysteine (Cys). For example, Li *et al.* have

synthesized glutathione responsive disulfide cross-linked and self-assembled micelles from lipoic acid (LA) and cholic acid (CA). Within 24 h, 35 μg/ml of DOX was released without glutathione, while the release was increased up to 88.1% in the presence of glutathione at 37°C. Through confocal laser scanning microscopy, it was observed that DOX was released into the nuclei of HeLa cell lines after 8 h of incubation[160]. Kong *et al.* have synthesized DOX- disulfide–methoxy PEG conjugate, which can self-assemble to form micelles. About 67.90% DOX release was observed at pH 7.4 and GSH concentration of 1 mg/ml after 72 h[161]. Some of the stimuli-responsive bonds have been listed in **Table 1.4**.

Some pH-responsive linker conjugation with chitosan has been reported. Lee *et al.* have conjugated paclitaxel to chitosan *via* a succinate linker that gets cleaved under physiological condition. The conjugate showed enhanced water solubility, bioavailability, and tumor inhibition in mice model[162]. Lee *et al.* reported the synthesis of hyaluronic acid attached glycol chitosan nanoparticles for dual drug delivery. DOX was conjugated *via* a pH-sensitive linker, and celecoxib was coloaded to it. The conjugate was stable at pH 7.4 but released the drug at pH 6 and 4. The combination of the drugs showed a synergistic effect compared to pure drugs and the nanoparticle[163].

Table 1.4 List of some stimuli-responsive bonds/groups.

Internal Stimuli	**Stimuli**		**Cleavable bonds/ groups**	**Ref.**
	pH		Acylhydrazone	164
			Acetals	165
			Benzoic imine	166
			Carbamate	167
			Ester	168
			Histidine	169
	Enzyme	Cathepsine B	Vat-Cit, Phe-Lys dipeptide	170
		Esterase	Ester	171
	Redox	Glutathione	Disulfide, Thioether	160,172
External stimuli	Photo		Derivatives of *o*-nitrobenzyl, carbonyl and benzyl.	88,157,159

1.6. Formulation of biomaterials from chitosan and SF for anti-cancer agents

1.6.1. Chitosan nanoparticles and microparticles

Polymeric nanoparticles made up of biopolymers find significant application in drug delivery, gene delivery, and tissue engineering. They provide many advantages while delivering a drug, such as biocompatibility, biodegradability, lesser toxicity, stability increase of volatile agents, targeted drug delivery, and non-immunogenicity.

Chitosan nanoparticle has been one of the widely used biopolymeric nanoparticles for cancer drug delivery. Various mechanisms are associated with the drug release from the chitosan nanoparticle, such as swelling, erosion, and diffusion. Some of the methods used for its preparation are ionic gelation, emulsification solvent diffusion, microemulsion, emulsion-based solvent evaporation, and emulsification solvent diffusion. Among these, ionic gelation is the simplest one, which avoids using any toxic chemicals, organic solvents, and high temperature. Li *et al.* reported the synthesis of chitosan nanoparticles by ionic gelation for the dual delivery of hydrophilic drugs 5-FU and leucovorin (LV). The drugs were encapsulated in the nanoparticles by electrostatic interactions. XRD results showed that both the drugs were distributed on the nanoparticles in amorphous state. In the cumulative drug release profile, an initial burst release of drugs was observed, but after some time, continuous-release occurred[173]. Aydin *et al*. has reported the synthesis of 5-FU encapsulated chitosan nanoparticles by ionic gelation to study the controlled release of 5-FU from chitosan nanoparticle for tumor environment due to pH sensitivity of chitosan nanoparticle. On testing, the pH sensitivity of the nanoparticle with phosphate buffer of varying pH values (3, 4, 5, 6, 7.4) showed a significant swelling response for pH 5. The In vitro release studies showed a controlled and sustained release of 5-FU from chitosan nanoparticles with 29–60% release amounts after 408 h of the incubation period[174]. **Table 1.5** shows some examples of chitosan nanoparticles used for anti-cancer agents.

Microparticles/microspheres/beads are hollow spheres that are in 1-1000 µm in range and are generally made of protein or polymer, which are used for oral and depot delivery of drugs. Chitosan microparticles are made up of cross-linked chitosan chains with a tangled mesh structure, providing a matrix for the entrapment of drugs[175]. There are various methods available for its synthesis, which includes ionic interactions, thermal cross-linking, solvent evaporation, interfacial acylation, coating on preformed microparticles, chemical cross-linking, etc. Ionic gelation technique, which comes under ionic interaction, has been widely used because of the non-toxic nature of the TPP anion, mild reaction conditions, and non-solvent steps used in this method. Lin *et al.* have reported the synthesis of 5-FU loaded chitosan/PEG microparticles by using TPP as the cross-linking agent. Various factors affecting the drug release behavior were studied. It was found that the drug release was retarded with various factors such as (a) increasing chitosan concentration due to the increase in viscosity and greater ionization of amine group; (b) increasing the pH of PBS buffer due to the destruction of the structure of microparticles at lower pH; (c) increasing TPP concentration due to increasing cross-linking density resulting in extra compact structure and retarding diffusion; (d) increasing cross-linking time which increases the interaction of 5-FU and microparticles[16]. **Table 1.5** shows some examples of chitosan microparticles used for anti-cancer agents.

Table 1.5 Chitosan nanoparticles and microparticles for anti-cancer agents.

Material	Techniques	Delivering molecule/drug	Ref.
Chitosan Nanoparticles	Ionic gelation (TPP)	5-FU	173
	Ionic gelation (TPP)	5-FU and LV	174
	Ionic gelation (TPP)	5-FU	176
	Ionic gelation (TPP)	5-FU	96
	Solvent evaporation	Tamoxifen	74
	Ionic interaction	DOX	177
	Ionic gelation (TPP)	DOX	178
Chitosan Microparticles	Emulsion	5-FU	179
	Emulsion and ionic gelation	5-FU	180
	Phase inversion	5-FU	16
	Ionic gelation	Capecitabine	181
	Ionic gelation	Curcumin	182
	Emulsion	DOX	183

1.6.2. Chitosan-based metal nanoparticles

Metal nanoparticles are nanometer-sized metal particles ranging between 1-100 nm. They are getting attention in the biomedical sector owing to their extraordinary optical, magnetic, thermal, catalytic, and electrical properties, which in turn depend on their shapes, size, and chemical composition. The nanoparticle's size is one of the critical factors of its interaction and behavior towards cell components. It is widely believed that particles below 100 nm have the potential of penetrating the cell barriers[184]. Chitosan consists of a large number of hydroxyl groups with the ability to form a complex with metal ions. It helps in controlling the shape and size of the nanoparticles and reduces its toxicity toward mammalian cells[185,186]. It has been used to synthesize nanoparticles of gold, silver, titanium dioxide, iron oxide, etc., for anti-cancer agents. Gold nanoparticles reduced and stabilized by chitosan has been used for paclitaxel[187] and DOX[47,188]. Similarly, silver nanoparticles synthesized using chitosan has been used for DOX[189]. Various other metal nanoparticles like titanium oxide[190], zinc oxide[191], iron oxide[192], etc., using chitosan have been used for anti-cancer therapy.

1.6.3. SF based coating systems and nanomaterials

SF has been a versatile biocompatible coating material that is used to coat several materials like nanoparticles, microparticles, liposomes, membranes, scaffolds, and other complexes. There are several advantages of SF coating, depending upon its application. Wang *et al.* reported the coating of SF on PLGA and alginate microsphere for the delivery of protein. The coating was found to retard the degradation of PLGA. The release of the model protein drug was significantly delayed by the coating, which was due to the diffusion barrier created by the coating. Thus, SF coating can be used for sustained and long term release of drugs[110]. They have also found that the SF coating layer can reduce the initial burst of release[193]. Gobin *et al.* have reported SF coated liposomes, which also showed long-term drug release and increased cell adhesion and uptake behavior upon coating[194]. Zhou *et al.* have reported SF coated poly (ε-caprolactone) microspheres for retarded vancomycin release with reduced initial burst release[195]. Kwon *et al.* have synthesized solid lipid nanoparticles (SLNs) of stearic acid (SA) and ceramide (Cer) using sodium lauryl sulfate as a stabilizing agent by emulsification and solidification process. The skin permeation of SF coated particles was two times larger than the uncoated ones due to the interaction of positively charged with negatively charged skin[196]. Thus, SF coating can be a beneficial approach in drug delivery applications.

SF nanoparticles have been used for various anti-cancer agents like PTX[197], 5-FU[198], curcumin[199], DOX[200] etc. for their controlled and target specific drug release. Moreover, various targeting moieties are attached to SF based materials that have been already shown in **Table 1.3**.

1.7. Conclusions

Cancer has been one of the leading malignant diseases worldwide. Looking into the present scenario of an increase in the rate of cancer cases and deaths, the development of cost-

effective, environmentally friendly, and effective drug delivery systems has been of high requirement. Thus, biopolymers can be a useful vehicle for the delivery of anti-cancer drugs. Chitosan and SF have shown advantages in terms of abundant availability, cost-effectiveness, biocompatibility, and non-toxicity, presence of large functional groups in their backbones, and easy material formulation.

Nanoparticles below 100 nm size show exclusive physicochemical and biological properties as they can easily penetrate the cell barriers and provide a high surface to volume ratio, which helps in better drug attachment. Polymeric nanoparticles and metal nanoparticles formulated from natural biopolymers can be an effective drug-carrying tool possessing uniform shape and size, lower cytotoxicity, and functional groups that can be used for attaching drug targeting moieties.

1.8. Objectives of research work

The aim of this thesis is to synthesize nanomaterials derived from biopolymers for controlled and targeted delivery of anti-cancer agents. We have used two types of biopolymers, low molecular weight chitosan, and silk fibroin.

The following objectives have been formulated:

(1) Development of a photoresponsive nanocarrier by covalently conjugating 5-FU to LMWC *via* a photocleavable linker. The covalent conjugation is expected to help in avoiding premature drug leakage and allowing drug release only upon irradiating the system with the light of wavelength 365 nm. Thus, acting as a photo-controlled drug delivery nanocarrier.

(2) Synthesis of 5-FC loaded LMWC stabilized silver nanoparticles for an enzyme-prodrug combinatorial system using non-mammalian enzyme cytosine deaminase. As 5-FC is less toxic to mammalian cells and release 5-FU under the action of CD, the

system is expected to behave as an enzyme-mediated system releasing 5-FU in a controlled manner.

(3) Synthesis of folate and fluorescein conjugated SF coated LMWC stabilized gold nanoparticles for anti-cancer agents. The SF coating is expected to provide a diffusion barrier and helps in long term drug release. Folic acid conjugation can provide cell targeting properties, and fluorescein conjugation can be utilized for imaging purposes.

(4) Formulation of SF coated LMWC stabilized gold nanoparticle beads for DOX. The beads are expected to be useful for oral and depot delivery and the SF coating to promote sustained and long term drug release.

(5) Fabrication of biotin conjugated LMWC-SF based carbon dots for targeted delivery of anti-cancer agents. Biotin conjugation can provide cell targeting properties, and fluorescence carbon dots can be utilized for cell-imaging purposes.

Chapter 2 Development of photoresponsive chitosan conjugated prodrug of 5-fluorouracil as a nanocarrier for controlled delivery of the antitumor drug.

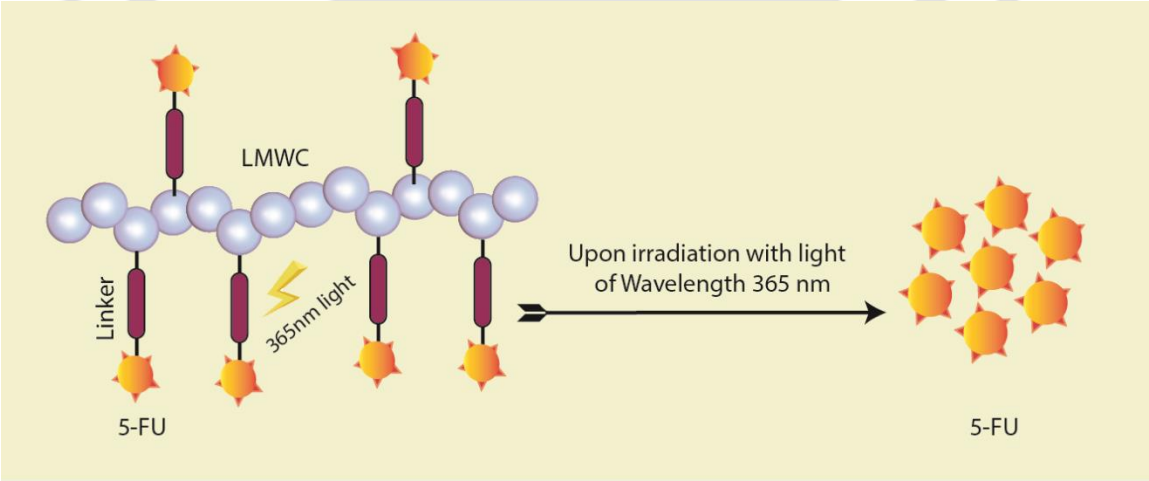

2.1. Overview

Polymer-drug conjugates have been a significant invention in the field of controlled drug delivery. The polymer and the drug are covalently conjugated *via* stimuli-responsive linkers that get cleaved upon exposure to a specific stimulus, thus releasing the drug in a controlled manner. They have several advantages over physically loaded drugs, as covalent conjugation increases the stability of the attached drug in the DDS, thus preventing its premature leakage and loss. It also provides high drug loading efficiency and sustained drug release, which can be externally controlled.

Natural polymers have been of great importance in various pharmaceuticals and biomedical applications because they are biocompatible, non-toxicity, and undergo enzymatic or non-enzymatic hydrolysis inside the cells, making them attractive candidates as potential drug carriers[201–203]. Chitosan has been widely used in cancer drug delivery as it is mucoadhesive[162] and easily gets degraded by lysozyme, which is an enzyme present in the human fluid; thus, no separate steps are needed for the removal of the drug carrier after the administration of the drug[203]. Besides, low molecular weight chitosan has come out with even enhanced properties like greater water solubility, narrower molecular weight distribution, lower cytotoxicity, and antioxidant properties[204].

Nanocarriers have been known to enhance the pharmacological and therapeutic properties of conventional drugs. Nanoparticles below 100 nm show unique biological and physicochemical properties as they can potentially penetrate the cell barriers[184]. Chitosan nanoparticles have been extensively used as drug carriers as they can be easily formulated due to its cationic nature, which allows it to undergo ionic cross-linking in the presence of multivalent anions[205]. Ionic gelation technique for chitosan nanoparticle preparation is advantageous as it avoids the use of toxic chemicals, organic solvents, and high temperature[206].

Herein, we have designed a model drug delivery system for photo controlled delivery of 5-FU. The drug has been covalently conjugated to LMWC *via* a photocleavable linker, an *o*-nitrobenzyl derivative that gets decomposed when exposed to a light of wavelength 365 nm. Thus, when the system is exposed to that particular wavelength of light, the linker gets decomposed and releases the drug. The present drug delivery system was designed primarily for surface application. E.g., Skin cancer. The conjugated was further formulated into nanoparticles *via* ionic gelation technique for effective cell-penetration. In some DDS, premature drug leakage and an initial burst release of the drug occurs, which leads to an increase in the concentration of the drug release resulting in toxicity, damage of organs, and various other side effect[207]. In our proposed system, no premature drug leakage and burst release is expected as it is covalently attached to the carrier and can only get detached on photoactivation. This was also evident from the cleavage study of *o*-nitrobenzyl derivatives, reported earlier[159,208]. The synthesized prodrug-polymer conjugate is expected to improve hydrophilicity as well as increase the retention time of the drug.

2.2. Experimental Procedures

2.2.1. Materials

All the reagents used were of analytical grade and were used without further purification. LMWC (Mv =130 kDa, 94% deacetylation), 5-FU, TPP and bis(trimethylsilyl)acetamide,4-bromomethyl-3-nitrobenzoic acid (BSA) were purchased from Sigma Aldrich. 2-(N-morpholino)ethanesulfonic acid (MES) buffer was purchased from Himedia. 1-Ethyl-3-(3-dimethylaminopropyl) carbodiimide (EDC) was procured from Spectrochem and N-Hydroxysuccinimide (NHS) and purchased from Alfa Aesar.

2.2.2. Characterization of LMWC

The LMWC used in the experiment was characterized for its percentage degree of deacetylation (DD %) and viscosity average molecular weight (M_v). The DD % was determined by pH-metric titration and supported by FTIR spectroscopic method. The M_v was determined by viscometric measurement.

(A) Determination of degree of deacetylation of LMWC

For pH-metric titration, 0.05 g of LMWC was dissolved in 0.1 M HCl and was titrated against 0.1 M NaOH. The pH of the solution was recorded with dropwise addition of 0.1 M NaOH. A graph of pH vs. ml of NaOH added was plotted, and the DD % was then calculated using the equation **Eq.2.1**.

$$DD\ \% = 16.1\ (y-x)\ f/w \qquad \textbf{(Eq. 2.1)}$$

where, y and x are the consumed NaOH volume at two equivalent points; f is molarity of the NaOH solution and w is the initial weight of LMWC[209,210].

(B) Determination of viscosity average molecular weight of LMWC by viscometric measurement

The viscosity average molecular weight of LMWC was performed by viscometric measurement using Ubbelohde viscometer. Different concentrations of LMWC: 0.033 g/dl, 0.5 g/dl and 0.7 g/dl was prepared in 0.1 M CH_3COONa/ 0.2 M CH_3COOH solution. Blank 0.1 M CH_3COONa/ 0.2 M CH_3COOH solution and the prepared LMWC solutions were allowed to flow through the viscometer at 30°C, and the time taken for the flow was recorded. From the time of flow of LMWC solution and time of flow of blank solvent, relative viscosity was determined using the equation **Eq. 2.2**.

$$\text{Relative viscosity, } \eta_r = t/t_0 \qquad \textbf{(Eq. 2.2)}$$

Where t is the time of flow of solution, and t_0 is the time of flow of the solvent.

From relative viscosity, inherent viscosity was calculated using the equation **Eq. 2.3**, which was then plotted against the concentration of LMWC, and extrapolating it to zero concentration gives intrinsic viscosity.

Inherent viscosity, $\eta_{inh} = \ln (t/t_0)/c = \ln \eta_r/c$ (**Eq. 2.3**)

Where c is the concentration of LMWC.

From Inherent viscosity, the viscosity average molecular weight was calculated using Mark-Houwink-Sakurada equation **Eq.2.4**.

$[\eta] = KM_v^{\alpha}$ (**Eq. 2.4**)

where, $[\eta]$ is the intrinsic viscosity; M_v is the viscosity average molecular weight; K and α are constants at a given temperature and solute solvent system[211].

2.2.3. Attachment of 5-fluorouracil and linker (5-FU-linker)

5-FU-linker was synthesized following an already reported procedure, with minor modification[159]. In brief, bis (trimethylsilyl)acetamide (2.3 ml, 9.60 mmol) was added to 5-FU (0.5 g, 3.85 mmol) under an inert atmosphere. The reaction mixture was allowed to stir at room temperature until 5-FU gets completely dissolved. 4-bromomethyl-3-nitrobenzoic acid, the linker (1.3 g, 5.0 mmol, dissolved in acetonitrile), was added to it and was refluxed for 18 h. Finally, the reaction was quenched with methanol, and the solvent was evaporated to obtain a pale yellow powder with a 42% yield.

2.2.4. Preparation of low molecular weight chitosan conjugated 5-FU-linker prodrug (LMWC-5-FU)

5-FU-linker (0.150 g, 0.48 mmol), EDC (0.102 g, 0.53 mmol), and NHS (0.061g, 0.53 mmol) was dissolved in 50 mM MES buffer of pH 6.0 and was allowed to stir for 4 h for activation of the carboxyl group, at room temperature. LMWC (0.097 g, 0.0019 mmol) suspended in MES buffer was added to the reaction mixture and was allowed to react for 24 h at room temperature. The product was dried at 50°C and repeatedly washed with methanol followed

by centrifugation to remove all the unreacted 5-FU and other organic reagents. The supernatant was checked in UV-Visible spectrophotometer until no trace of 5-FU was found. Further, the product was dialyzed using a dialysis membrane (MW cut off 13 kDa) for 72 h to eliminate the presence of any small molecules as an impurity followed by lyophilization.

2.2.5. Preparation of low molecular weight chitosan conjugated 5-FU-linker prodrug nanoparticles (LMWC-5-FU nanoparticles)

The nanoparticles were synthesized by the conventional ionic gelation technique[206]. The LMWC-5-FU conjugate was dissolved in 0.1 % (v/v) acetic acid solution. The acetic acid concentration taken was 1.75 times more than the conjugate. The pH of the solution was adjusted to 5.5 by 0.5 M NaOH. Then 0.21 mg/ml of aqueous TPP solution was dropwise added to the conjugate solution by taking conjugate: TPP ratio of 2:5 (w/w) under constant stirring at room temperature. The solution was stirred overnight at room temperature, and then the resultant nanoparticles were centrifuged for 30 min at a temperature of 14°C and rotation speed of 13,000 rpm to remove any suspended materials and finally lyophilized and stored at 4°C.

2.2.6. Determination of percentage conjugation

The percentage of the conjugation of 5-FU-linker to the free amino group of LMWC was determined by calculating the amount of 5-FU conjugated by UV-Visible spectroscopy. The calibration curve of 5-FU was prepared in distilled water. The concentration of 5-FU in the conjugate was determined by comparing the absorbance of the conjugate to the calibration curve of 5-FU at 266 nm.

2.2.7. UV-Visible spectroscopy

The percentage conjugation and release of 5-FU were determined by UV-Visible spectroscopy at room temperature using Agilent Carry 100 UV-Visible spectrophotometer.

2.2.8. Fourier Transform Infrared Spectroscopy (FTIR)

The FTIR spectra of the dry LMWC and the conjugate were recorded on Perkin Elmer Spectrum 2 FTIR spectrometer at room temperature using KBr pellet, over a frequency range of 4000-400 cm^{-1}.

2.2.9. Field Emission Scanning Microscopy/Energy Dispersive X-ray Analysis (FESEM-EDX)

The elemental mapping to check the presence of fluorine of 5-FU in the conjugate was done by Zeiss Sigma Field Emission Scanning Electron Microscope by EDX Analysis. The conjugate was lyophilized and grounded to fine powder, spread in on carbon film for the analysis.

2.2.10. Thermogravimetric analysis (TGA)

The change in the thermal properties before and after conjugation was studied by TGA using Netzsch STA 449 F3 Jupiter® thermal analyzer. The mass of the sample taken was in the range of 5-8 mg. The temperature was raised at a rate of 10°C/min from 25°C to 700°C under an inert atmosphere.

2.2.11. Powder X-Ray Diffraction (Powder-XRD)

The change in crystallinity before and after conjugation was determined by powder XRD using Bruker D8-Advance Powder X-Ray diffractometer with CuK_{α} radiation (λ=1.54 Å) in a 2θ range of 5-80°.

2.2.12. Field Emission Transmission Electron Microscope (FETEM)

The particle size of the nanoparticles was determined by Jeol 2100F Field Emission Transmission Electron Microscope. For the analysis, a droplet of the nanoparticle suspension was cast on a copper grid without being stained. The excess liquid was removed by touching

the edge of the copper grid with a small piece of filter paper and further dried overnight in a desiccator.

2.2.13. Dynamic Light Scattering (DLS)

DLS studies were conducted to determine the hydrodynamic diameter of the particles using a Malvern Zetasizer Nano Series at 25±0.1°C. Diluted nanoparticle suspension was used for the analysis.

2.3. Results and Discussions

2.3.1. Synthesis of LMWC-5-FU conjugate prodrug

The conjugate was synthesized in two steps, as shown in **Scheme 1**:

(i) Attachment of 5-FU (**1**) with 4-bromomethyl-3-nitrobenzoic acid (**4**), the cleavable linker *via* formation of a reactive intermediate **(3)** using BSA **(2)**. The drug-linker attachment gives (**5**).[88,159]

(ii) Coupling of the free carboxyl group of **(5)** to the free amine of LMWC (**6**) to from the desired conjugate **(7)**.

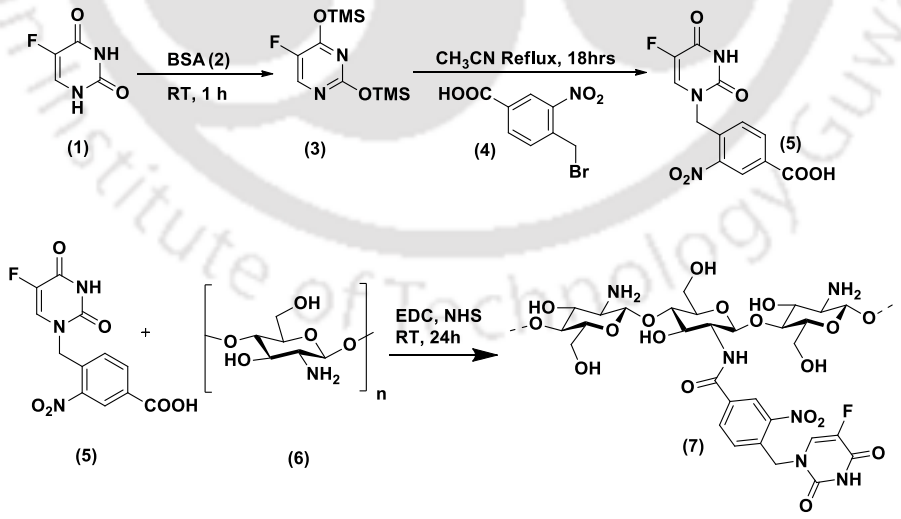

Scheme 2.1 Schematic representation for the stepwise synthesis of LMWC-5-FU conjugate (7).

2.3.2. Purification of LMWC-5-FU conjugate prodrug

The prepared conjugate **(7)** was purified in two steps. At first, the unreacted 5-FU and linker were removed by washing three to four times with methanol followed by centrifugation. The washing was monitored by UV-Visible spectra of the supernatant until the peak for 5-FU was null. Secondly, for further removal of any other unreacted compounds and impurities, the compound **(7)** was dispersed in distilled water and dialyzed for 72 h using dialysis membrane (MW cut-off 13 kDa).

2.3.3. Determination of percentage conjugation

The percentage of 5-FU-linker conjugated to LMWC was calculated to be 30 wt% from the calibration curve of 5-FU.

2.3.4. Synthesis of LMWC-5-FU conjugate prodrug nanoparticles

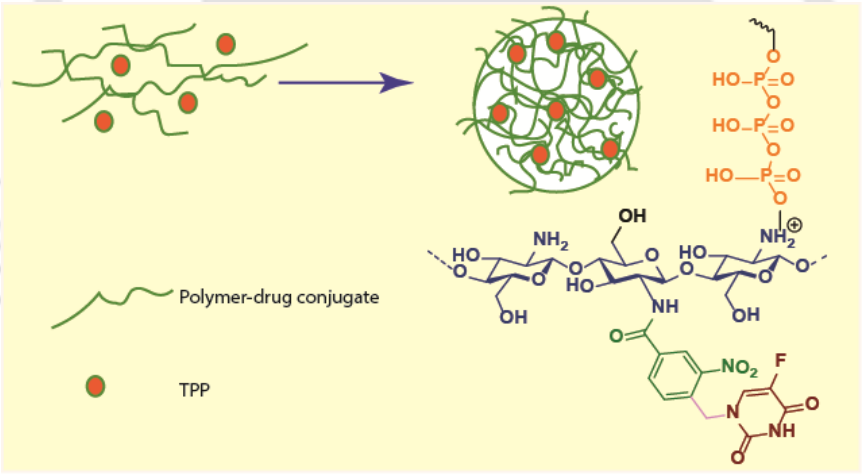

Figure 2.1 Formation of LMWC-5-FU conjugate prodrug nanoparticles by ionic gelation technique using TPP.

LMWC-5-FU conjugate prodrug was formulated into nanoparticles as particles with a size less than 100 nm are potentially capable of penetrating cell membranes, making them an attractive choice as drug delivery vehicles. LMWC-5-FU nanoparticles were synthesized by the ionic gelation technique as shown in **Figure 2.1**. It is a one-step process in which the prepared LMWC-5-FU conjugate prodrug **(5)** was treated with sodium tripolyphosphate

(TPP). In slightly acidic pH, the glucosamine residue of chitosan carries a positive charge, making it a poly-cationic biopolymer that can interact with poly-anionic tripolyphosphate molecule leading to the formation of the nanoparticles. Various other processes are available for the synthesis of chitosan nanoparticles, but this is the most preferred and best suited for pharmaceutical application as it involves the use of non-toxic TPP, aqueous and mild processing conditions, and requirement of less energy[212].

2.3.5. Drug releasing mechanism

5-FU was covalently conjugated to LMWC *via* a photocleavable linker containing *o*-nitrobezyl derivative, which is known to get decomposed upon irradiation with λ=365 nm UV-A light to form *o*-nitroso-benzaldehyde **(8)** as in **Figure 2.2** and release 5-FU **(1)**. The linker can be cleaved in a controlled manner on irradiation, thereby releasing the drug 5-FU from the conjugate over a specific time interval. The cleavable bond is indicated by red color in **Figure 2.2**. Thus, the duration and rate of drug delivery can be controlled by varying the intensity of the light and the time of exposure to attain the preferred therapeutically effectual concentration.

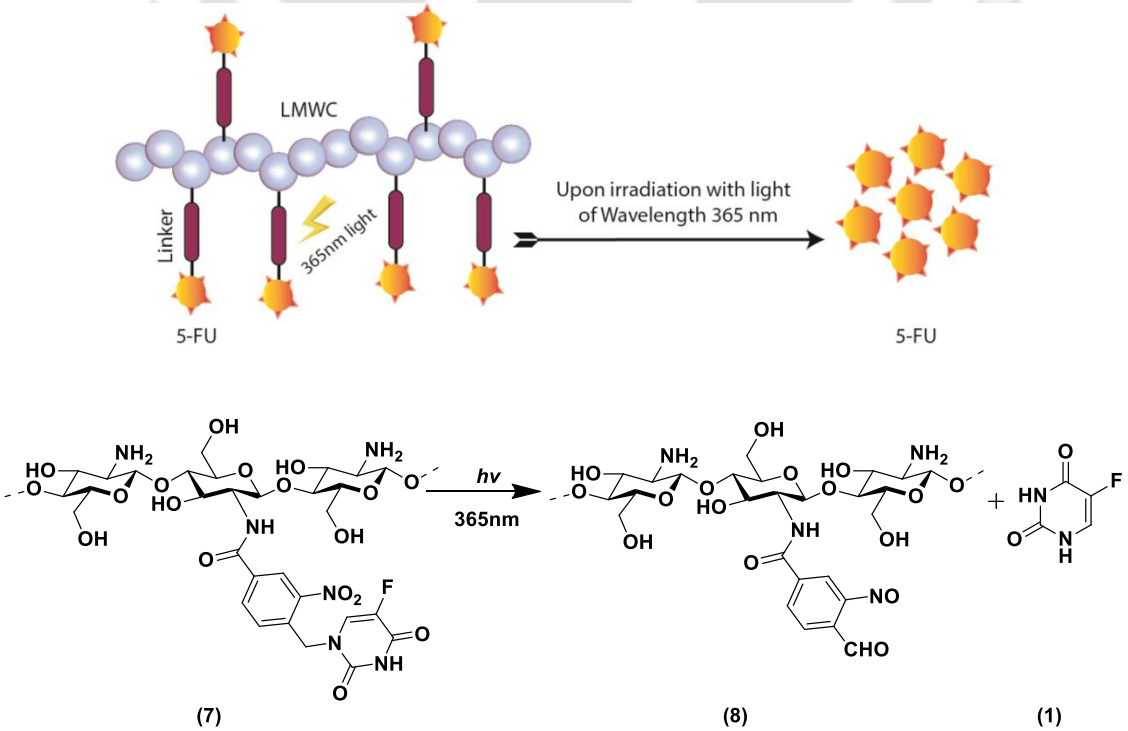

Figure 2.2 Release mechanism of 5-FU from the LMWC-5-FU conjugate prodrug upon irradiating with λ = 365 nm light.

2.3.6. Characterization of LMWC

A. Determination of the degree of deacetylation of LMWC

The DD % of the LMWC was calculated by pH-metric titration. The pH vs. ml of NaOH added was plotted as shown in **Figure 2.3 (B)** from which two equivalence points were determined using the second derivative plot, as in **Figure 2.3 (C)** and using **Eq. 2**, the degree of deacetylation was calculated to be 93.05 %. It was further confirmed by FTIR spectroscopy in **Figure 2.3 (A)**, which gave a value of 94.45 % using the equation (A_{1656}/ A_{3450}) (100/1.33) where A_{1655} and A_{3450} are absorbances at 1655 cm^{-1} and 3450 cm^{-1} respectively[213].

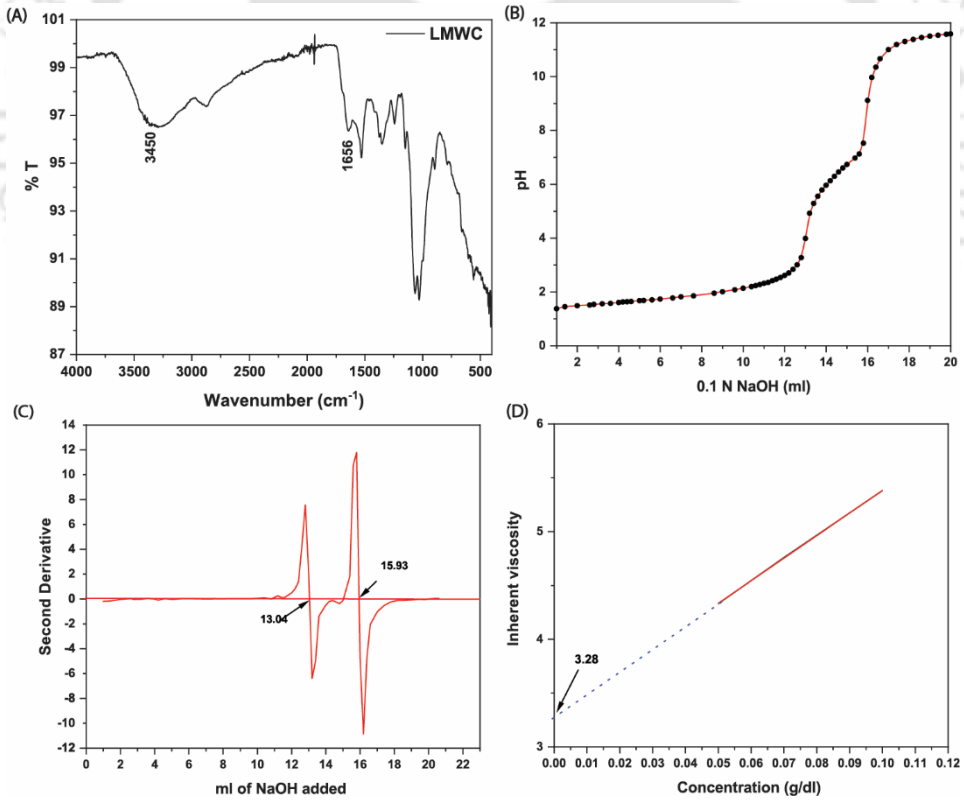

Figure 2.3 (A) FTIR spectra of LMWC; **(B)** Plot of pH vs. ml of NaOH added; **(C)** Second derivative plot of pH vs. ml of NaOH added; **(D)** plot of inherent viscosity vs. concentration LMWC.

B. Determination of viscosity average molecular weight

Different concentration of LMWC was dissolved in 0.1 M CH_3COONa/ 0.2 M CH_3COOH solution, and the viscosity was determined at 30°C using Ubbelohde viscometer. From viscosity data, relative viscosity (η_r) was calculated from which inherent viscosity ($\eta_{inh}=\ln \eta_r /c$) was determined. Then the η_{inh} was plotted against the concentration (c) shown in Figure **2.3 (D)**, which on extrapolating to zero concentration gave intrinsic viscosity as 3.28 dl/g. The viscosity average molecular weight was then calculated using **Eq.2.5**.

$[\eta] = KM_V^{\alpha}$ **(Eq. 2.5)**

The value of K and α was determined using the following equation[211].

$K= 1.64 \times 10^{-3} \times DD^{14.0}$ **(Eq. 2.6)**

$\alpha = -1.02 \times 10^{-2} \times DD + 1.82$ **(Eq. 2.7)**

For DD = 94 %, the value of $K = 6.89 \times 10^{-3}$ and $\alpha = 0.86$

Therefore,

$[\eta] = KM_V^{\alpha}$

$3.28= 6.89 \times 10^{-3} M_v^{0.86}$

$M_v = 1298.82$ dl/g = 129882 cm^3/g = 129883 Da

2.3.7. Determination of conjugation of 5-FU-linker to LMWC

The conjugation of the 5-FU-linker to LMWC has been analyzed by UV-Visible spectroscopy, FTIR spectroscopy, and FESEM-EDX. The change in the thermal property of the material upon conjugation was studied by TGA, and the crystalline behavior was studied by powder-XRD.

(A) UV-Visible Spectroscopic study

An indication of the coupling between 5-FU-linker and LMWC could be determined from the UV-Visible spectroscopic study. The UV-Visible spectra of LMWC and 5-FU-linker conjugate are shown in **Figure 2.4 (A)** and **(B)**, respectively. A noticeable difference between

LMWC and the conjugate prodrug can be seen from the spectra. The conjugate shows an absorption peak at 266 nm, which is the characteristic peak of 5-FU, which is absent in blank LMWC[159,214]. This concludes the linkage of 5-FU with LMWC.

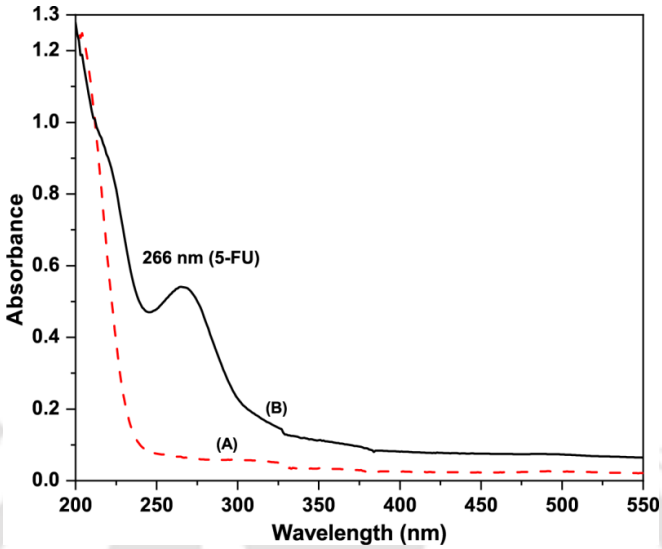

Figure 2.4 UV-Visible Spectra of **(A)** LMWC; **(B)** LMWC-5-FU conjugate in 1% acetic acid solution. The absorption maxima at 266 nm in (B) prove the presence of 5-FU in the conjugate prodrug.

(B) FTIR spectroscopic study

The formation of the conjugate was further supported by the FTIR study. **Figure 2.5 (A)** shows the FTIR spectrum of LMWC. The absorption band at around 3317 cm^{-1} is assigned to the stretching vibration of amine (-NH_2) and hydroxyl (O-H) group of chitosan. The bands at 2938 and 2882 cm^{-1} are attributed to the symmetric stretching vibration of –CH_3 and asymmetric stretching vibration of –CH_2, respectively. The peak at 1643 cm^{-1} is assigned to the carbonyl (C=O) stretching vibration and 1537 cm^{-1} to N-H bending vibration. After being covalently attached to the linker, the carbonyl peak intensity is increased and is slightly shifted to 1651 cm^{-1}, as shown in **Figure 2.5 (B).** The N-H peak is also shifted to a higher wavenumber of 1590 cm^{-1}, confirming the successful attachment of 5-FU-linker to the LMWC[215,216].

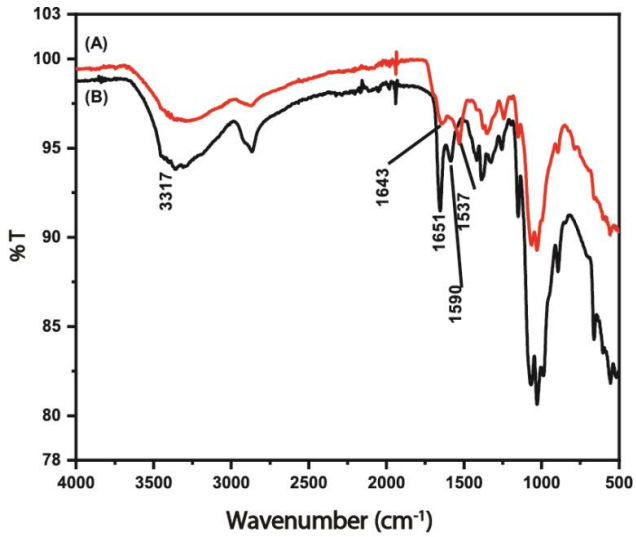

Figure 2.5 FTIR spectra of **(A)** LMWC; **(B)** LMWC-5-FU conjugate as obtained using KBr pellets.

(C) FESEM-EDX

The elemental mapping of LMWC-5-FU conjugate was done by FESEM-EDX. EDX of LMWC, as given in **Figure 2.6 (A)**, shows large peaks of carbon (C) and oxygen (O), indicating the two main components of chitosan along with a small amount of nitrogen (N). But the elemental analysis of synthesized conjugate in **Figure 2.6 (B)** showed peaks for 8.1% of fluorine (F) along with carbon, oxygen, and nitrogen, indicating the presence of 5-FU.

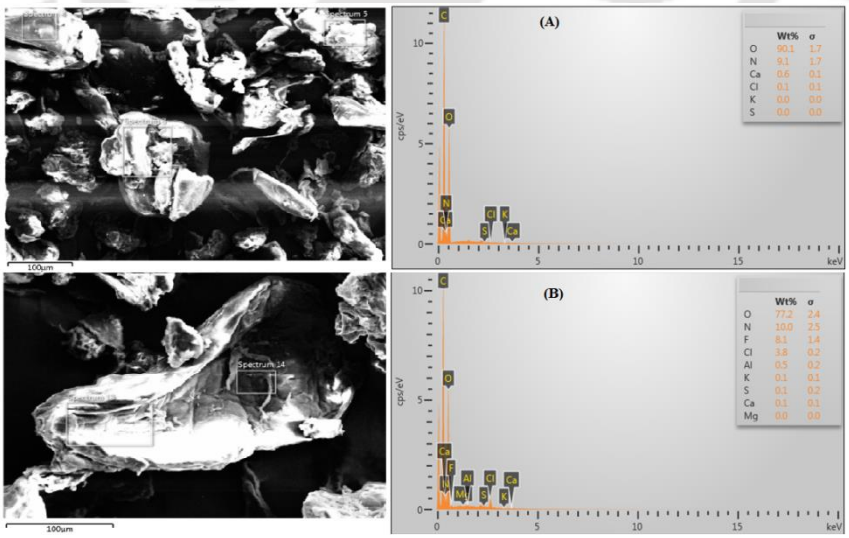

Figure 2.6 FESEM/EDX of **(A)** LMWC; **(B)** LMWC-5-FU conjugate powder spread on a carbon film.

(D) Thermogravimetric Analysis

The thermal stability of LMWC and LMWC-5-FU conjugate was compared by thermogravimetric analysis (TGA). The TGA thermogram of LMWC and conjugate is shown in **Figure 2.7 (A)**. Three consecutive weight loss steps for both LMWC and conjugate were observed. At first, 6% weight loss can be seen in both the thermograms from 66°C, which is due to moisture loss. The second weight loss of about 40% occurred in LMWC due to ether linkage scission in chitosan from 256°C. The third weight loss of 26% occurred from 338°C due to glucosamine residue of LMWC. Whereas, in the conjugate, the second weight loss started earlier than LMWC, which is at about 191°C. This may be due to the new covalent bond formation with 5-FU, which blocks the free -NH_2 group of chitosan, thereby decreasing intermolecular interactions between the polymeric chains. It was also seen that, at the end of the experiment, the residue percentage of LWMC was more than that of LMWC-5-FU, showing the decrease of thermal stability of LMWC on covalent attachment to the drug[217]. A plot of temperature vs. percentage decomposition has been shown in **Figure 2.7 (B)** which is inferred from transient thermogravimetric plot over a temperature 25°C to 700°C in **Figure 2.7 (A).** In transient thermogravimetric analysis, the mass is recorded by changing the temperature linearly while in static thermogravimetric analysis, the mass at a fixed temperature is recorded. The thermal degradation data are shown in **Table 2.1**.

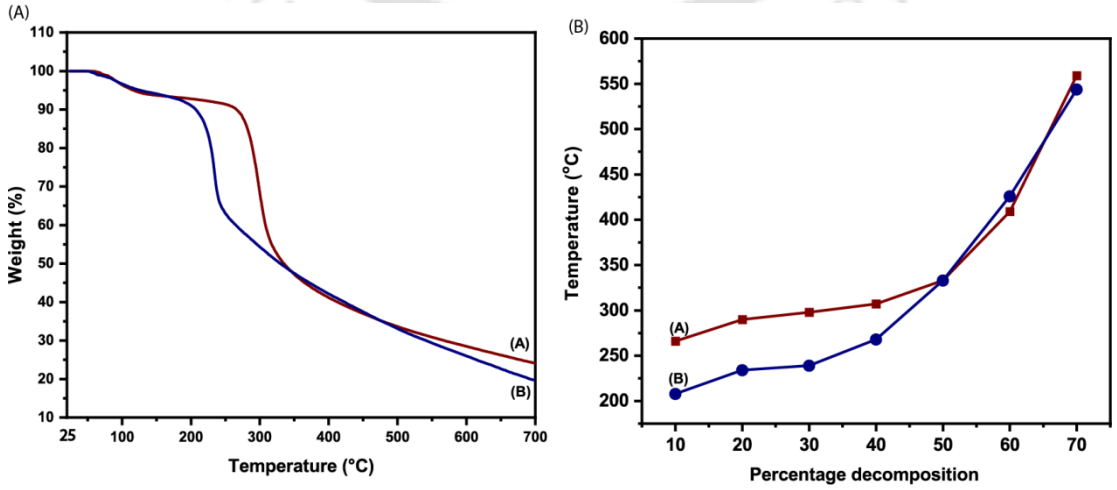

Figure 2.7 (A) TGA thermogram of **(a)** LMWC and **(b)** LMWC-5-FU conjugate at a heating rate of 10°C/ min from 25°C to 700°C under N_2 atmosphere; **(B)** Thermal study plot of **(a)** LMWC and **(b)** LMWC-5-FU conjugate obtained from TGA plot.

Table 2.1 Thermal degradation data of LMWC and LMWC-5-FU conjugate.

	T_i (°C)	T_{max} (°C)	T_f (°C)	Residual wt %
LMWC	256	298	362	25
LMWC-5-FU conjugate	191	236	257	20

T_i=Temperature corresponding to the beginning of the decomposition; T_{max}= temperature corresponding to the maximum rate of mass loss; T_f = temperature corresponding to the ending of the decomposition.

(E) Powder-XRD

The Powder XRD pattern of LMWC and the conjugate are given in **Figure 2.8 (A)** and **(B),** respectively. LMWC exhibits two diffraction peaks at 2θ =10° and 2θ =20°, which are the typical fingerprint peaks of crystal chitosan showing its high degree of crystallinity[217–219]. In the XRD pattern of the LMWC-5-FU conjugate **(5)**, the peak of LMWC at 10° disappears and at 20° weakens, and a broad, amorphous peak at 20-25° appears. With the attachment of the aromatic moiety of the 5-FU-linker to the LMWC chain, the non-coplanarity of the chain might have increased. The intermolecular force of attraction between the chains has decreased compared to the unsubstituted LMWC due to loose packing. As a result, the crystallization tendency is lowered, and even the conjugate's solubility is enhanced compared to LMWC[217,218]. The amorphous nature of the LMWC-5-FU conjugate, as obtained from XRD, is in good agreement with the TGA analysis.

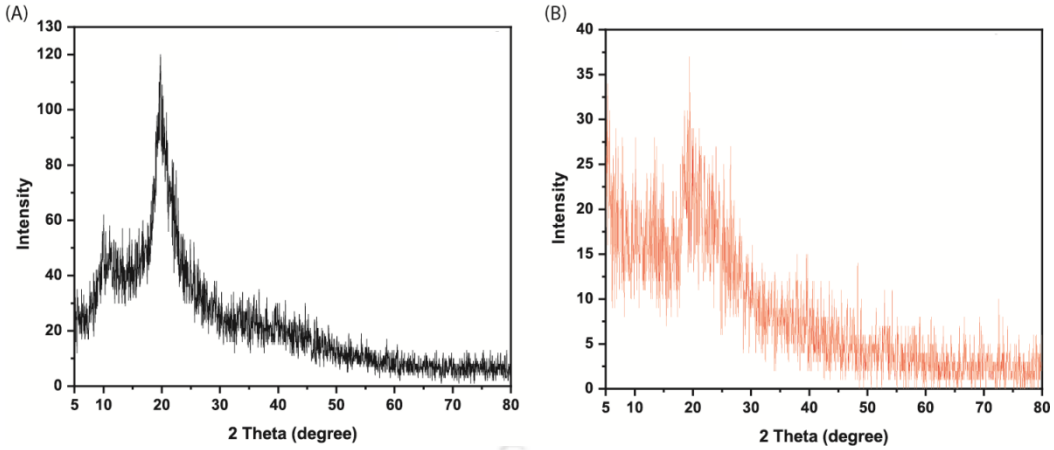

Figure 2.8 XRD pattern of **(A)** LMWC with sharp peak at 2θ = 10 and 20°; **(B)** LMWC-5-FU conjugate prodrug with broad amorphous peak at 2θ = 20-25° taken under CuK_{α} radiation in a 2θ range of 5-80°.

2.3.8. Gelation of LMWC-5-FU conjugate prodrug

The prepared conjugate was found to form gel in water (hydrogel) and DMSO (organogel) with a specific concentration, which is a very desirable property for a drug's surface application. The gelation concentration and gelation time of the conjugated prodrug were studied, which is shown in **Table 2.2**.The gelation time for the hydrogel was found to be 10 s with a concentration of 0.45 wt%, and for DMSO gel was found to be 10 min with a concentration of 12.5 wt%. The images of the inverted vial tests of both the gels are shown in **Figure 2.9.**

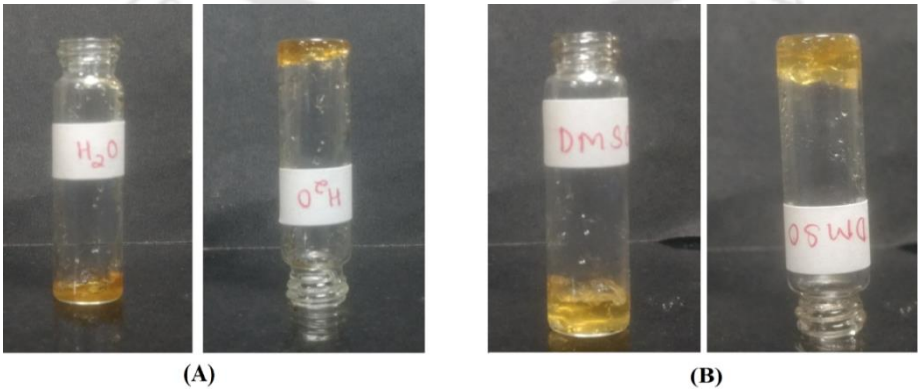

Figure 2.9 Inverted vial test of **(A)** 0.45wt% of hydrogel (left) and **(B)** 12.5wt% of DMSO gel (right) at a time interval of 10 s and 10 min, respectively.

Table 2.2 The gelation concentration and gelation time of the conjugated prodrug.

	Gelation concentration (wt.%)	**Gelation Time**
Hydrogel (in H_2O)	0.45	10 s
Organogel (in DMSO)	12.5	10 min

2.3.9. Determination of LMWC-5-FU conjugate nanoparticles formation

The size of the LMWC-5-FU conjugate nanoparticles was determined by FETEM analysis. DLS was done to obtain the hydrodynamic diameter, polydispersity index (PDI), and the size distribution of the nanoparticles.

(A) FETEM Analysis

The FETEM micrographs of the nanoparticles are shown in **Figure 2.10.** The images clearly show nanoparticles of mostly spherical shape with a narrow particle size distribution of 70-90 nm.

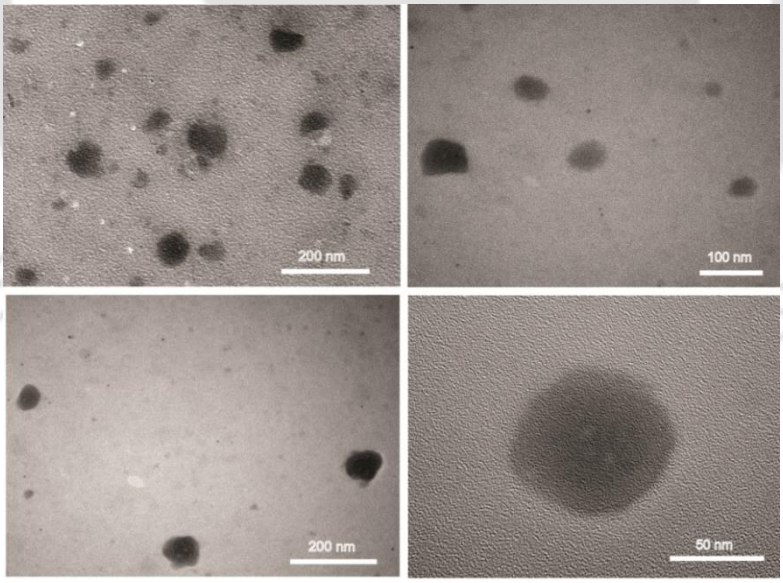

Figure 2.10 FETEM micrographs of LMWC-5FU conjugate nanoparticles showing nanoparticles of spherical shape with a narrow particle size distribution of 70-90 nm. The scale bar corresponds to 200 nm (top and bottom left), 100 nm (top right), 50 nm (bottom right).

(B) DLS study

DLS studiey was performed using dilute nanoparticle suspension in water. The final value was an average of three measurements. The z-average particle size was obtained to be 178.90±12 nm diameters with a PDI of 0.127. **Figure 2.11** shows the DLS spectrum of LMWC-5-FU conjugate nanoparticles.

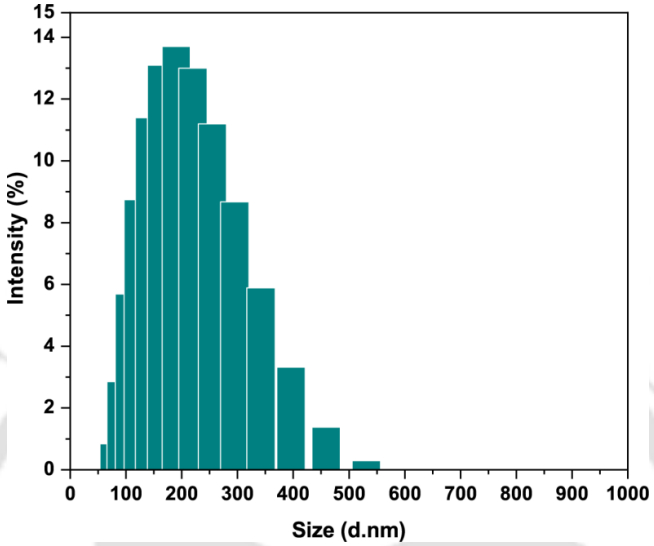

Figure 2.11 DLS spectrum of LMWC-5-FU conjugate nanoparticles suspension in water.

2.3.10. In vitro release study of 5-FU from LMWC-5-FU conjugates nanoparticles prodrug.

The in vitro release study of 5-FU from the conjugate nanoparticles was performed by irradiating it under LED UV bulb (λ= 365 nm) of 48 W at 25°C. Nanoparticles (0.4 mg/ml) dispersed in 2% acetic acid in water/acetonitrile (50:50) mixture was taken in a quartz cuvette and kept for irradiation. After an interval of 1 h, 1 ml aliquot was taken out in a dialysis membrane (MW cut-off 13 kDa) and dialyzed against 15 ml of distilled water. After 12 h of dialysis, approximately 500 µl samples were taken out from the solution outside the dialysis membrane and analyzed by UV-Visible spectrophotometry. This was done to measure the released concentration of 5-FU, as the cleaved 5-FU comes out of the dialysis membrane while the conjugate remains inside the membrane. The procedure was repeated for three more aliquots after 2, 3, and 4 h of irradiation. The drug release percentage (weight percent based

on initial drug taken) at different time intervals is shown in **Figure 2.12 (A),** which displays a steady release of 5-FU with a drug release of about 53% achieved after an interval of 4 h.

The UV-Visible absorption spectra of the irradiated samples were also recorded during the course of the photochemical reaction, i.e., after 0.5, 1, 1.5, 2, 3, 3.5, and 4 h to study the uniform cleavage of the linker with time. The changes in the UV-Visible absorption spectra are shown in **Figure 2.12 (B)**. An absorption peak between 300-325 nm increased gradually, which is the characteristic peak of *o*-nitroso-benzaldehyde[220] that forms upon decomposition of the linker and thus releases 5-FU, proving successful uniform cleavage of the linker.

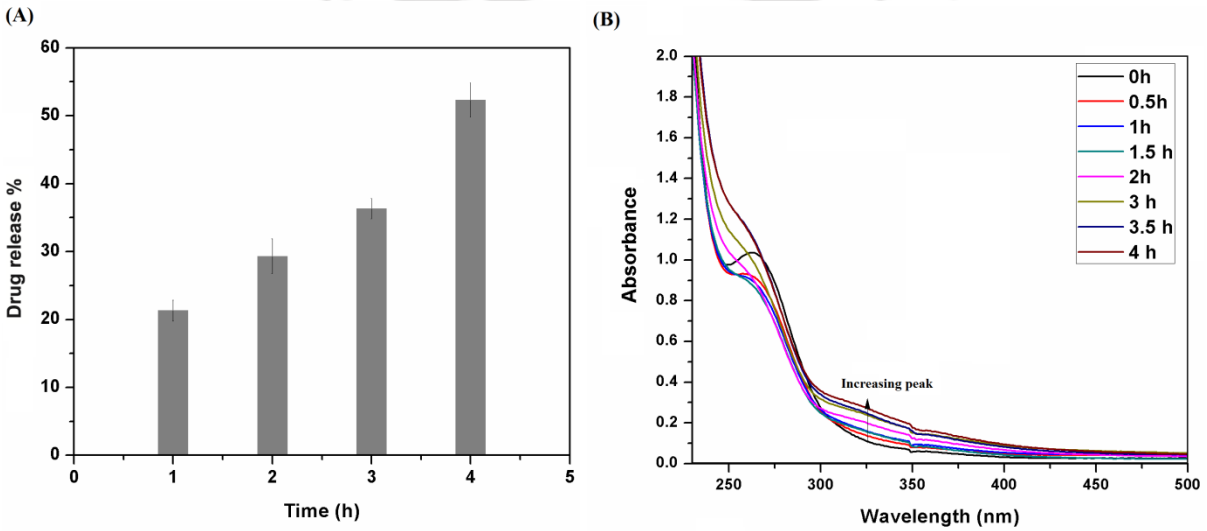

Figure 2.12 (A) Drug release kinetics of LMWC-5-FU conjugate nanoparticles after irradiation at 365 nm at a different time interval of 1, 2, 3, and 4 h with an initial drug concentration of 0.4 mg/ml; **(B)** Overlaid UV-Visible Spectral changes of the conjugate prodrug upon irradiation with UV light of λ=365 nm for different time interval.

2.4. Conclusions

A controlled drug delivery system of 5-FU, an antitumor drug covalently conjugated to low molecular weight chitosan *via* a photocleavable linker, has been designed and successfully tested in vitro for the release of the drug. The conjugate prodrug releases the effective drug 5-FU only on external stimulation, using the light of wavelength 365 nm. The concentration

and rate of the drug release could be controlled by monitoring the dose of the external stimulus. Nanoparticles of the covalently conjugated polymer-prodrug were synthesized to achieve better cell penetration ability. The average size distribution of the nanoparticles obtained was 70-90 nm, and as it is widely believed that nanoparticles having a size less than 100 nm are potentially capable of penetrating cell membranes, the synthesized LMWC-5-FU nanoparticles could be a suitable model for effective delivery of antitumor drugs as well as for their dose-dependent release in a controlled manner.

2.5. Individual FTIR spectra

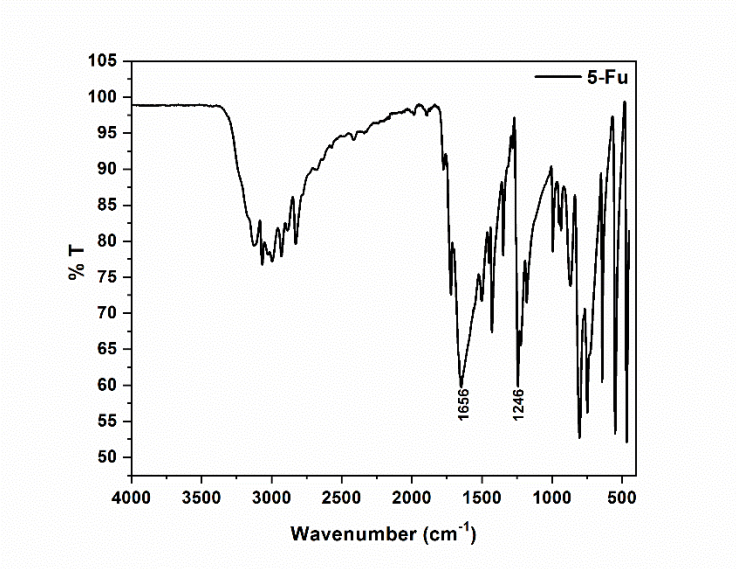

Figure 2.13 FTIR spectra of 5-FU.

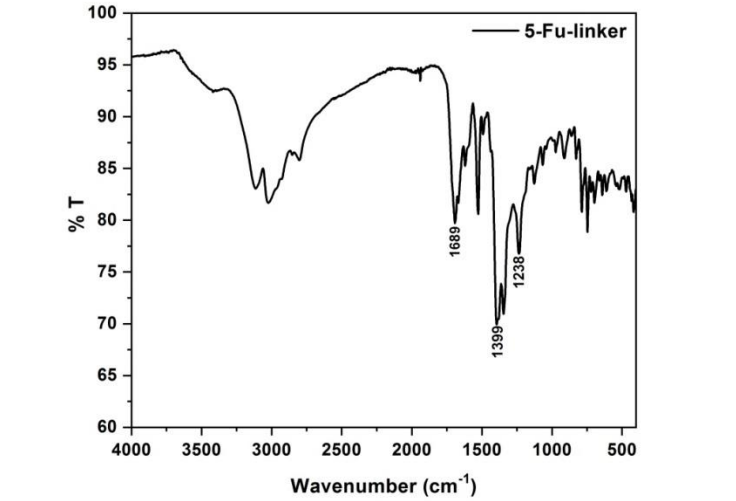

Figure 2.14 FTIR spectra of 5-FU-liker.

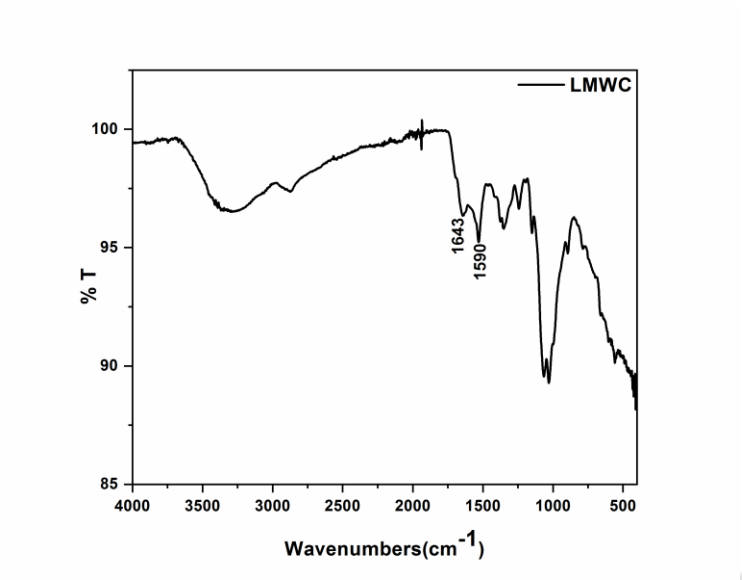

Figure 2.15 FTIR of LMWC.

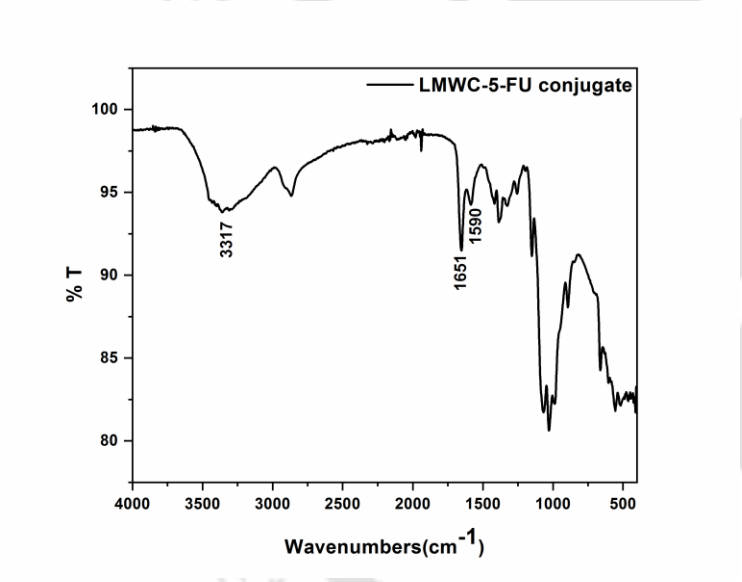

Figure 2.16 FTIR of LMWC-5-FU conjugates.

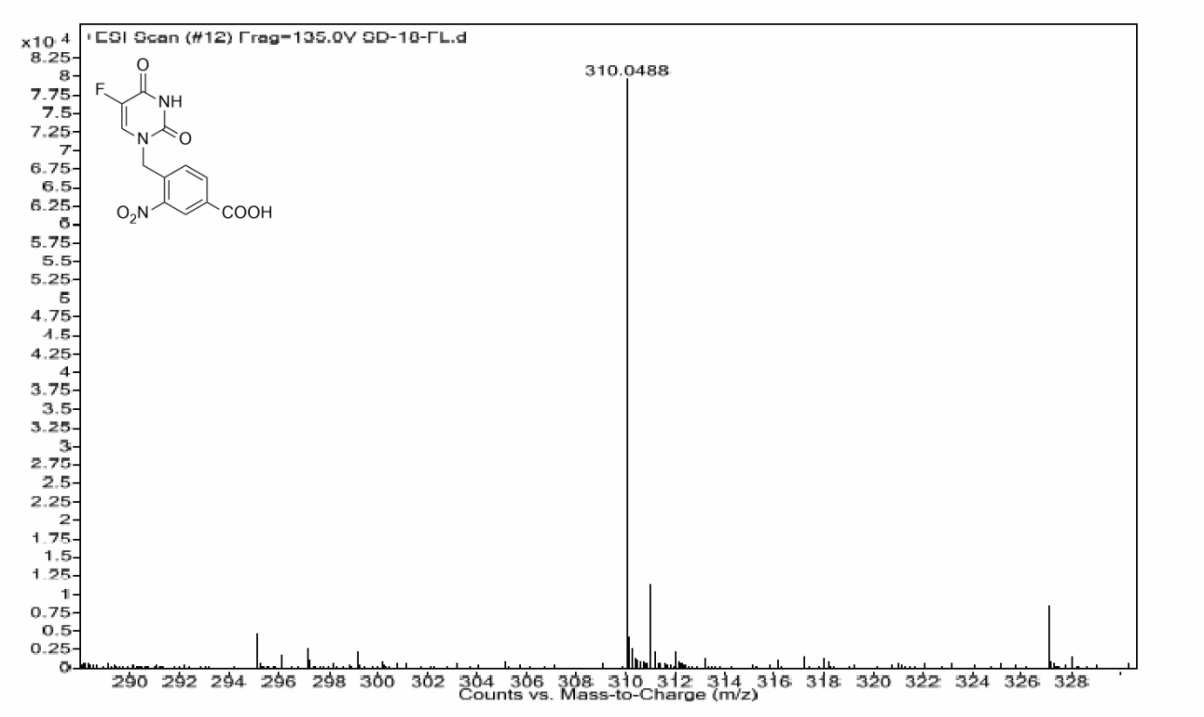

Figure 2.17 HRMS spectra of 5-FU-linker.

Chapter 3 Synthesis of 5-fluorocytosine loaded chitosan stabilized silver nanoparticles as a prodrug in combination with cytosine deaminase for controlled drug delivery

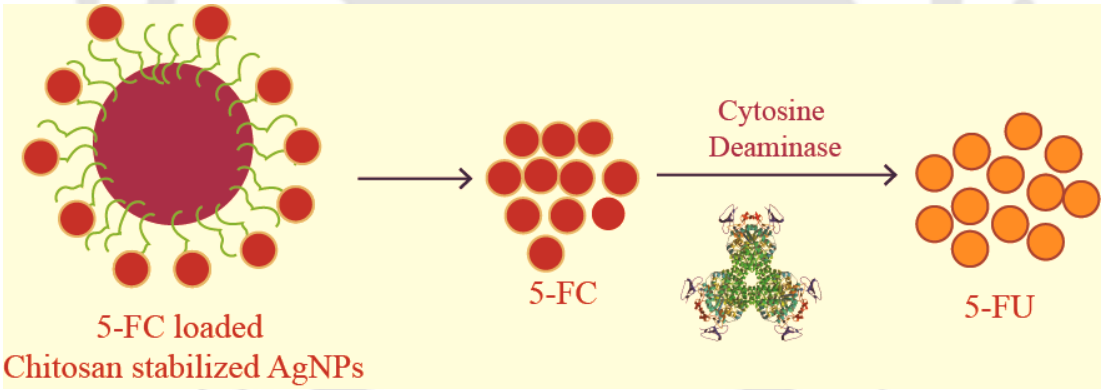

3.1. Overview

Nanomaterials-mediated drug delivery has conceived great importance in the field of drug delivery due to their prominent dominance in improving efficacy in affected tumor cells[221]. Exceptional properties of nanomaterials such as small size, promising physicochemical properties, prolonged blood circulation, and high surface-area-to-volume ratio allow them to penetrate the affected cells and release the drug in an effective and controlled manner [222]. Such nanoparticle cargos also have the potential to control both the pharmacodynamic and pharmacokinetic profiles of the therapeutic agents, thus enhancing their therapeutic index[17].

Biopolymer-stabilized silver nanoparticles (AgNps) have earned much attention in the biomedicine and healthcare sectors because of their excellent antimicrobial, anti-inflammatory, anti-cancer, and anti-angiogenic properties. Its application in cancer diagnosis and treatment exhibited promising results as a targeted drug delivery tool, preliminary cancer detection probe, and as a therapeutic molecule by itself [223–225]. The overall toxicity of AgNps has been lesser-known, and a few studies on its toxic effects in biological systems reported results that are unmatched and conflicting [186,226,227]. AgNps have decidedly less or no toxicity to the mammalian cells at a lower dosage compared to other metal nanoparticles [224,228]. Green synthesis of AgNps using plant extracts, microorganisms, and biopolymers has been in trend for environmental friendliness. Synthesis of the nanoparticles using biopolymers such as chitosan has been worthwhile and has been reported by various researchers [50,229,230], where chitosan acts as both a reducing and a stabilizing agent. Chitosan possesses a large number of hydroxyl groups with the ability to form a complex with metal ions. It helps in controlling the shape and size of the nanoparticles and reduces its toxicity to mammalian cells[185,186]. Moreover, the size of the nanoparticles obtained was found to be less than 30 nm, which has the potential to penetrate the cell barriers[184]. Chitosan has attained great importance in

pharmaceutical research because of its biocompatibility, non-toxicity, biodegradability, mucoadhesiveness, and lysozyme degradability[162,203].

5-FU is an antimetabolite used for the treatment of various types of cancer. It exerts its anticancer activity by converting itself to FdUMP, which irreversibly inhibits the action of TS, causing scarcity of dTTP and thereby preventing DNA synthesis, which ultimately leads to apoptosis[2]. Due to its toxicity and adverse side effects, 5-FU is often introduced *via* a suicide gene therapy approach. This technique adds a 'killer gene,' generally an enzyme that transforms a nontoxic prodrug into a lethal drug. The concept of prodrug has previously been reported for controlled and safe administration of drugs [231–234]. Bacterial cytosine deaminase (CD), along with 5-FC, has been widely used as an enzyme-prodrug system for suicidal gene therapy for the treatment of cancer. The prodrug 5-FC is a fluoropyrimidine, primarily used for the treatment of systemic mycoses and fungal infections that affect internal organs and is known to be less toxic to mammalian cells than 5-FU. The advantage of using CD lies in the fact that there is minimal off-target effects as this gene is exclusively expressed only in certain types of fungi and bacteria and is absent in mammalian cells. CD encodes a protein that catalyzes the deamination of 5-FC to 5-FU. Thus, 5-FC acts as a prodrug that gets converted to 5-FU, an active antitumor agent upon the action of the gene[13]. To increase the cellular uptake of CD to the cancer cells, various carriers such as antibodies, polymers [235], chitosan, and its nanoparticles, have been previously reported [31,236].

Herein, to facilitate enhanced delivery into the target cell, we have demonstrated a procedure for antiproliferation of the cancer cells using a combination of nanoparticle prodrug and a non-mammalian enzyme CD. Activity assay showed high selectivity and efficiency of ECD towards 5-FC encapsulated chitosan-silver nanoparticles, converting it into the active antitumor agent 5-FU *in situ*. The synthesized nanoparticles manifested negligible cytotoxicity in human breast carcinoma cell line MDA-MB-468.

3.2. Experimental Procedures

3.2.1. Materials

All the reagents and the solvents were of analytical grades and were used without further purification. LMWC (M_v =129 kDa; 94% deacetylation) and 5-FU were procured from Sigma Aldrich, and 5-FC was purchased from Alfa Aesar. Glacial acetic acid was purchased from Merck (India), and Silver nitrate was purchased from Himedia laboratories, Mumbai.

3.2.2. Synthesis of 5-fluorouracil/5-fluorocytosine loaded LMWC stabilized silver nanoparticles (CAg-FU)/(CAg-FC).

The nanoparticles were synthesized following a reported protocol with some modifications[237]. LMWC (6.9 mg/ml) was dissolved in 1% aqueous acetic acid solution. 5-FU or 5-FC was added to it with LMWC: 5-FU/5-FC ratio of 1:1 (w/w) and stirred until a clear solution was obtained. 54 mM $AgNO_3$ (0.4 ml/ml LMWC solution) was added into each of the solutions containing 5-FU and 5-FC respectively and stirred at 90°C for 6 h for nanoparticle formation and then kept overnight at 37°C for proper drug loading. The color of the solution changes from colorless to light yellow, followed by dark brown. The solutions were then centrifuged at 13,000 rpm for 30 min, and the drug loaded nanoparticle pellets are collected and stored at 4°C.

3.2.3. Drug loading efficiency

The drug loading efficiency was determined by spectrophotometric analysis. After the formation of nanoparticles and loading of the drugs, the reaction mixture was centrifuged at 13,000 rpm for 20 min. The absorbance of the supernatant was analyzed in UV-Visible spectroscopy at a wavelength of 266 nm and 276 nm for CAg-FU and CAg-FC, respectively. Comparing with a calibration curve of pure 5-FU and 5-FC, the drug loading efficiency was calculated.

3.2.4. *In vitro* drug release study

The *in vitro* release of 5-FU and 5-FC from CAg-FU and CAg-FC, respectively, were carried out by suspending a known amount of drug loaded nanoparticles in phosphate buffer saline (PBS) of pH 7.4. The suspension was transferred to the dialysis membrane (MW cutoff 13 kDa) and immersed in 20 ml of PBS buffer maintained under constant stirring. At the chosen time interval, 500 µL aliquot of sample was taken out and replaced with the same quantity of fresh PBS buffer. The collected aliquots were analyzed spectrophotometrically at 266 nm and 276 nm for 5-FU and 5-FC, respectively, and the percentage of drug release was calculated using a standard calibration curve of pure 5-FU and 5-FC.

3.2.5. Cytosine deaminase activity study

CD gene was amplified from *Escherichia coli* K12 genomic DNA and cloned in pET28a vector using forward primer 5'-CGCGGATCCGTGTCGAATAACGCTTTA-3' and reverse primer 5'-CGGGGTACCTCAACGTTTGTAATCGAT-3'. After validation of the clone by the Sanger sequencing method, the clone was transformed in *E. coli* BL21 (DE3) Rosetta cells. 1 L of culture was overexpressed with 1 mM IPTG at 25°C. His-tagged ECD protein was purified using a standard Ni-NTA affinity chromatography method described previously, with some modifications. Cells were lysed using 50 mM Tris-HCl (pH 7.5), 300 mM NaCl, 3 mM imidazole. After binding to Ni-NTA resin, the column was washed with 50 mM Tris-HCl (pH 7.5), 300 mM NaCl and 10 mM imidazole. The protein was eluted in 50 mM Tris-HCl (pH 7.5), 200 mM NaCl, 200 mM imidazole. The elution fractions were checked on 15% SDS-PAGE for purity, and pure fractions were pooled and desalted in 25 mM Tris-HCl (pH 7.5), 200 mM NaCl.

To test the specificity of CD towards 5-FC, Berthelot assay was performed [238–240]. CAg-FC nanoparticle was used as a substrate for CD. Control experiments were also performed with commercially available 5-FC along with CAg and CAg-FU nanoparticles. 100 nM of purified

ECD and 1 mM of the substrate were incubated in phosphate buffer (pH 7.4) at 37°C for 1 h. The reaction was quenched with 2/3 N H_2SO_4 and 10% (w/v) sodium tungstate. The released ammonia was detected by the addition of phenol color reagent and alkaline hypochlorite, which develops blue coloration and can be measured spectrophotometrically at 630 nm. All the experiments were done in triplicates, and the error was estimated from standard deviation using origin software (version: OriginPro 8.0).

3.2.6. Cell lines and cell culture conditions

Human breast carcinoma cell line MDA-MB-468 was obtained from National Centre for Cell Science, Pune, India. The cells were maintained in Dulbecco's Modified Eagle Medium (DMEM) medium containing 10% (v/v) heat-inactivated fetal bovine serum (FBS), 50 g/ml streptomycin, and 50 IU/ml penicillin incubated at 37°C humidified atmosphere at 5% CO_2.

3.2.7. MTT assay for Cytotoxicity determination

The effect of the synthesized silver nanoparticles on cancer cells was assessed by MTT (3-(4,5-dimethylthiazol-2-yl)-2,5 diphenyl tetrazolium bromide) assay. MDA-MB-468 cells were seeded in triplicates on a 96-well tissue culture plate. The cells were incubated overnight in the CO_2 incubator for attachment. Subsequently, the cells were treated with increasing concentrations of the synthesized drug nanoparticles and blank nanoparticles. After 12 h of treatment, the treatment media was removed and analyzed by MTT assay.

3.2.8. Antibacterial activity

The antibacterial activities of the nanoparticles were determined by the agar well diffusion method against *E.Coli* bacteria (MTCC 1696). Pure *E.Coli* culture was subcultured on Luria Bertani (LB) broth (Sisco Research Laboratories). The LB agar plates were prepared, and 50 µl of *E.Coli* was spread using sterile L-Spreader. Using sterile gel puncture, 10 mm diameter wells were punctured on the plates and 50 µl of each of the samples (a) LMWC; (b) 5-FC; (c)

5-FU; (d) CAg; (e) CAg-FC; (f) CAg-FU was poured on separate wells. The plates were incubated at 37°C overnight to observe various levels of inhibition zone, and the zone's diameter was measured. The experiments were carried out in triplicates.

3.2.9. UV-Visible spectroscopy

The formation of silver nanoparticles, drug loading efficiency, and drug release percentage was determined by UV-Visible spectroscopy at room temperature using Agilent Carry 100 UV-Visible spectrophotometer

3.2.10. FTIR spectroscopy

The FTIR spectra of LMWC and drug loaded nanoparticles were recorded on Perkin Elmer Spectrum 2 FTIR spectrometer at room temperature using KBr pellet, over a frequency range of 4000-400 cm^{-1}.

3.2.11. FESEM-EDX

The elemental mapping to check the fluorine of 5-FU and 5-FC in the nanoparticle was done by Zeiss Sigma Field Emission Scanning Electron Microscope by EDX Analysis. 5-FU and 5-FC loaded nanoparticles were spread on carbon film for the analysis.

3.2.12. FETEM

The particle size of the drug loaded silver nanoparticles was determined by Jeol 2100F Field Emission Transmission Electron Microscope. For the analysis, a droplet of the nanoparticle suspensions was cast on a copper grid without being stained. The excess liquid was removed by touching the edge of the copper grid with a small piece of filter paper and further dried overnight in a desiccator.

3.2.13. Dynamic Light Scattering (DLS)

DLS studies were conducted to determine the hydrodynamic diameter of the nanoparticles using a Malvern Zetasizer Nano Series at 25±0.1°C. Diluted nanoparticle suspension was used for the analysis.

3.3. Results and Discussions

3.3.1. Synthesis of CAg-FU and CAg-FC

A green synthesis protocol was adopted to synthesize drug loaded chitosan stabilized silver nanoparticles: CAg-FU and CAg-FC, without using any toxic reducing and stabilizing agents. Low molecular weight chitosan stabilizes the nanoparticles and acts as a platform for loading the antitumor drug 5-FU and the prodrug 5-FC, respectively. Chitosan contains free -NH_2 and –OH functional groups, which may act as chelating sites and form weak, non-covalent interactions with the hydrophilic drugs [96]. The formation of the nanoparticle is confirmed by a change in color of the solution from colorless to dark brown. For comparative study, chitosan-silver nanoparticles (CAg) without any loaded drug, was also synthesized. Our objective in this study is to develop a nanomaterial prodrug, which in combination with an external enzyme, could be used for effective delivery of the active therapeutic molecule.

3.3.2. Mechanism of action of CAg-FU and CAg-FC in cancer cell death

It is well known that 5-FU promptly kills the tumor cells while 5-FC is mostly non-toxic to the mammalian cells. Only on activation by non-mammalian enzyme CD, 5-FC is hydrolyzed to 5-FU, thereby killing the cells. Thus, 5-FC loaded CAg can be used as a prodrug and consequently acting as an enzyme-mediated drug delivery system. The mechanism of action of CAg-FU and CAg-FC in cancer cell death is demonstrated in **Figure 3.1**.

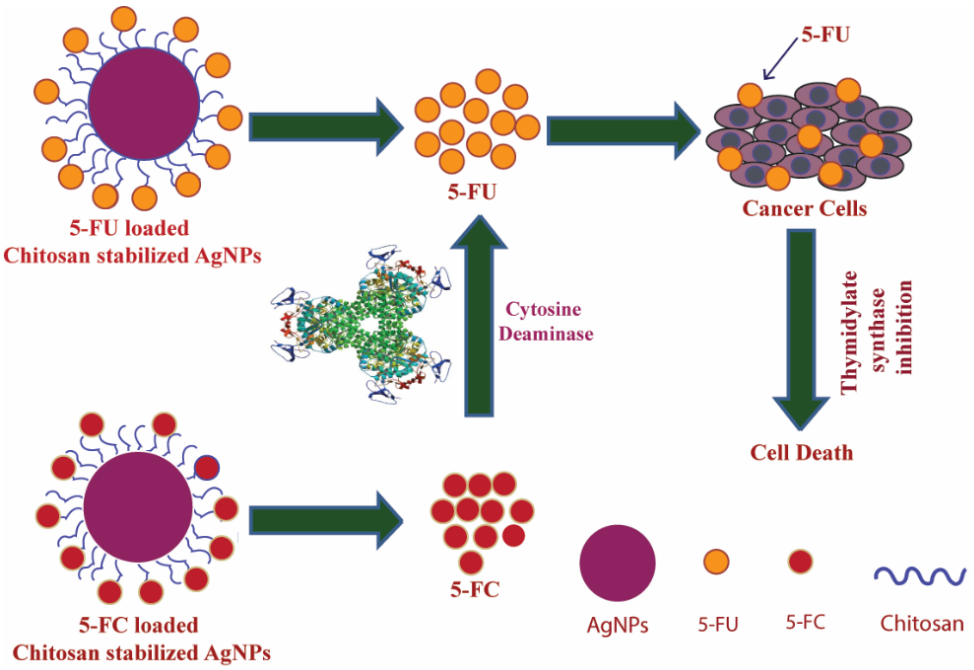

Figure 3.1 Mechanism of action of CAg-FU and CAg-FC in cancer cell death**.**

3.3.3. Determination of formation of silver nanoparticles

The formation of AgNps was investigated by the change in color of the reaction solution and UV-Visible spectroscopy. The size of the nanoparticles was determined by FETEM analysis and DLS study.

(A) Color change and UV-Visible spectroscopy

As the reaction proceeds and the silver nanoparticles start forming, the color of the reaction solution starts changing from colorless to light yellow, followed by dark brown. **Figure 3.2 (A)** and **(B)** show the color change in CAg-FU and CAg-FC, respectively.

The formation was further confirmed by monitoring through UV-Visible spectroscopy. AgNps exhibit an intense absorption peak between 400-430 nm due to surface plasmon resonance (SPR)[229]. At a different interval of time, 1h, 3h, and 6h, 500 µL of the reaction mixture were taken out and analyzed. **Figure 3.2 (C)** and **(D)** show the UV-Visible absorption spectra of CAg-FU and CAg-FC, respectively, which shows that with an increase in reaction time, there is a gradual increase in absorbance of both CAg-FU and CAg-FC, indicating the formation of the AgNps with time.

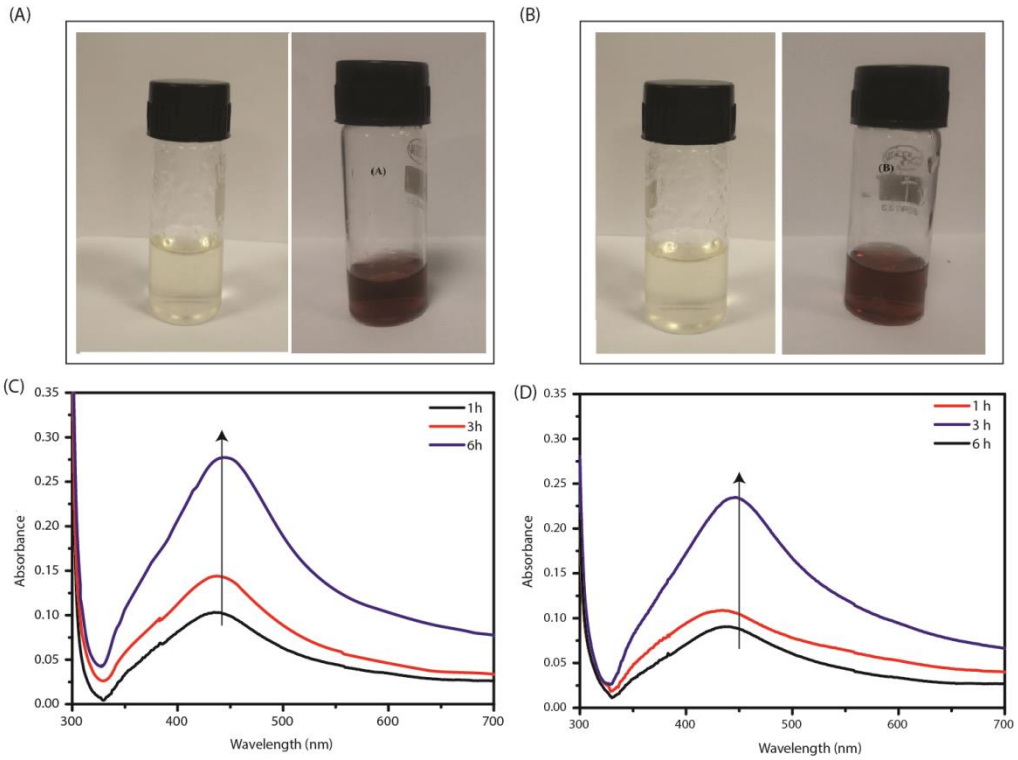

Figure 3.2 Image showing the formation of silver nanoparticles from colorless solution to dark brown in **(A)** CAg-FU and **(B)** CAg-FC; UV-Visible Spectroscopic time-dependent plot of **(C)** CAg-FU and **(D)** CAg-FC showing an increase in the peak of silver nanoparticles with time.

(B) Size determination by FETEM analysis

The size of the drug loaded AgNps was estimated from FETEM images. It can be evident from the micrographs in **Figure 3.3 (A)-(D)** and image J size distribution plot in **Figure 3.3 (E)** and **(F)** that the synthesized CAg-FU nanoparticles were of size 5-25 nm and CAg-FC were of size 5-15 nm and nearly quasi-spherical in shape. It is widely believed that nanoparticles with a size of less than 100 nm are capable of penetrating cell membranes. Hence, the synthesized nanoparticles carrying 5-FU or 5-FC are expected to penetrate the affected cells and effectively release the drugs.

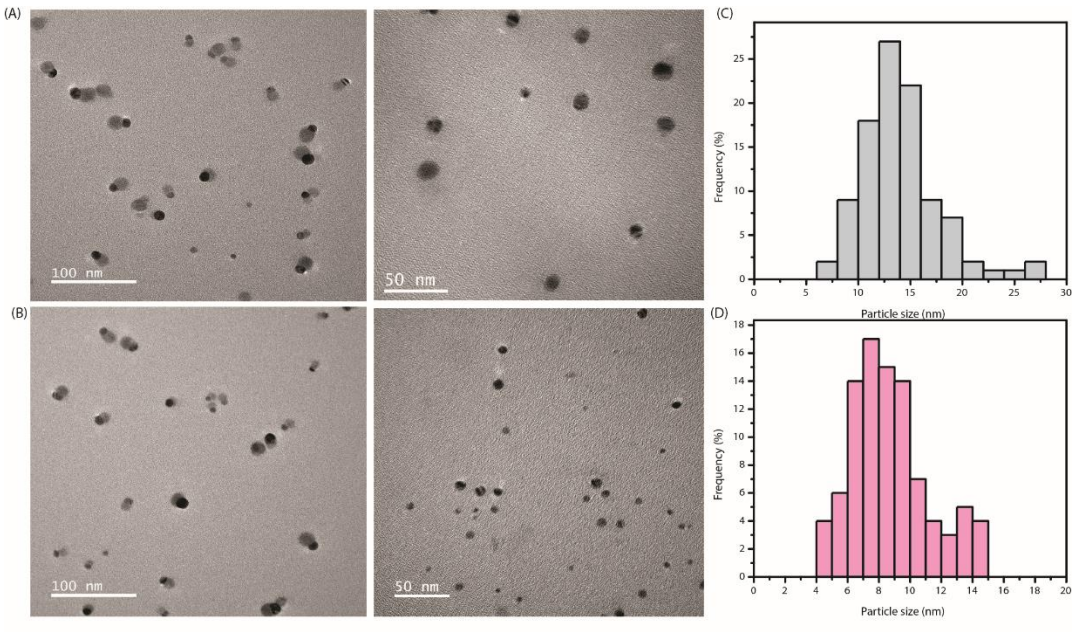

Figure 3.3 FETEM micrographs of **(A)** CAg-FU (scale: left 100 nm and right 50 nm) and (**B**) CAg-FU (scale: left 100 nm and right 50 nm); Image J size distribution histogram of **(C)** CAg-FU and **(D)** CAg-FC.

(C) Size determination by DLS studies

DLS studies of CAg, CAg-FU, and CAg-FC were performed using dilute aqueous nanoparticle suspensions. **Figure 3.4** shows the DLS spectrum of the synthesized nanoparticles. The hydrodynamic diameter of CAg, CAg-FU, and CAg-FC nanoparticles were found to be 185±20 nm, 213±13 nm, and 220±15 nm, respectively. The massive difference in the particle size in FETEM and DLS is due to the presence of the chitosan capping on the nanoparticle surface, which increases the hydrodynamic diameter of the nanoparticle [241]. The respective PDI was calculated to be 0.395, 0.363, and 0.374.

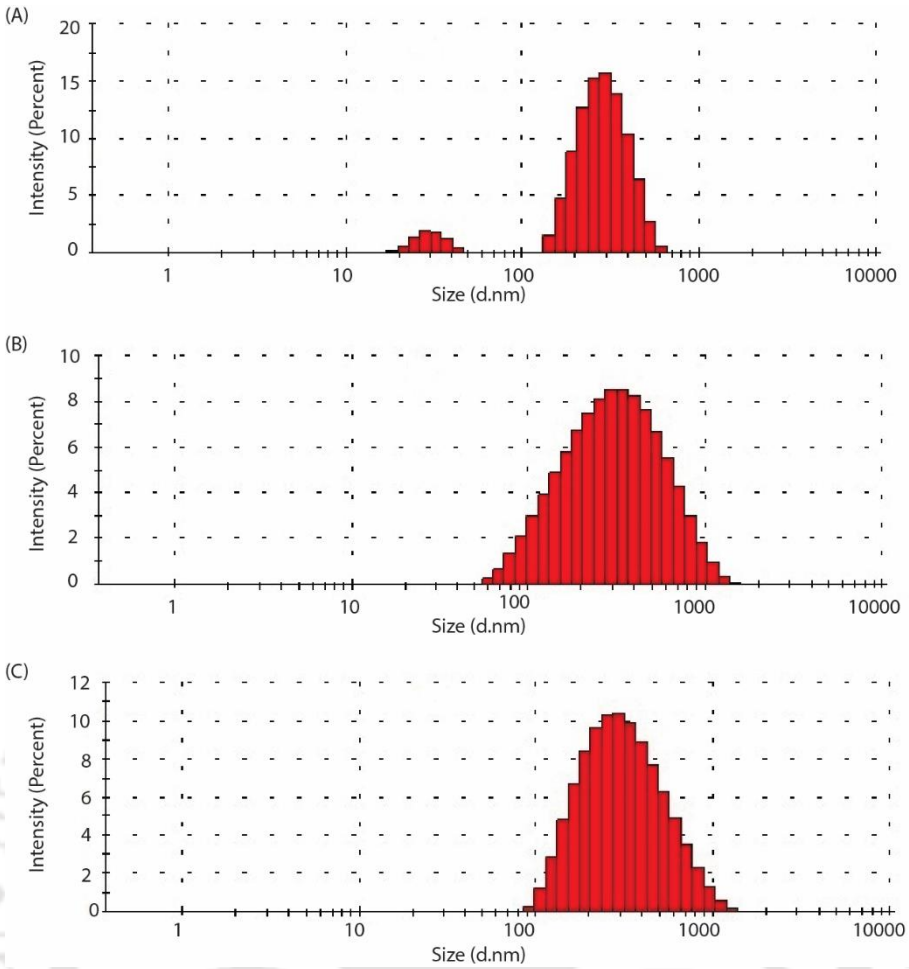

Figure 3.4 Dynamic light scattering data of **(A)** CAg; **(B)** CAg-FU; **(C)** CAg-FC

3.3.4. Determination of drug loading on silver nanoparticles

The loading of the drugs on the silver nanoparticles was analyzed by UV-VIS spectroscopy, FTIR spectroscopy, and EDX.

(F) UV-Visible Spectroscopic study

The loading of the drug was also determined using UV-Visible spectroscopy**.** CAg-FU and CAg-FC nanoparticle pellets were dispersed in water by sonication and measured. **Figure 3.5 (A)** and (**B)** show the absorption spectra of CAg-FU and CAg-FC, respectively. In **Figure 3.5 (A)**, the peak at 266 nm is the characteristic peak of 5-FU [242], and in **Figure 3.5 (B)**, the peak at 276 nm is the characteristic peak of 5-FC [243]. Therefore, the presence of the characteristic

peaks of AgNps, as well as the 5-FU and 5-FC, prove the successful loading of the drugs on the nanoparticles.

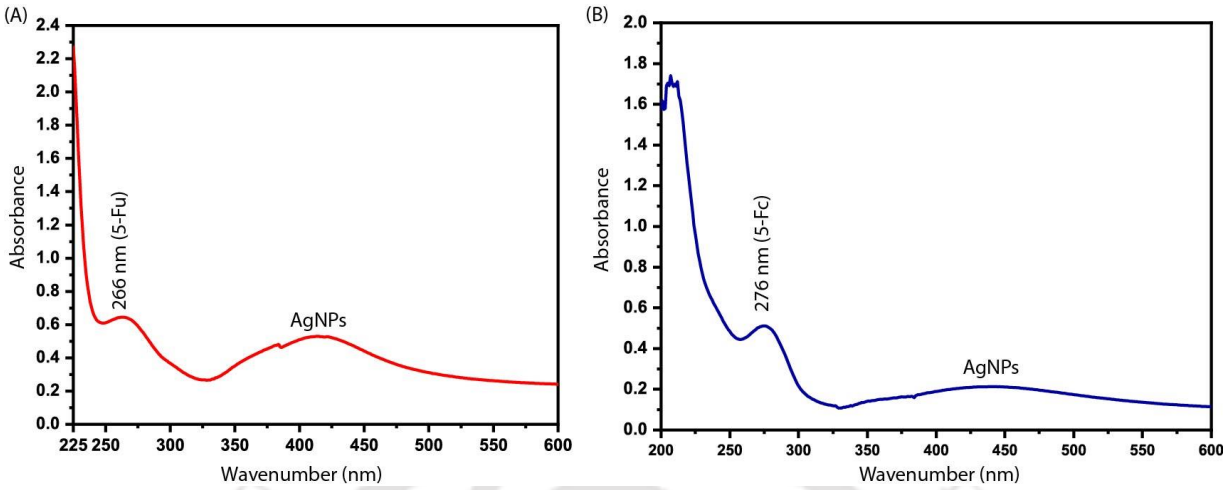

Figure 3.5 UV-Visible absorption spectra of **(A)** CAg-FU, showing a peak at 266 nm, characteristic peak of 5-FU and 420 nm, characteristic peak of AgNPs; **(B)** CAg-FC, showing a peak at 276 nm, characteristic peak of 5-FC and 420 nm, characteristic peak of AgNPs

(G)FTIR spectroscopic study

The loading of the drug was further supported by FTIR spectroscopy. The FTIR spectra of CAg-FU, CAg-FC, and LMWC are shown in **Figure 3.6 (A), (B), and (C),** respectively. Spectra of the drug loaded nanoparticles resemble well with the pure LMWC spectrum apart from minor deviations, which shows the presence of the drug in the nanoparticles. The FTIR spectrum of LMWC shows a peak at 3370 cm^{-1}, which corresponds to the stretching vibration of N-H and O-H bonds, a peak at 2920 to 2866 cm^{-1} corresponds to the C-H stretching vibrations and the bands at 1651 cm^{-1} and 1590 cm^{-1} corresponds to the amide I and amide II vibrations, respectively. The other bands in the range 1000–1155 cm^{-1} are due to chitosan's saccharide structure and the C-O and C-O-C stretching vibrations of the glycosidic bonds [215]. FTIR spectra of CAg-FU shown in **Figure 3.6 (B)** displays a sharp peak at 1656 $cm^{-1,}$ which is due to the C=O stretching vibration, and a peak at 1254 cm^{-1} is due to C-F stretching vibration of 5-FU. Similarly, the FTIR spectra of CAg-FC in **Figure 3.6 (A)** shows an additional sharp peak at 1651 cm^{-1} due to C=O stretching vibration and peak at 1277 cm^{-1}

due to C-F stretching vibration of 5-FC. Thus, from the FTIR studies, it can be seen that **Figure 3.6 (A)** and **Figure 3.6 (B)** consists of characteristic peaks of chitosan along with the respective drugs, confirming the successful loading of the drugs to the chitosan stabilized nanoparticles[244].

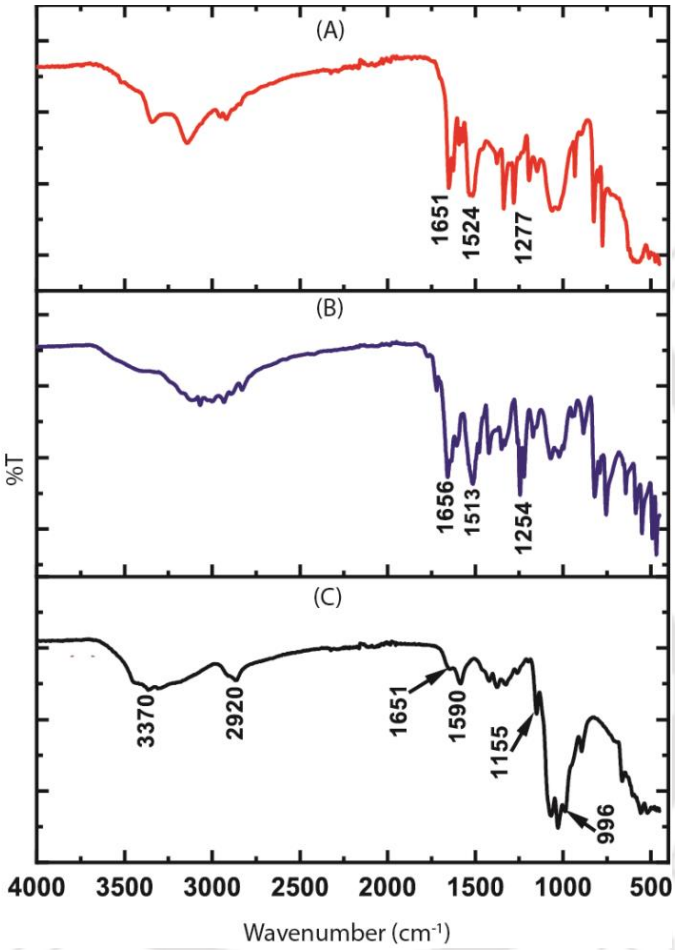

Figure 3.6 Stacked FTIR spectra of **(A)** CAg-FC; **(B)** CAg-FU; **(C)** LMWC using KBr pellet.

(H)FESEM-EDX

The loading of the drugs is further supported FESEM-EDX. The elemental mapping of CAg-FU and CAg-FC was performed by FESEM to examine the presence of silver (Ag) and fluorine (F) in the drug loaded CAg. Powdered samples were spread on carbon film for analysis. The EDX of CAg-FU, as shown in **Figure 3.7 (A)**, shows large peaks of carbon (C),

oxygen (O), and a small quantity of nitrogen (N), which are the fundamental element of chitosan, along with 6.4 % of fluorine and 1.5 % of silver. The EDX, therefore, further confirms the loading of 5-FU in AgNps. Similarly, the EDX analysis of CAg-FC, as shown in **Figure 3.7 (B)**, also reveals large peaks for chitosan along with 7.8 % of fluorine and 1 % of silver, indicating the presence of silver and 5-FC in the nanoparticles.

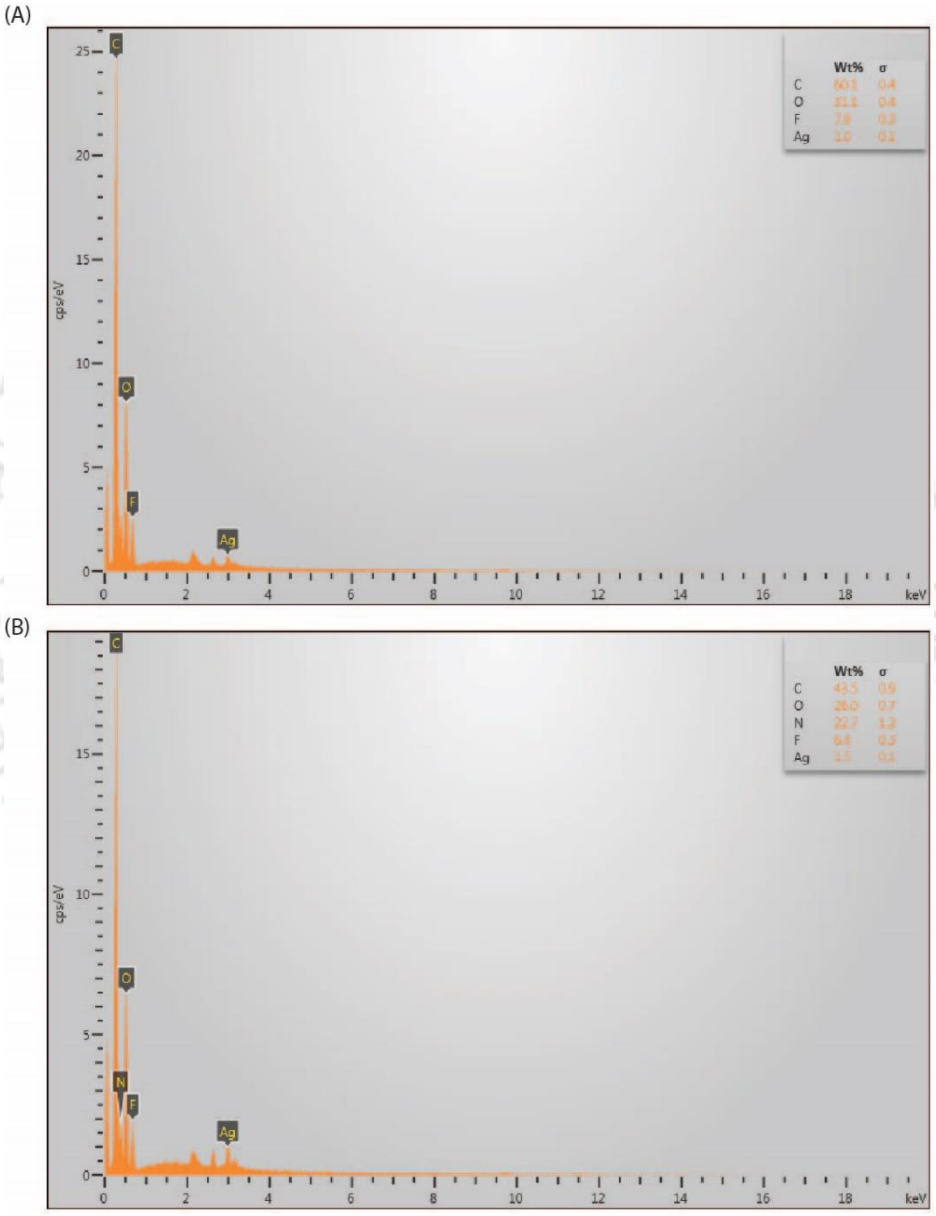

Figure 3.7 FESEM-EDX spectra of **(A)** CAg-FU showing 1.5 wt % Ag and 6.4 wt % F; **(B)** CAg-FC showing 1 wt % Ag and 7.8 wt % F.

3.3.5. Drug loading efficiency

The drug loading efficiency was calculated to be 96% for CAg-FU and 97% for CAg-FC nanoparticles. The following equation was used to calculate the drug loading efficiency.

$$\textbf{\textit{Loading efficiency}}\ (\%) = \frac{\textbf{\textit{drug loaded}}}{\textbf{\textit{drug initially fed}}} \times \mathbf{100}$$

3.3.6. *In vitro* drug release study

The *in vitro* release curve of 5-FU and 5-FC from CAg-FU and CAg-FC are shown in **Figure 3.8 (A) and (B).** The equation used for calculation is as follows:

$$\textbf{\textit{Perecentage of Drug release}} = \frac{\textbf{\textit{Amount of drug released at time 't'}}}{\textbf{\textit{Total drug content}}} \times \mathbf{100}\%$$

The release from both the nanoparticles was done in triplicates, and the error was estimated from the standard deviation using origin. Uniform release of drug from both the nanoparticles can be seen. The percentage drug release in CAg-FU and CAg-FC was found to be 78% and 79% respectively after 62 h.

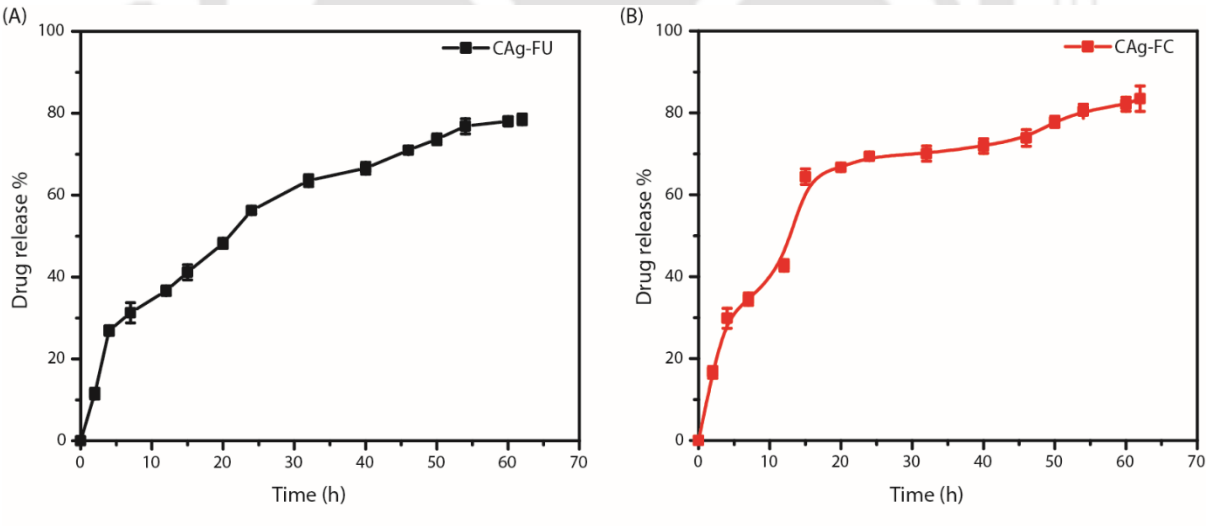

Figure 3.8 The drug release percentage of **(A)** 5-FU from CAg-FU; **(B)** 5-FC from CAg-FC in PBS buffer of pH 7.4 using dialysis membrane of MW cutoff 13 kDa upto 62 h.

3.3.7. Cytosine deaminase activity test

Berthelot assay was performed on CAg, 5-FU deloaded from CAg-FU, 5-FC deloaded from CAg-FC, and commercially available pure 5-FC. The kinetics of CD activity on 5-FC has been reported.[245,246] To confirm whether the drug is accessible after it is released from nanoparticles and to comprehend the efficiency of release, a comparative activity-analysis was performed before and after deloading of 5-FC. The amount of ammonia released from commercially available 5-FC is taken as 100% and compared with the amount of ammonia released from CAg-FC. The activity graphs in **Figure 3.9** indicate that 5-FC present in CAg-FC nanoparticles is released with more than 96% efficiency. No deamination activity was observed with CAg as well as with deloaded 5-FU from CAg-FU. The absence of deaminase activity in blank nanoparticles and 5-FU ensures that the activity seen in deloaded 5-FC is upon deamination brought about by CD. This comparative study shows that the loading of 5-FC on nanoparticles has not affected the specificity of the enzyme.

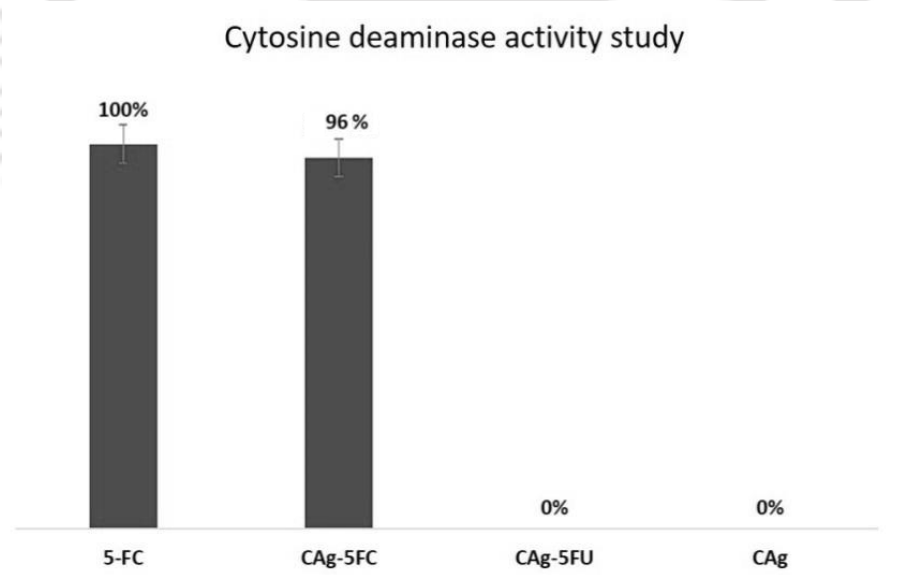

Figure 3.9 Comparative study of CD activity test showing 96% activity from deloaded 5-FC from CAg-FC as compared against 100% activity by commercial 5-FC. No activity was observed from CAg-FU and CAg.

3.3.8. Cell viability assay

In order to examine the versatility of the CAg-FC nanoparticles as a prodrug, we have tested the cell viability of the human breast carcinoma cell line MDA-MB-468 after the treatment of cells with different concentrations of CAg, CAg-FU, and CAg-FC, as shown in **Figure 3.10**. The percentage of cell viability was calculated compared to the untreated cells. Maximum cytotoxicity was observed on the treatment of the cell with CAg-FU with an estimated half-maximal inhibitory concentration (IC_{50}) of 21.60 µg/ml. Blank AgNps showed cytotoxicity with an IC_{50} value of 130µg/ml, which showed the anticancer property of AgNps. CAg-FC showed the minimum cytotoxicity, thus showing the low cytotoxic nature of 5-FC.

It was seen that CAg-FC showed even lower cytotoxicity as compared to the blank AgNps. As been reported[247], pure 5-FC is inert to the MDA-MB-468 cell lines. Upon loading, it covers the surface of the AgNps and blocks its activity also, which is also evident from the elemental analysis (EDX) data, which shows lower silver content compared to the fluorine of the drugs. Thus, it is evident that the CAg-FC having low cytotoxicity can be used as a prodrug, which on activation generates 5-FU, which can be used as an active anticancer agent. The error was estimated from the standard deviation of all the experiments done in triplicates.

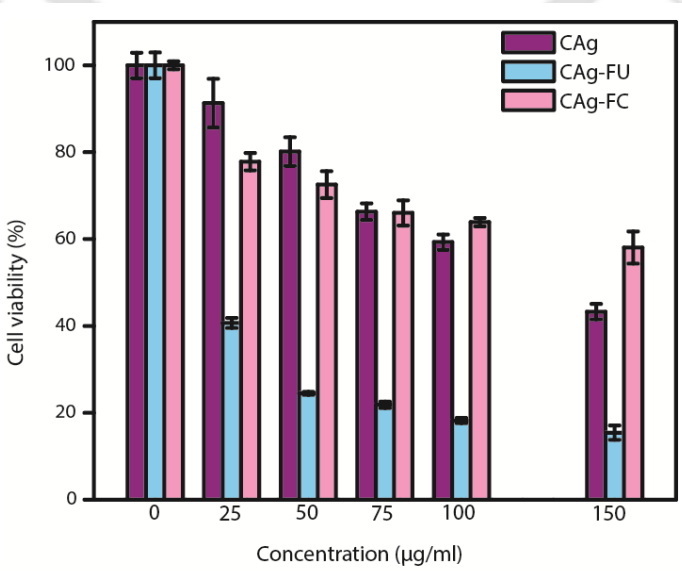

Figure 3.10 Concentration-dependent cytotoxicity of CAg, CAg-FU, and CAg-FC to human breast carcinoma cell line MDA-MB-468 at a compound concentrations range of 25 µg/ml to 150 µg/ml.

3.3.9. Antibacterial activity study

The antibacterial activity of the compounds was tested using *E. coli* strain. The antimicrobial activity test of CAg-FC and CAg-FU showed in **Figure 3.11 (E)** and **(F)** were compared with LMWC, 5-FC, 5-FU, and CAg as in **Figure 3.11 (A)**, **(B)**, **(C),** and **(D)** respectively. The tests showed that the maximum zone of inhibition was obtained for CAg-FU followed by CAg-FC, compared to pure drugs, chitosan, and silver nanoparticles. Thus, the antimicrobial activity of silver nanoparticles has been enhanced by the addition of the drugs.

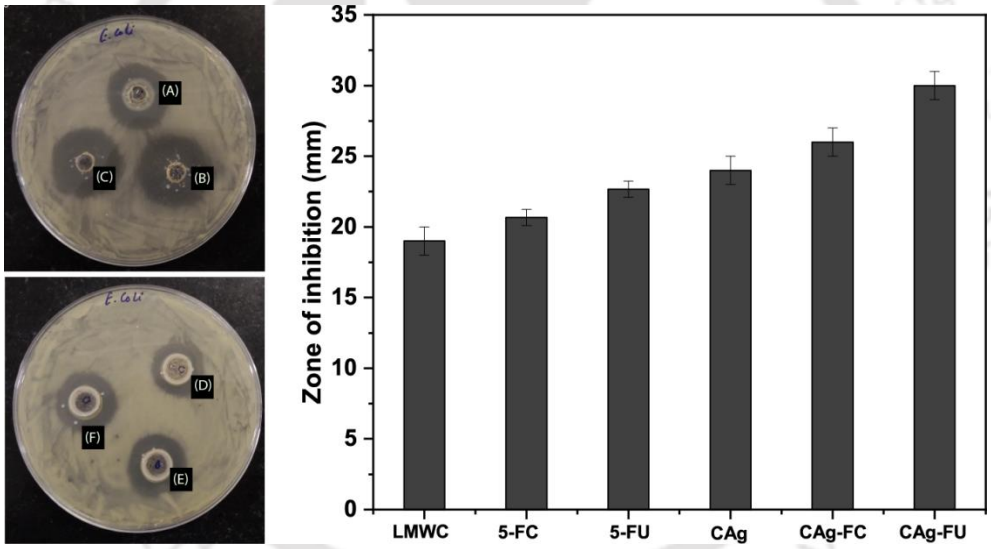

Figure 3.11 Antimicrobial activity test (by well diffusion method) against *E. coli* and plot of the zone of inhibition of **(A)** LMWC; **(B)** 5-FC; **(C)** 5-FU; **(D)** CAg; **(E)** CAg-FC; **(F)** CAg-FU.

3.4. Conclusions

CD is a class of protein that catalyzes the deamination of nucleobase cytosine into uracil. CD, isolated and overexpressed in *E. coli*, is also known to transform 5-FC into 5-FU, the active chemotherapeutic molecule. In the present study, a combination of CD and 5-FC loaded

nanoparticle-prodrug is proposed as a therapeutic tool for improved antitumor activity. We have synthesized 5-FC and 5-FU loaded chitosan-silver nanoparticles in an environmentally benign, green chemistry method without the use of additional reducing and stabilizing agents. Cell viability assay of CAg-FC, performed in human breast carcinoma cell line MDA-MB-468, resulted in negligible cytotoxicity in cells, signifying the prodrug nature of CAg-FC nanoparticles. The activity study with CD confirmed high substrate specificity towards 5-FC in CAg-FC and was found to hydrolyze 5-FC into the active molecule 5-FU.

3.5. Individual FTIR spectra

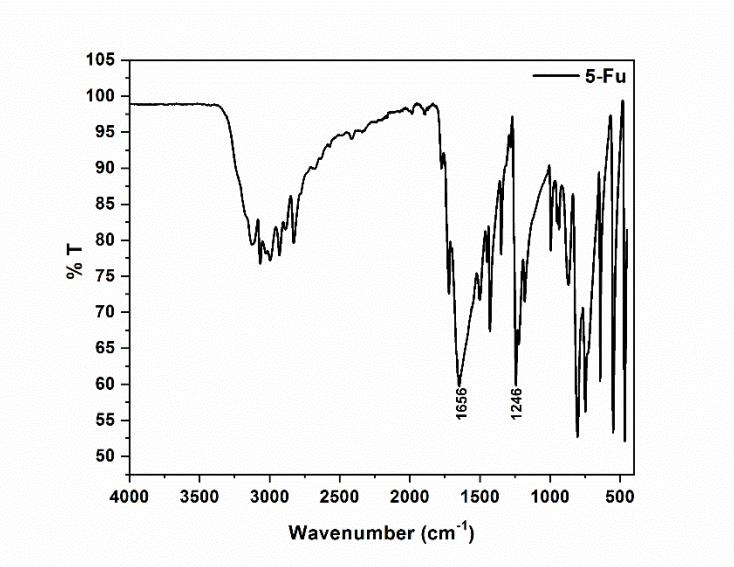

Figure 3.12 FTIR spectra of 5-FU.

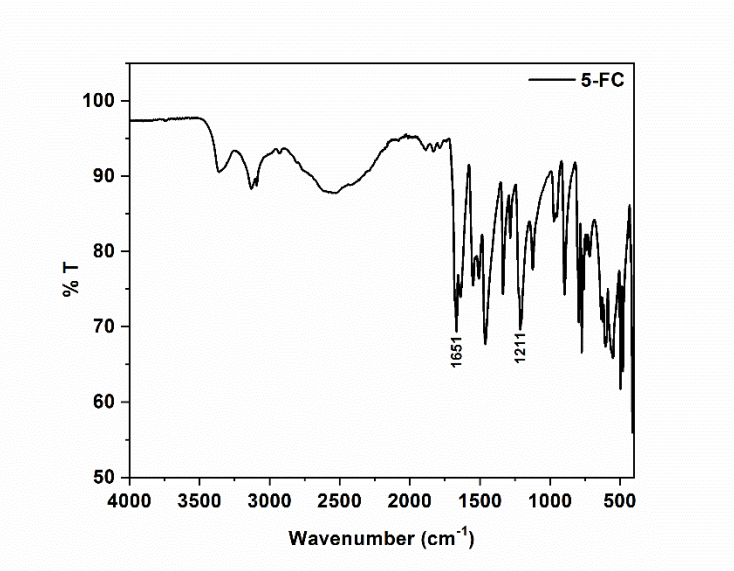

Figure 3.13 FTIR spectra of 5-FC.

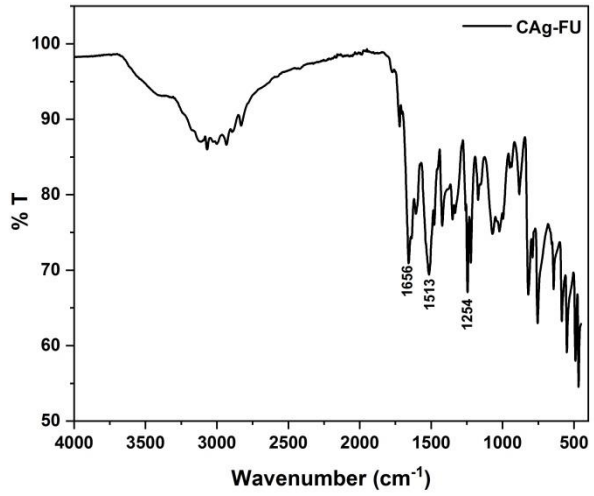

Figure 3.14 FTIR spectra of CAg-FU.

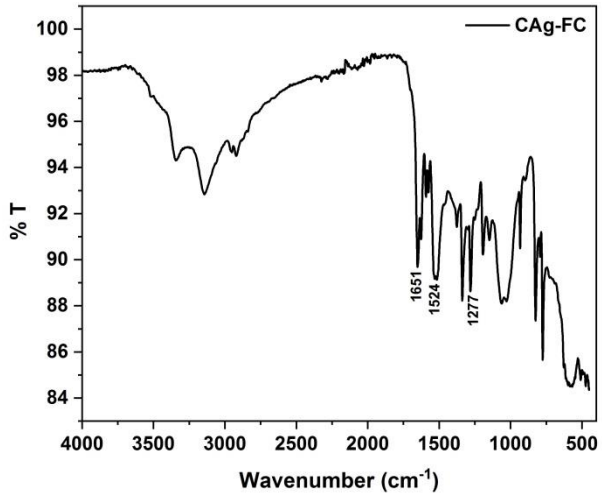

Figure 3.15 FTIR spectra of CAg-FC.

3.6. UV-Visible Spectroscopic data of pure drugs.

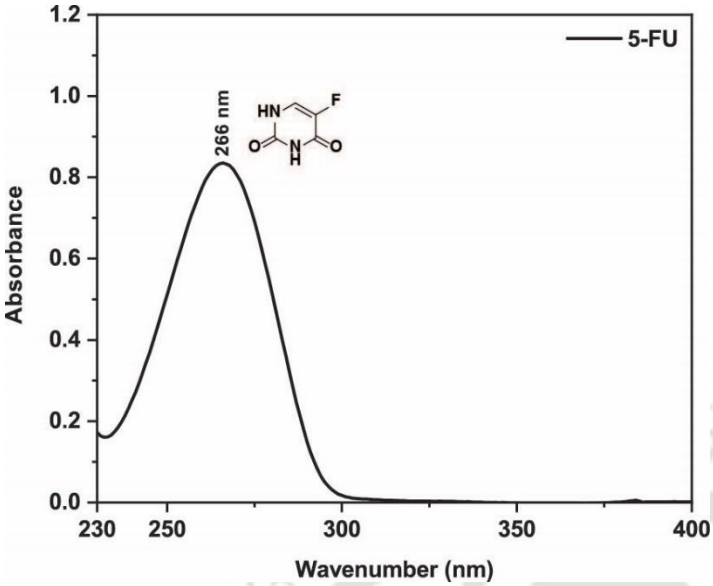

Figure 3.16 UV-Visible Spectra of 5-FU.

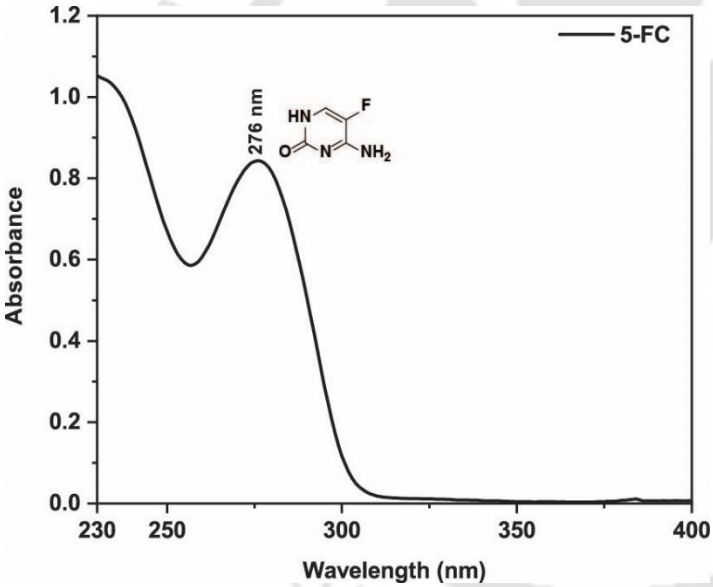

Figure 3.17 UV-Visible Spectra of 5-FC.

3.7. Gel elecrophoresis.

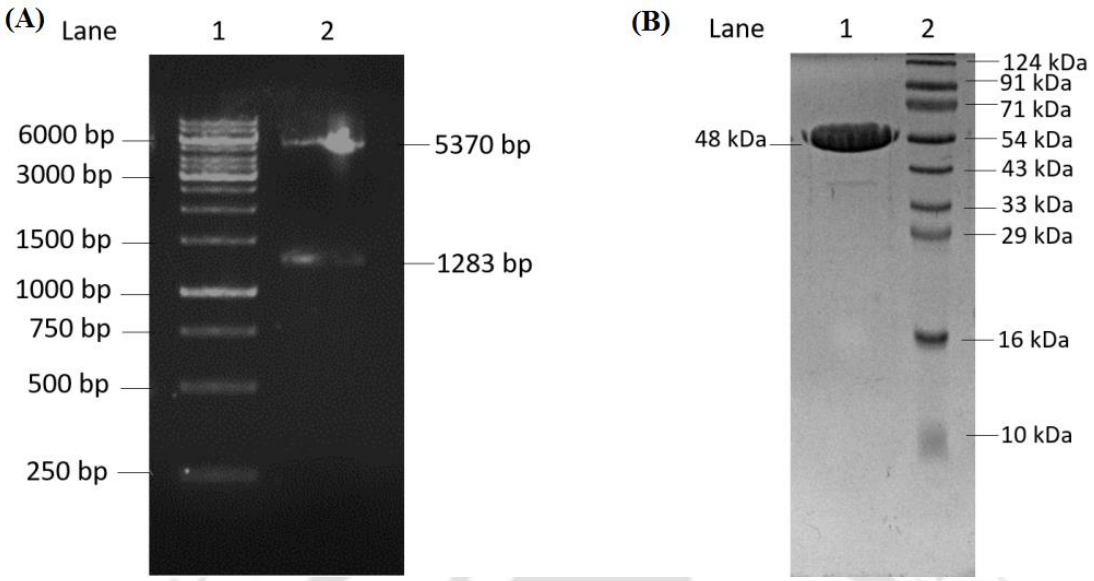

Figure 3.18 (A) 0.8% agarose gel of double restriction digestion of ECD in pET vector. Lane 1 is ladder, and lane 2 is ECD gene at 1283bp and pET vector at 5370bp; **(B)** 15% SDS gel of purified ECD. Lane 1 is ECD protein with a molecular weight of 48kDa, and lane 2 is molecular weight marker.

Chapter 4 Synthesis of folate functionalized silk fibroin coated chitosan/gold nanoparticles for targeted delivery of doxorubicin

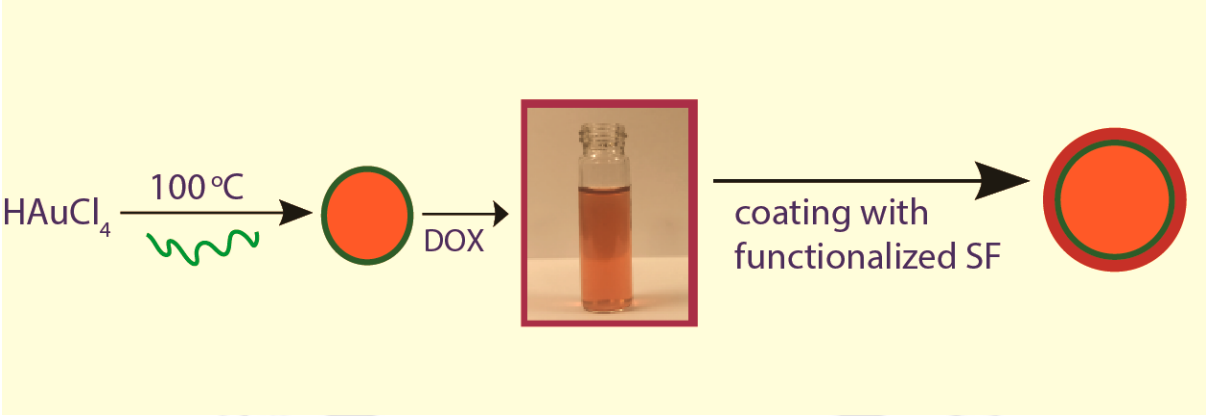

4.1. Overview

Gold nanoparticles have proved to be an effective cancer drug delivery tool because of its highly significant properties likes inertness; non-toxicity[248]; easy synthesis protocols of mono-disperse particles below 100 nm; ability to alter light/radio frequency into heat, enabling thermal ablation of the targeted cancer cells and ability to get easily functionalized, mostly by thiol chemistry[96,249,250]. Green synthesis of gold nanoparticles using chitosan has been reported[26,47,49,118,248], where chitosan acts as both a reducing and a stabilizing agent. Chitosan consists of free hydroxyl groups that form a complex with the metal ions, thus aids in the shape and size control of the nanoparticles and also reduces its toxicity towards mammalian cells[186].

The development of a biocompatible and simple coating to increase the stability, strength and provide a matrix to impart functionalization to the coated materials can be a significant approach for targeted and sustained drug release. SF has been a versatile biocompatible coating material known to impart mechanical stability and provide a diffusion barrier to the encapsulated drugs, which prevent premature drug leakage and enable sustained and long-term drug release, thus increasing bioavailability and decreasing dose frequency. It also provides sites for easy functionalization, which can be used for the attachment of drug targeting moieties. It has been reported that drug release has been significantly retarded upon SF coating. Moreover, it can be easily formulated due to its aqueous processibility and offers the ability to control the thickness of coating[60,193–195,251].

Here, we have synthesized gold nanoparticles using low molecular weight chitosan, loaded with a model chemotherapeutic drug, doxorubicin. Then we have coated the nanoparticles with folic acid and fluorescein conjugated SF. The SF was used as a matrix for providing necessary functional groups for covalent attachment of the FA and FL and also provides a diffusion barrier that can promote the slow and sustained release of the drug. FA has been

used as a cancer-targeting ligand as it binds with the folate receptors, which is mostly overexpressed in cancer cells, thus delivering the drug into the cancer cells [33,89,118,252]. Fluorescein can be utilized for cell imaging purposes if non-fluorescent drugs are used.

4.2. Experimental Procedures

4.2.1. Materials

LMWC (Mv =129 kDa; 94% deacetylation) and FL was purchased from Sigma Aldrich. DOX was purchased from Tokyo Chemical Industry (TCI). Gold chloride, lithium bromide, and EDC were procured from Spectrochem. Glacial acetic acid, sodium carbonate, and ethylenediamine were purchased from Merck (India). FA and NHS were purchased from Alfa Aesar. *Bombyx mori* silk cocoons were acquired from local silk farms, Assam, India.

4.2.2. Synthesis of doxorubicin-loaded LMWC stabilized gold nanoparticles (CAu-DOX)

LMWC (2 wt%) was dissolved in 30 ml of 1% aqueous acetic acid solution and was stirred overnight until a clear solution was obtained. It was then filtered using a 0.45-micron syringe filter, and 30 µl of 125 mM $HAuCl_4$ was added to it in a dropwise manner under continuous stirring. After 45 min of reaction at 100°C, a blushing red-colored solution was observed, which indicated the formation of gold nanoparticles. After cooling, DOX (0.005 w/v %) was added into the nanoparticle solution and stirred for 30 min, followed by incubation at 37°C for 12 h.

4.2.3. Extraction of silk fibroin

The extraction of SF was done using a reported procedure [253]. Briefly, dried *bombyx mori* silk cocoons were cut into small fragments, and the dead pupae were discarded. 5 g of cocoon fragments were boiled in 1000 ml of 0.02 M sodium carbonate solution for 1 h to remove the sericin. The gummy sericin part was discarded, and the degummed silk fibers were repeatedly

washed with deionized water and dried at room temperature overnight. The dried silk fibers were melted in 9.3 M LiBr solution (2.5 g fibers/10 ml) at 70°C for 4 h. The SF-LiBr solution was dialyzed for 3 days by changing the water every 6 h. The solution was then centrifuged at 9000 rpm for 20 min at 4°C. The concentrated silk solution was stored at -20°C. To check the amount of dry SF/ml of solution, a known amount of SF solution was dried and weighed.

4.2.4. Preparation of folate and fluorescein functionalized silk fibroin (SF-FA-FL)

2 ml of silk fibroin solution was dropwise added to 47 ml water at 4°C with mild stirring. The carboxyl groups of SF were activated using EDC (25 mg) and NHS (25 mg) at pH 6 under continuous stirring for 3 h in the dark. 1 ml of ethylenediamine was added dropwise into the solution and reacted for 12 h at room temperature. The reaction mixture was dialyzed against deionized water for 2 days. 40 mg of FA was dissolved in 40 ml DMSO/H_2O (1:1) mixture and activated using EDC (26 mg) and NHS (15 mg) under continuous stirring for 3 h in the dark. At the same time, FL dissolved in 20 ml PBS pH 6 was also activated using EDC (19 mg) and NHS (15 mg) for 3 h in the dark. The activated FA and FL was dropwise added to the ethylenediamine-SF conjugate and reacted for 24 h in the dark and then dialyzed against deionized water for 2 days. The dialyzed solution was stored at 4°C.

4.2.5. Coating of nanoparticles (SF-FA-FL coated CAu-DOX)

The prepared nanoparticles were dialyzed against distilled water using a dialysis membrane (MW cutoff 1kDa) for 48 h to separate the unloaded DOX from the solution. Then it was mixed with SF-FA-FL solution (2:1) for10 min with mild stirring. It was then lyophilized to collect the dried coated nanoparticles.

4.2.6. Drug loading efficiency

The drug loading efficiency on the nanoparticles was determined before coating by measuring the drug concentration in the nanoparticle solution before and after dialysis. The

UV-Visible absorbance of the drug loaded nanoparticle was determined at a wavelength of 480 nm, and then the solution was dialyzed against distilled water for 48 h for removing the unbound drug from the solution. The absorbance was again analyzed. Using the calibration curve of DOX, the amount of drugs before and after dialysis was obtained.

4.2.7. *In vitro* drug release study

For the *in vitro* drug release study, the uncoated as well as coated nanoparticles were dried using the freeze-drying technique. The lyophilized nanoparticles were then suspended in PBS buffer of pH 7.4 and kept inside a dialysis membrane of molecular weight cutoff 1 kDa. The membranes were dipped inside 15 ml of water at room temperature. After equal intervals of time, 500 µL aliquots of the samples were taken out from the water outside the membrane and replaced with the same quantity of fresh buffer. The collected samples were analyzed spectrophotometrically at 480 nm for the released drug concentration with time. All the reactions were performed in triplicates, and the error was determined from the standard deviation using the Origin software version 2020.

4.2.8. Cell lines and cell culture conditions

Human cervical cancer cells (HeLa) were procured from National Centre for Cell Science, Pune, India. The cells were maintained in DMEM medium containing 10% (v/v) FBS and 1% penicillin-streptomycin and incubated at CO_2 incubator in a humidified atmosphere at 37°C having 5% CO_2.

4.2.9. MTT assay for Cytotoxicity determination

The effect of the synthesized nanoparticles on cancer cells was assessed by MTT assay. HeLa cells were seeded at a density of 5×10^3 cells/well, in triplicates on a 96-well tissue culture plate. The cells were incubated in the CO_2 incubator overnight for attachment. Subsequently, the cells were treated with increasing concentrations of the synthesized nanoparticles. For the

cytotoxicity study, cells were treated with four treatment groups, which are as follows: blank gold nanoparticles (CAu), pure DOX, CAu-DOX and SF-FA-FL coated CAu-DOX. After 48 h treatment, the treatment media was removed and 0.5 mg/ml MTT solution dissolved in PBS (phosphate buffer saline) was added to the cells followed by 2 h incubation. Next, DMSO was added, and absorbance at 570 nm was recorded using Tecan multiplate reader having a reference of 630 nm.

4.2.10. Confocal imaging to study the uptake

Cell imaging was performed to study the uptake efficiency of the synthesized nanoparticles. 1 x 10^5 cells were seeded in glass-bottomed live-cell imaging plates and incubated for 12 h for attachment. Subsequently, cells were treated with 1.5 µM of CAu-DOX, and SF-FA-FL coated CAu-DOX each for 2 h. For the visualization of the nucleus, the cells were counterstained with Hoechst stain. After that, the cells were washed gently with PBS, and colorless DMEM media was added for confocal visualization. The plates were visualized under a confocal microscope (LSM 880) at an excitation wavelength of 480 nm and emission of 590 nm.

4.2.11. UV-Visible spectroscopy

The formation of nanoparticles, drug loading efficiency, and drug release percentage was determined by UV-Visible spectroscopy at room temperature using Agilent Carry 100 UV-Visible spectrophotometer.

4.2.12. FTIR spectroscopy

The FTIR spectra of the dried SF, FA, FL, and SF-FA-FL were recorded on Perkin Elmer Spectrum 2 FTIR spectrometer at room temperature using KBr pellet, over a frequency range of 4000-400 cm^{-1}.

4.2.13. FETEM analysis

The size of the uncoated and coated nanoparticles was determined by Jeol 2100F Field Emission Transmission Electron Microscope. For FETEM analysis, a droplet of the gold nanoparticle suspension was cast on a copper grid without being stained. The excess liquid was removed with a piece of filter paper and further dried overnight in a desiccator

4.2.14. Dynamic Light Scattering (DLS)

Zeta potential of the blank gold nanoparticles and drug loaded nanoparticles was measured using Anton Paar Litezetasizer 500 at 25±0.1°C. Diluted nanoparticle suspension was used for the analysis.

4.3. Results and Discussions

4.3.1. Synthesis of LMWC stabilized gold nanoparticles and doxorubicin loading.

Gold nanoparticles were synthesized using a green synthesis protocol using LMWC as both the reducing as well as the stabilizing agent, without adding any other toxic reagents. The formation of the nanoparticles was indicated by a change in color of the solution from colorless to light pink and finally into a blushing red color solution. The model anti-cancer drug, DOX, was loaded into the nanoparticles, where LMWC acts as a platform for loading the drug. LMWC contains free -NH_2 and -OH functional groups, which may serve as chelating sites and form weak, non-covalent interactions with the hydrophilic drugs[96].

4.3.2. Synthesis of coating material and coating of nanoparticles

The traditional layer by layer coating is based on the deposition of alternative oppositely charged species. But SF coating is mainly due to hydrophobic interactions[251]. As been reported, the maximum deposition occurred on a silk concentration of 0.1 % (w/v), so we have prepared the coating materials using the same composition [254]. SF was extracted from *bombyx mori* silk cocoons by discarding the sericin. As shown in **Scheme 4.1**, amine-

functionalized SF **(3)** was prepared to increase the number of the free amino group in SF **(1)** by covalently conjugating it to en **(2)** *via* amide coupling reaction. The amine-functionalized SF **(3)** was then covalently conjugated to the free carboxyl group of FA **(4)** and FL **(5)** *via* amide coupling reaction. The FA and FL conjugated SF were used for coating the nanoparticles. The FL might also be useful for cell imaging.

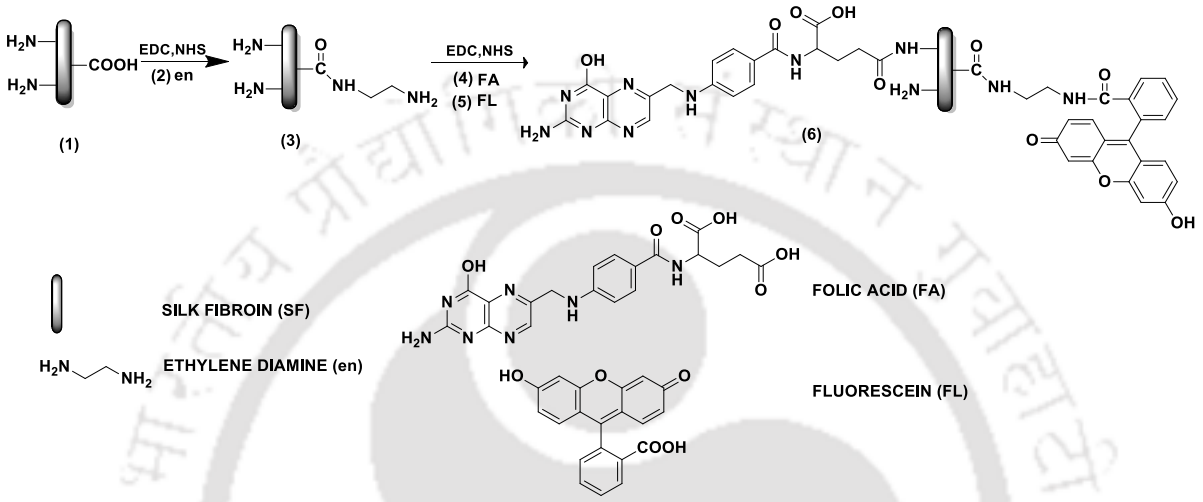

Scheme 4.1 Stepwise synthesis of folic acid and fluorescein conjugated silk fibroin.

4.3.3. Determination of formation of gold nanoparticles

The formation of gold nanoparticles was confirmed by the change in the color of the solution, UV-Visible spectroscopy, and FETEM analysis.

(A) Color change and UV-Visible spectroscopy

The formation of gold nanoparticles is primarily indicated by the change in color of the solution from colorless to blushing red, as shown in **Figure 4.1 (B).** It was further confirmed by UV-Visible spectroscopy. **Figure 4.1 (A)** shows the UV-Visible spectra of CAu showing absorption maxima at 518-520 nm, the characteristic peak of gold nanoparticle due to SPR[255].

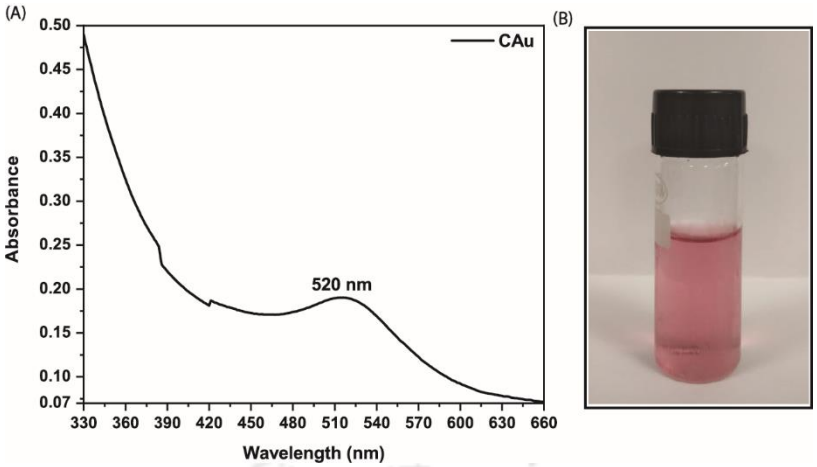

Figure 4.1 (A) UV-Visible Spectroscopic plot of CAu; **(B)** Image showing the formation of gold nanoparticles from colorless solution to blushing red.

(B) Size determination by FETEM analysis

The FETEM micrographs and size distribution histogram of CAu are shown in **Figure 4.2 (A)** and **(B)**, respectively, which reveals that the nanoparticles were quasi-spherical in shape with a narrow size distribution of 8±3 nm. The size distribution histogram was obtained by size analysis using ImageJ.

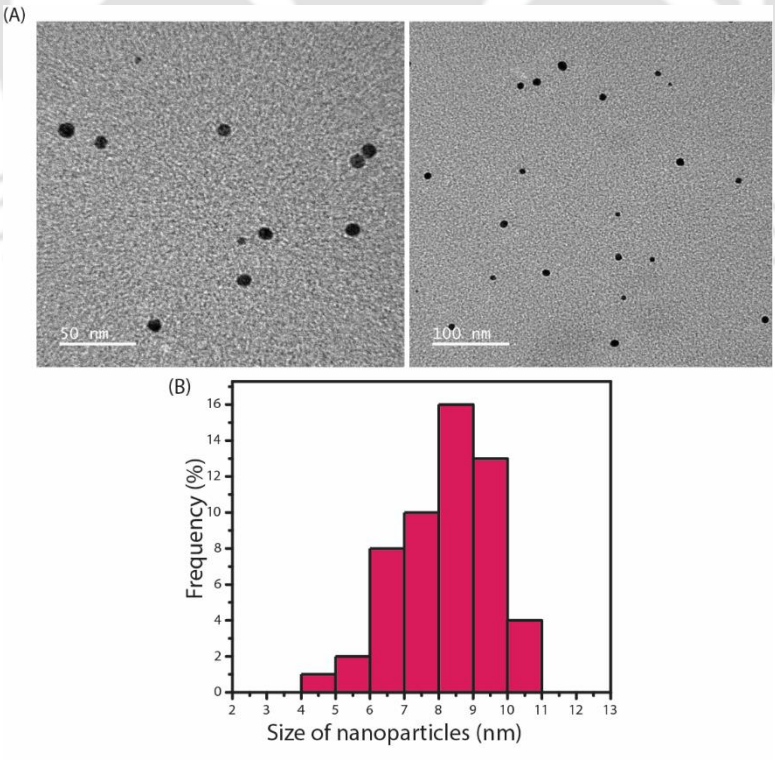

Figure 4.2 (A) FETEM micrograph of CAu with scale 50 nm (left) and 100 nm (right); **(B)** Size distribution histogram.

(C) Determination of drug loading on gold nanoparticles by DLS

The loading of DOX on the nanoparticles after dialysis was determined by zeta potential measurement. At acidic pH of 4, the zeta potential of the CAg was found to be 37.77 mV due to the gold nanoparticles being capped by cationic chitosan. After loading of DOX, the zeta potential was found to be 58.70 mV. The increase in the value is the indication of the presence of positively charged DOX[47,256]. The zeta potential curve of CAu and CAu-DOX is shown in **Figure 4.3 (A)** and **(B)**, respectively.

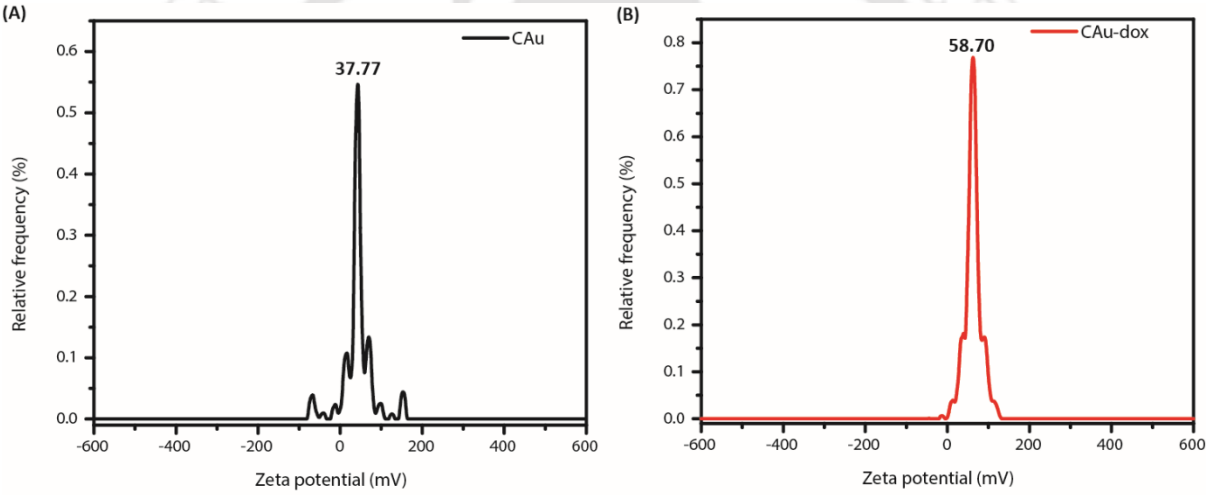

Figure 4.3 Zeta potential curves of **(A)** CAu; **(B)** CAu-DOX.

4.3.4. Determination of conjugation of FA and FL to SF by FTIR spectroscopy

The FTIR spectra of SF shown in **Figure 4.4 (A)** shows typical peaks of amide I (C=O stretching), amide II (N-H bending), and amide III (C-N stretching) at 1620, 1520, and 1236 cm^{-1} respectively[121]. Pure FL in **Figure 4.4 (C)** shows a wide band between 3428-3072 $cm^{-1,}$ which corresponds to the hydroxyl group, H-bonded-OH stretch; peaks from 1468-1316 cm^{-1} which is due to carboxylic acid salt; peak at 1636 cm^{-1} and 1600 cm^{-1} due to the aromatic ring vibrations which appear as a pair of band structures, often with some splitting; peaks between 1110-607 cm^{-1} due to the aromatic C-H out of the plane bend and between 587-461 cm^{-1} due

to O-H out of plane bend[257]. **Figure 4.4 (D)** shows FTIR spectra of SF-FA-FL, where along with the peaks of SF, new peaks of FA and FL can also be seen. The appearance of a peak at 1673 cm^{-1} is due to the C=O stretching vibration of FA. The peak at 1445 cm^{-1} and 1410 cm^{-1} is attributed to the -C=C- phenyl ring aromatic stretching vibration and OH deformation of phenyl skeleton, thus indicating the presence of FA[258]. The peak from 876-652 cm^{-1} is due to due to the aromatic C-H out of plane bend of FL.

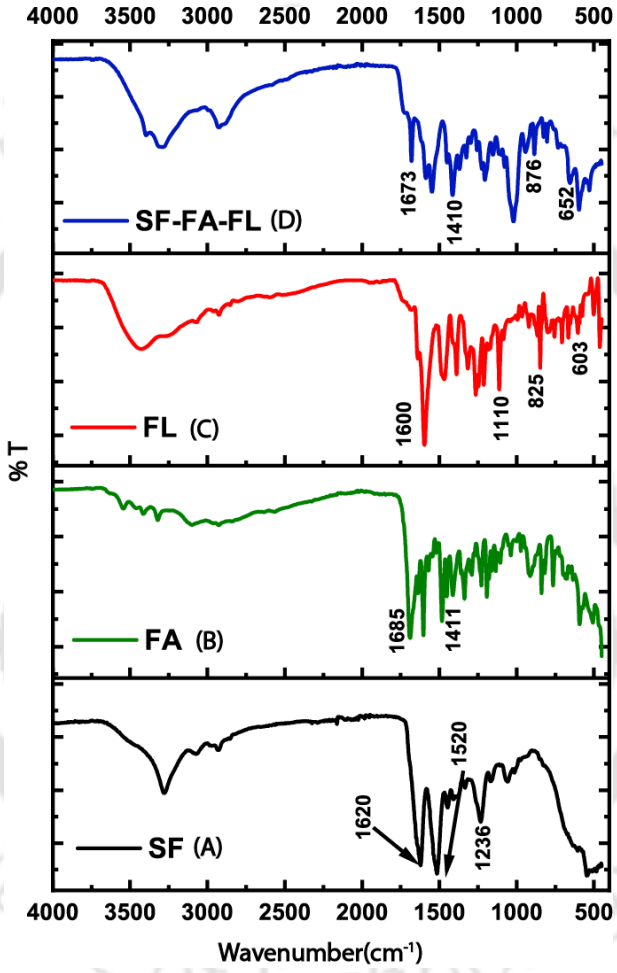

Figure 4.4 Stacked FTIR spectra of **(A)** SF; **(B)** FA; **(C)** FL; **(D)** SF-FA-FL.

4.3.5. Evaluation of SF-FA-FL coated CAu-DOX nanoparticle by FETEM analysis

The silk coating on the CAu-DOX was evaluated by FETEM analysis. **Figure 4.5 (A)** and **(B)** show the FETEM micrographs of uncoated and coated CAu-DOX nanoparticles, respectively. The size of the uncoated nanoparticles was 8±3 nm, whereas, upon coating, the size of the nanoparticles increases to 80±15 nm.

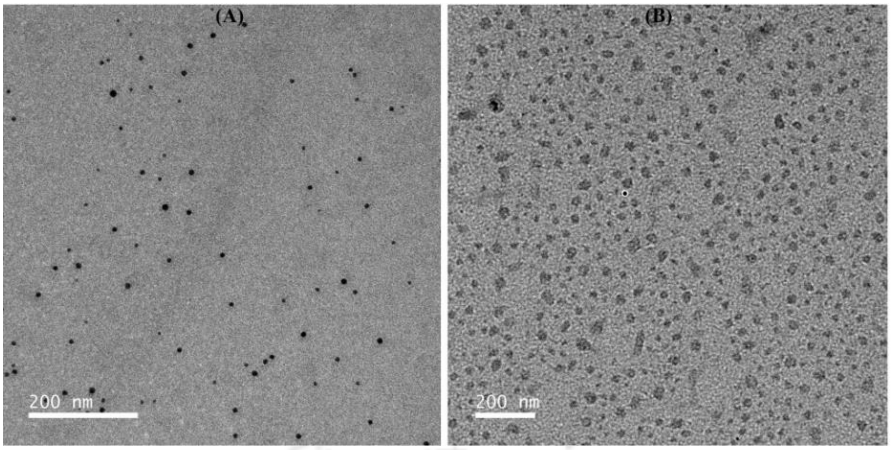

Figure 4.5 FETEM micrograph of **(A)** uncoated CAu-DOX nanoparticles; **(B)** SF-FA-FL coated CAu-DOX nanoparticles.

4.3.6. Drug loading efficiency

The drug loading efficiency on the nanoparticles, as determined by the drug concentration in the nanoparticle solution before and after dialysis, was calculated to be 70.83 %. The drug loading efficiency was calculated using the following equation.

$$\textit{Drug loading efficiency}(\%) = \left(\frac{\textit{drug content before dialysis} - \textit{drug content after dialysis}}{\textit{drug content before dialysis}}\right) \times 100$$

4.3.7. *In vitro* drug release study

The plot of the percentage drug release vs. time of uncoated and coated nanoparticles is shown in **Figure 4.6 (A)** and **(B)**, respectively. It can be seen that the coated nanoparticles showed slower release of DOX compared to uncoated ones, which is due to the diffusion barrier created by the SF coating. This is beneficial for the sustained and long term release of the drugs. The uncoated nanoparticles exhibited an initial burst release of 44% within 6 h. While upon surface-coating, the burst release was drastically reduced to 14%. The percentage

drug release in uncoated and coated nanoparticles was found to be 90% and 60% respectively after 32 h.

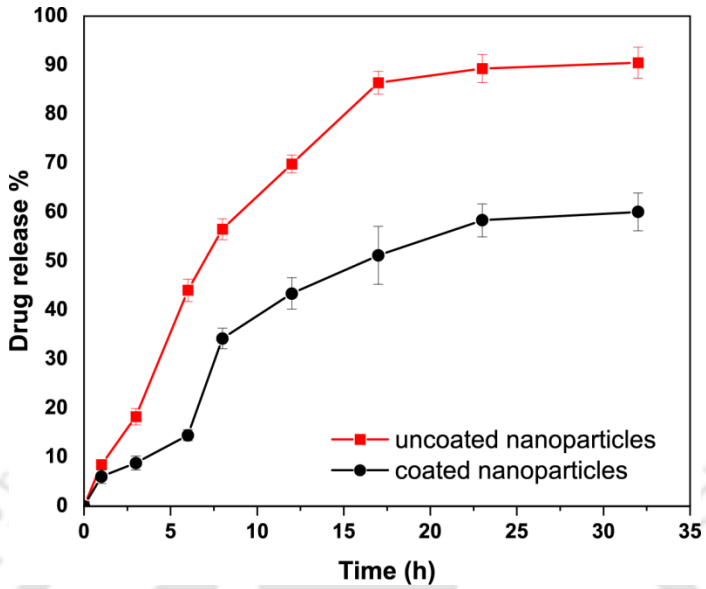

Figure 4.6 Percentage of drug release from **(A)** uncoated nanoparticles; **(B)** coated nanoparticles.

4.3.8. MTT assay for Cytotoxicity determination

A dose-dependent decrease in cell viability was observed for all four treatment groups in **Figure 4.7**. However, it should be mentioned here that there was very less cell death in the samples, which were treated with blank gold nanoparticles, as in **Figure 4.7 (A)**. Cell death was remarkably higher for the other three treatment groups in **Figure 4.7 (B)-(D)**. A maximum of cell death was observed in the samples of group D, which were treated with SF-FA-FL coated CAu-DOX. This can be attributed to the selective targeting of the FA ligand towards the HeLa cells, which are known to overexpress folic acid receptors.

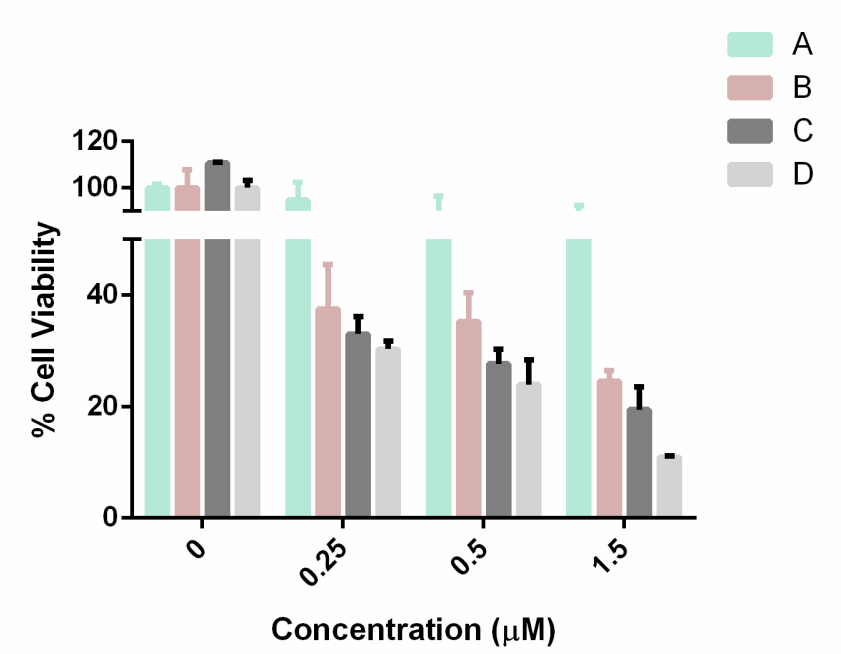

Figure 4.7 In vitro cell viability of HeLa cell lines treated with **(A)** CAu; **(B)** DOX **(C)** CAu-DOX; **(D)** SF-FA-FL coated CAu-DOX.

4.3.9. Confocal imaging to study the uptake

For the visual evaluation of the targeting efficiency of the synthesized nanoparticle, we performed live-cell imaging. The fluorescence of doxorubicin was probed in the cells treated with 1.5 μM of CAu-DOX and SF-FA-FL coated CAu-DOX for 2 h. Confocal microscopy images in **Figure 4.8 (B)** explicitly illustrate the abundance of fluorescence from the cells which were treated with the folic acid conjugated nanoparticles (SF-FA-FL coated CAu-DOX). This selective cellular uptake of the nanoparticles by the folic acid receptor overexpressing HeLa cells essentially emphasizes the improved targeting efficacy of the SF-FA-FL coated CAu-DOX making it an ideal candidate for cancer therapy.

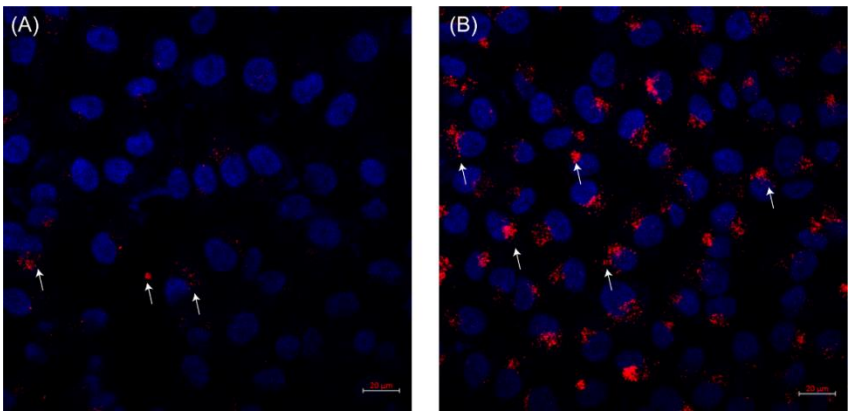

Figure 4.8 Confocal microscope images of the HeLa cells treated with **(A)** CAu-DOX; **(B)** SF-FA-FL coated CAu- DOX, depicting increased uptake of the SF-FA-FL coated CAu-DOX nanoparticles by the cells. The white arrows indicate successful uptake of the DOX loaded nanoparticles by the cells.

4.4. Conclusions

Nanoparticles fabricated using chitosan can act as a potent drug delivery vehicle for various types of anti-cancer drugs. In this study, the gold nanoparticles were formulated by a green synthetic route with uniform shapes and size of 8±3 nm. The loading of DOX on the nanoparticles was evident from zeta potential, which shows an increase in the value in loaded ones indicating the presence of positively charged DOX. The coating of nanoparticles was done, which was proved by FETEM, showing an increase in the size of nanoparticles upon coating to 80±15 nm. The coated nanoparticles showed slower drug release as compared to the uncoated ones, which can be useful for the long term and sustained drug release. SF-FA-FL coated CAu-DOX nanoparticles showed maximum cytotoxicity in HeLa cell lines as compared to the uncoated ones, which can be possibly due to the increased uptake of the coated ones due to the presence of FA as the folate receptors that are overexpressed on the surface of cancer cells rapidly bind to FA and triggers cellular uptake via endocytosis. This was further supported by cell imaging using confocal microscopy, which shows about 7 fold

increases in DOX concentration in the coated nanoparticles as compared to the uncoated ones.

4.5. Time Dependent UV-Visible spectroscopy of CAu.

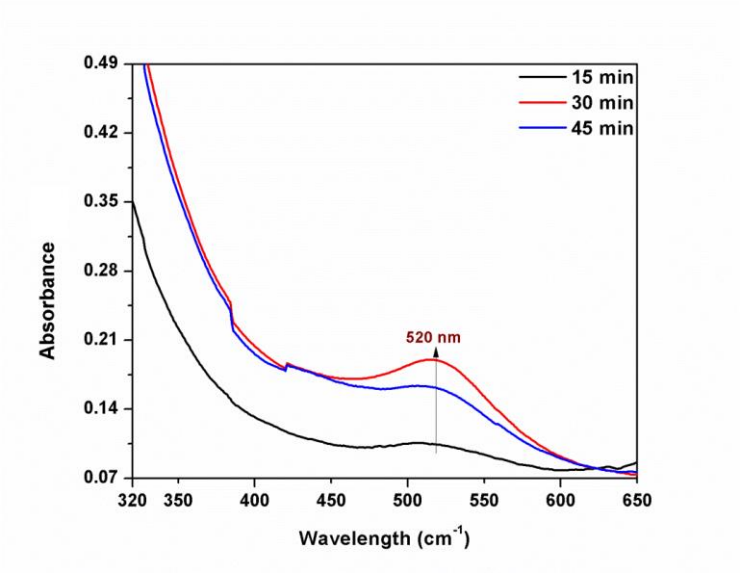

Figure 4.9 UV-Visible spectroscopic data of CAu showing the formation of nanoparticles with time.

4.6. Bright field images and image of untreated HeLa cells

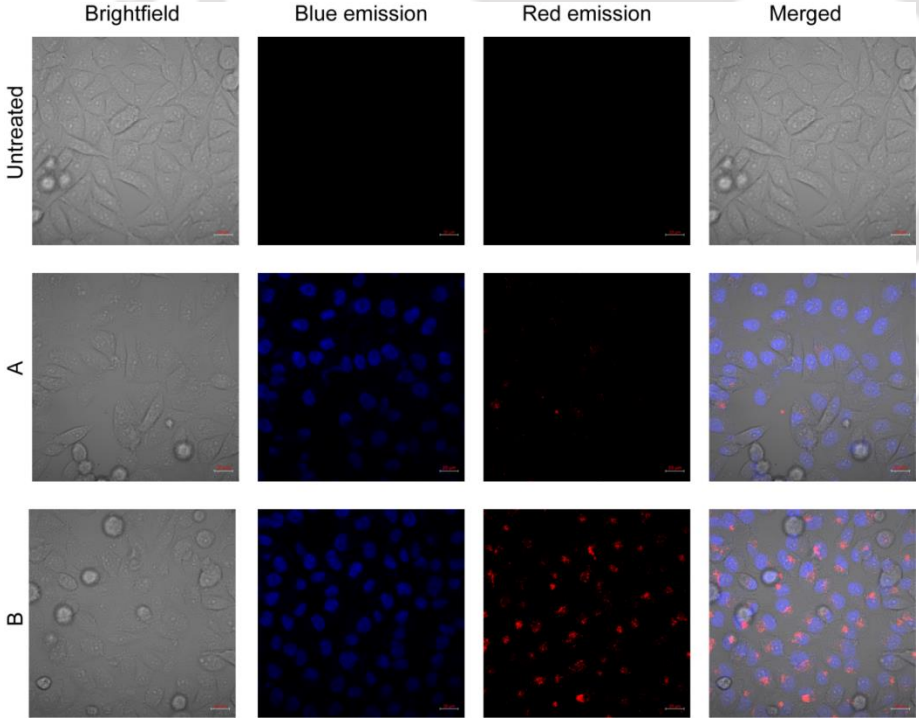

Figure 4.10 Confocal microscopy images of HeLa cells treated with with **(A)** CAu-DOX; **(B)** SF-FA-FL coated CAu-DOX.

4.7. Individual FTIR spectra

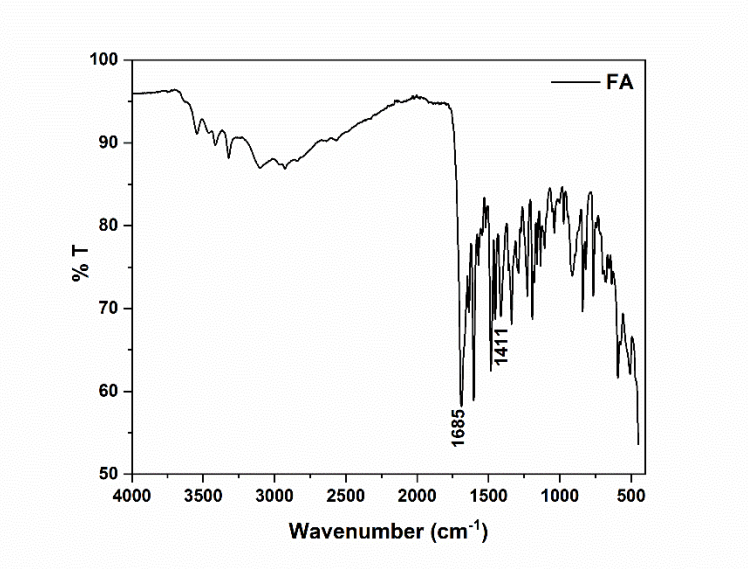

Figure 4.11 FTIR spectra of FA.

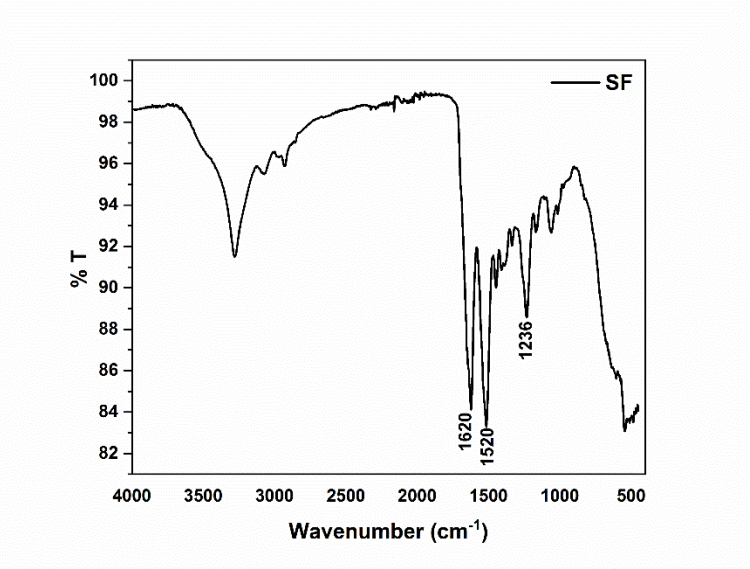

Figure 4.12 FTIR spectra of SF.

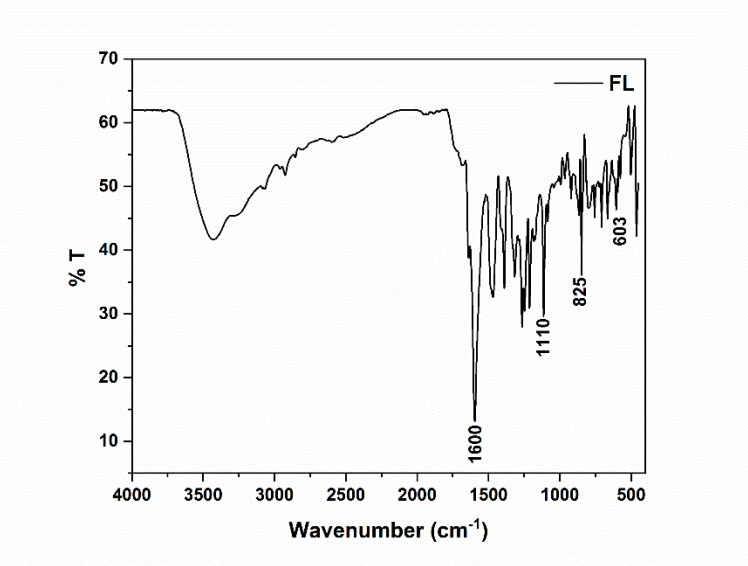

Figure 4.13 FTIR spectra FL.

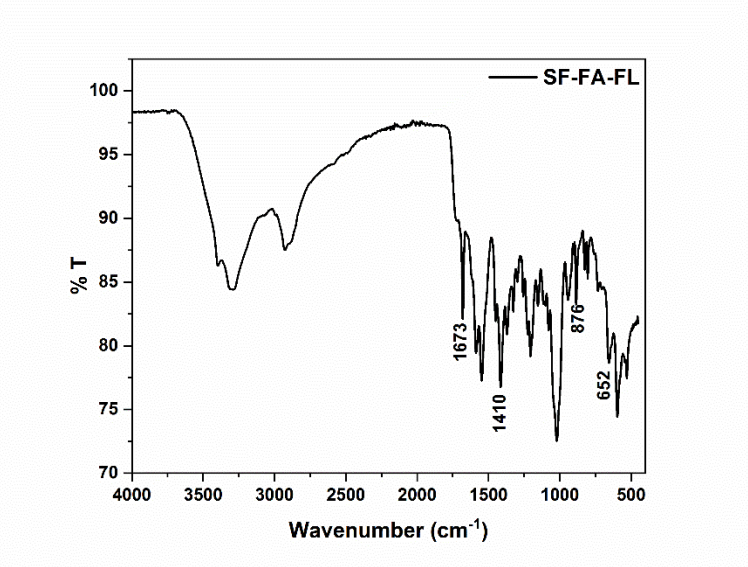

Figure 4.14 FTIR spectra SF-FA-FL.

Chapter 5 Formulation of silk fibroin coated chitosan/gold microparticles for oral delivery of doxorubicin

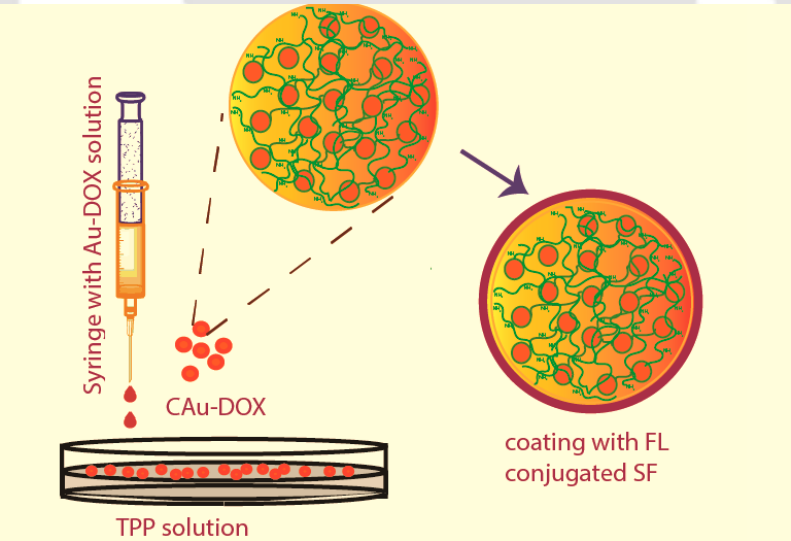

5.1. Overview

Hydrogel beads have been explored for the development of oral and depot drug delivery tools. Chitosan hydrogel beads are spherical, micron- or nano-sized polymeric substances that do not dissolve in physiological conditions instead of being swelled. They are made up of cross-linked chitosan chains with a tangled mesh structure, providing a matrix for the entrapment of drugs[175]. They are known to have high soft tissue biocompatibility and ease of drug dispersion in the matrix. The polymeric beads are beneficial over pellets because of their relatively greater intercellular uptake. Their charge properties influence Their uptake by intestinal epithelia. The microparticles formulated from hydrophobic polymers exhibit greater uptake as compared to the hydrophilic ones. Therefore, the surface charges and hydrophobicity of microparticles have been effective for gastrointestinal (GI) uptake. They are used for depot drug delivery where a large amount of drug can be administered into the body and can be tuned for its controlled and sustained release[44,259,260]. Generally, depot delivery involves particles greater than 5 µm in sizes[251], where the drugs are either adsorbed or encapsulated in it. The release of drug from the beads can be controlled by physical cross-linking of the beads instead of chemical cross-linking to reduce the toxicity. Sodium tripolyphosphate (TPP), a non-toxic multivalent anion, is generally used to crosslink chitosan ionically. It has been seen that by varying the concentration of TPP and cross-linking time, the rate of drug release can be controlled [16].

SF coated beads have been reported where the SF was observed to delayed the degradation of the polymeric beads, create a drug diffusion barrier, retard the drug release, and provide mechanical stability. Thus, the coating can impart sustained release of the drug and increase stability in the GI tract for oral delivery. It was also seen that by increasing the percentage of SF in the coating solution, there was an increase in the delay of drug release[195,251]. As already

discussed in chapter 4, SF coatings can be easily done due to its aqueous processibility. The thickness of the coating can also be easily controlled[60,194].

Both intravenous and oral chemotherapy route of drug administration has played a vital role in cancer treatment. Both ways require a specific drug carrier design and have their promising aspects and limitations. Oral therapy is mostly preferred as it is more convenient, painless, has a long shelf life, provides sustained drug release, and maintains an optimal concentration of the drug in the blood.

Here, we have synthesized hydrogel beads using LMWC stabilized gold nanoparticles that have been prepared in chapter 4. Upon formulation, the DOX gets encapsulated in the hydrogel beads. We have also synthesized FL conjugated SF, which was used for coating the beads for imparting stability and drug retardation properties. FL was used for detecting the SF coating on the beads by fluorescence microscopy.

5.2. Experimental Procedures

5.2.1. Materials

LMWC (M_v =129 kDa; 94% deacetylation), TPP and FL were purchased from Sigma Aldrich. DOX was purchased from Tokyo Chemical Industry. Gold chloride, lithium bromide, and EDC were procured from Spectrochem. Glacial acetic acid, sodium carbonate, and ethylenediamine (en) were purchased from Merck (India). NHS was purchased from Alfa Aesar. *Bombyx mori* silk cocoons were acquired from local silk farms, Assam, India.

5.2.2. Preparation of doxorubicin encapsulated LMWC stabilized gold nanoparticles beads (CAu-DOX beads)

The undialyzed DOX loaded LMWC stabilized gold nanoparticles (CAu) reported in chapter 4 was used for the preparation of the beads. The beads were formulated by the ionic-cross-linking method using TPP as the cross-linking agent. The viscous CAu-DOX nanoparticles

were dropped into TPP solution of 10 %(w/v) and 8 pH using a 22 G needle. It was allowed to crosslink for 3 h. The formed beads were then extracted from the TPP solution, washed several times with deionized water to wash the TPP and non-encapsulated drug. The drug encapsulated beads were dried at 40°C for 5 h and stored at 4°C.

5.2.3. Preparation of fluorescein functionalized silk fibroin (SF-FL)

The extraction of SF was done using a reported procedure[253], which has been described in detail in chapter 4. For the synthesis of SF-FL, 2 ml of SF solution was dropwise added to 47 ml water at 4°C with mild stirring. The carboxyl groups of SF were activated using EDC (25 mg) and NHS (25 mg) at pH 6 under continuous stirring for 3 h in the dark. 1 ml of ethylenediamine (en) was added dropwise into the solution and reacted for 12 h at room temperature. The reaction mixture was dialyzed against deionized water for 2 days. In a separate apparatus, FL dissolved in 20 ml PBS of pH 6 was also activated using EDC (19 mg) and NHS (15 mg) for 3 h in the dark. The activated FL was dropwise added to the en-SF conjugate and reacted for 24 h in the dark and then dialyzed against deionized water for 2 days. The dialyzed solution was stored at 4°C before further use.

5.2.4. Coating of beads (SF-FL coated CAu-DOX beads)

For coating, the SF conjugate solution is taken in a beaker. The prepared CAu-DOX beads were dipped in the solution. After 10 min of dipping, the beads were recovered from the solution and washed with deionized water. They were then dried in a hot air oven at 40°C for 1 h and stored at 4°C.

5.2.5. Drug loading efficiency

The drug encapsulation efficiency was calculated using an indirect method by measuring the drug concentration in the leftover TPP solution after the extraction of beads. The TPP solution was analyzed spectrophotometrically at 480 nm, and the DOX concentration was

obtained by the calibration curve of DOX. Then the encapsulation efficiency was calculated using the following formula.

5.2.6. *In vitro* drug release study

The in vitro drug release study from the coated and uncoated beads was also performed by suspending them in PBS buffer of pH 7.4 in conical flasks. The flasks were kept inside an incubator shaker maintained at a speed of 100 rpm at 37°C. At defined time intervals, 500 µL aliquots of samples were taken out from the flasks and analyzed in a spectrophotometer as was done for nanoparticles. All the reactions were performed in triplicates, and the error was determined from the standard deviation using the Origin software version 2020.

5.2.7. UV-Visible spectroscopy

The drug encapsulation efficiency and drug release study were performed by UV-Visible spectroscopy at room temperature using Agilent Carry 100 UV-Visible spectrophotometer.

5.2.8. FTIR spectroscopy

The FTIR spectra of the DOX, CAu beads, CAu-DOX beads, SF, FL and SF-FL were recorded on Perkin Elmer Spectrum 2 FTIR spectrometer at room temperature using KBr pellet, over a frequency range of 4000-400 cm^{-1}.

5.2.9. Optical microscopy

The precise size of the dried uncoated and coated beads was observed by optical microscopy using Leica DM 2500 M Optical microscope. The dried beads were directly kept under the microscope for observation.

5.2.10. FESEM analysis

The morphology of the beads was determined by Zeiss Sigma Field Emission Scanning Electron Microscope (FESEM). The uncoated and coated beads were pasted on top of two separate carbon film for the analysis.

5.2.11. Fluorescence microscopy

The SF coating on the beads was analyzed using fluorescence images recorded in Olympus CX41Upright Fluorescence Microscope. The FL conjugated on SF shows fluorescence at an excitation wavelength of 480 nm and an emission of 520 nm.

5.3. Results and Discussions

5.3.1. Synthesis of doxorubicin encapsulated LMWC stabilized gold nanoparticles beads.

The LMWC stabilized gold nanoparticles were formulated into beads by the ionic cross-linking technique using TPP as the cross-linking agent. The cationic chitosan capping in gold nanoparticle interacts with the anionic TPP by ionic interaction and get formulated into beads. Upon extraction of the beads from the TPP solution after crosslinking, the unloaded drug remains back in the TPP solution, which was analyzed for checking drug loading efficiency and then discarded. The schematic representation of the synthesis of CAu-DOX beads and SF-FL coated CAu-DOX beads is depicted in **Figure 5.1**.

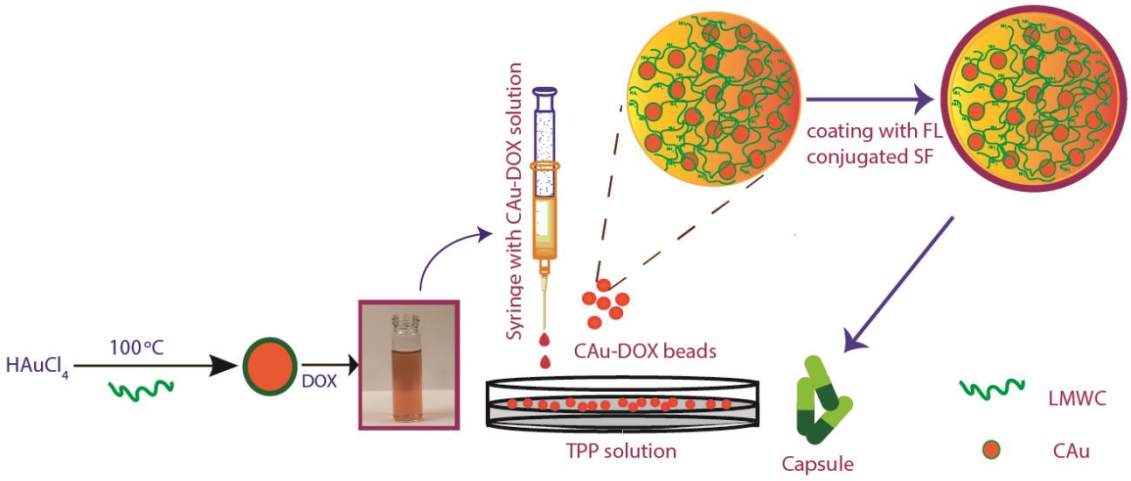

Figure 5.1 Schematic diagram of synthesis of CAu-DOX beads and SF-FL coated CAu-DOX beads.

5.3.2. Synthesis of coating material and coating of beads

The mechanism of coating of the beads is hydrophobic interactions[251]. The coating was done by 0.1 % (w/v) of SF in SF-FL. As shown in **Scheme 5.1**, the SF **(1)** was functionalized using ethylenediamine **(2)** to form amine-functionalized SF **(3)** to increase the number of the free amino group in SF. The amine-functionalized SF **(3)** was then covalently conjugated to the free carboxyl group of FL **(4)** via amide coupling reaction. The FL conjugated SF **(5)** was used for coating the beads. The FL was used to detect the SF coating on the beads by using fluorescence microscopy. This might also be useful for cell imaging. The coated beads can be used for oral delivery of DOX, even using capsules.

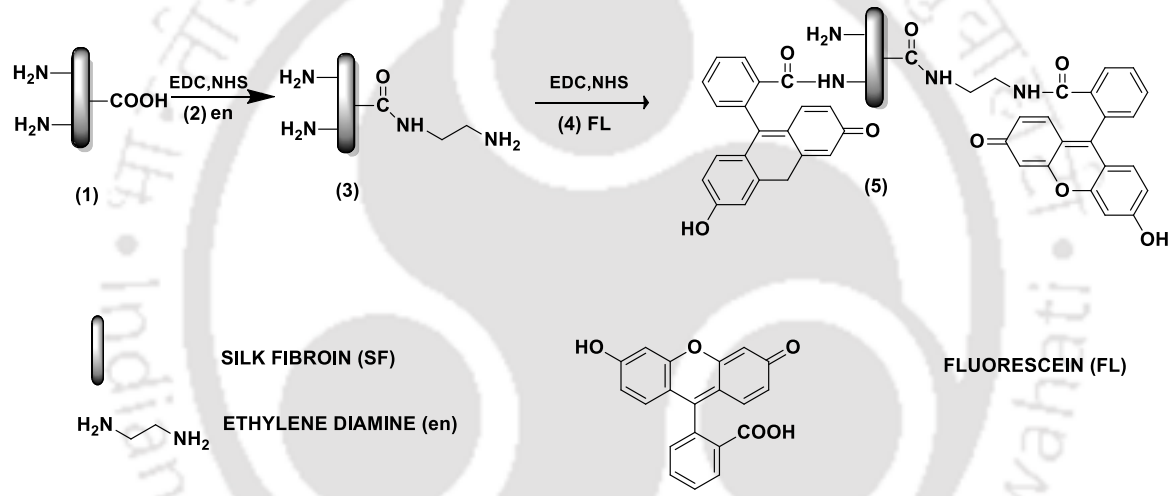

Scheme 5.1 Stepwise synthesis of fluorescein-conjugated silk fibroin.

5.3.3. Evaluation of bead formation and DOX encapsulation.

Figure 5.2 (A) and **(B)** show the image of CAu-DOX beads in TPP solution. The encapsulation of DOX in the beads was analyzed by FTIR spectroscopy. For comparative study, pure gold nanoparticles beads (CAu beads) were also synthesized following the same protocol as CAu-DOX beads**. Figure 5.2 (C)**, **(D)**, and **(E)** shows the FTIR spectra of CAu bead, pure DOX, and CAu-DOX beads, respectively. On comparing the spectra of CAu bead and CAu-DOX beads, two characteristic peaks of DOX can be seen in the spectra of CAu-DOX beads. The new peak at 1249 cm^{-1} is due to stretching bands of the C–O–C groups and

the peak at 814 cm^{-1} is due to the primary amine NH_2 wag of DOX[261,262], which shows the successful encapsulation of the drug in the microparticles.

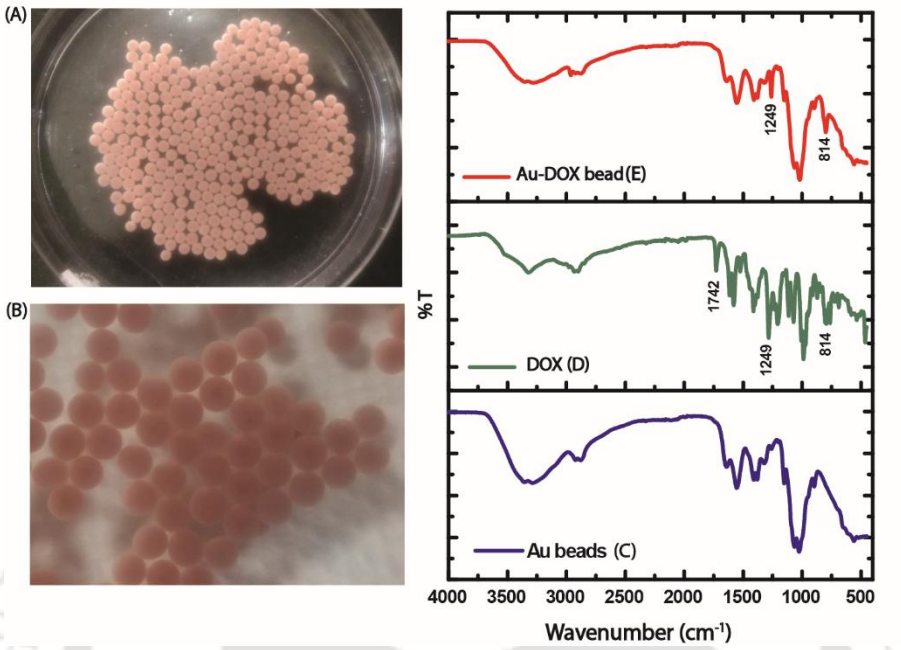

Figure 5.2 (A)-(B) Image of CAu-DOX beads in TPP solution; Stacked FTIR spectra of **(C)** CAu beads; **(D)** DOX; **(E)** Au-DOX beads.

5.3.4. Determination of conjugation of FL to SF by FTIR spectroscopy

5.3.5. Evaluation of SF-FL coating on CAu-DOX beads by fluorescence microscopy

The SF coating on the beads was determined by detecting the FL conjugated to SF by fluorescence microscopy at an excitation wavelength of 480 nm and an emission of 520 nm. **Figure 5.3 (A)** and **(B)** shows the fluorescence microscopy image of uncoated beads and coated beads, respectively. Upon excitation, the uncoated beads show no fluorescence, which is evident in **Figure 5.3 (A)**, showing a blank dark image. Whereas; the coated beads were surrounded by a uniform fluorescent layer, as in **Figure 5.3 (B)**, confirming the presence of FL conjugated SF.

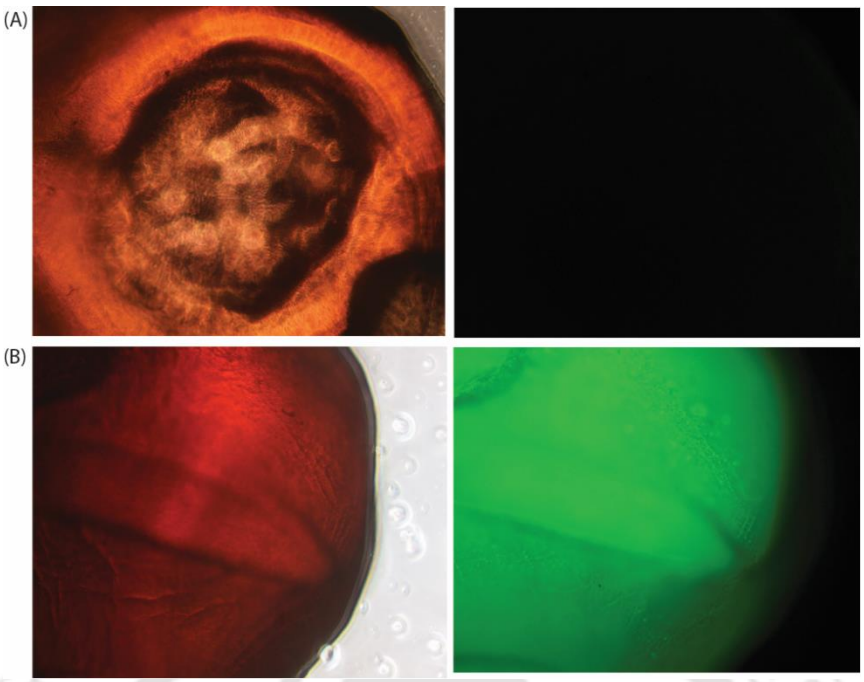

Figure 5.3 Fluorescence microscopy images of **(A)** uncoated beads; **(B)** coated beads.

5.3.6. Evaluation of size of the beads by optical microscopy

The size of the dried uncoated and coated beads was analyzed by optical microscopy and shown in **Figure 5.4 (A)** and **(B)**, respectively. The image showed that the average particle size of the coated and uncoated beads, were almost the same and in the range of 900-1000 µm. Upon coating, no significant increase in size was observed as the coating thickness might be negligible range compared to the bead size, unlike the nanoparticles in chapter 4, where the change was visible. The beads' size could be further controlled during its formulation, depending upon the application, by changing the diameter of the needle used for dropping.

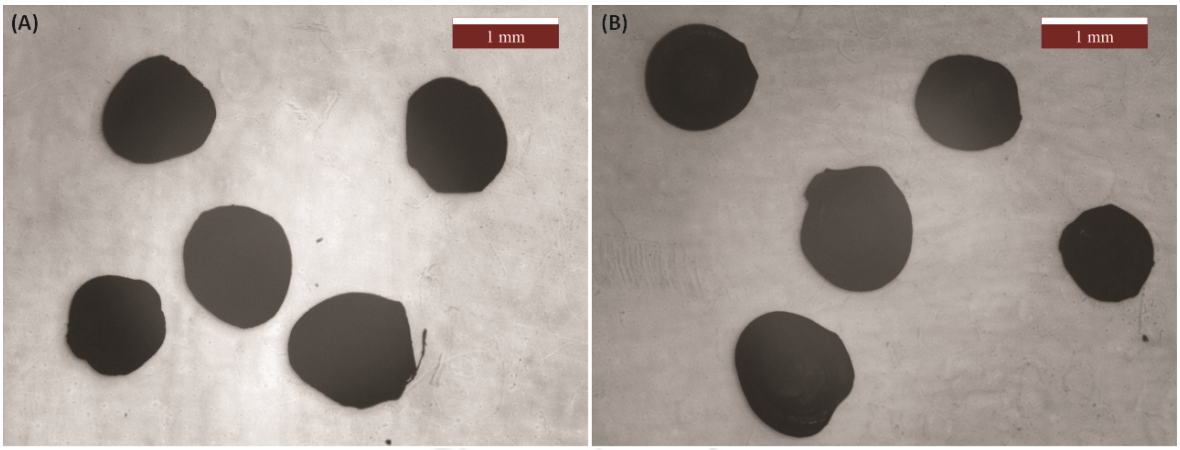

Figure 5.4 Optical microscopy images of **(A)** uncoated beads; **(B)** coated beads with size 900-1000 µm.

5.3.7. Evaluation of morphology of the beads by FESEM analysis

The morphology of the coated, as well as uncoated beads, was determined by FESEM. **Figure 5.5 (A)** and **(B)** show the FESEM micrographs of uncoated and coated beads, respectively. It was distinguishable that the coated beads possessed a smooth surface compared to the uncoated ones. Further, the shape of the coated beads was properly spherical compared to the uncoated ones.

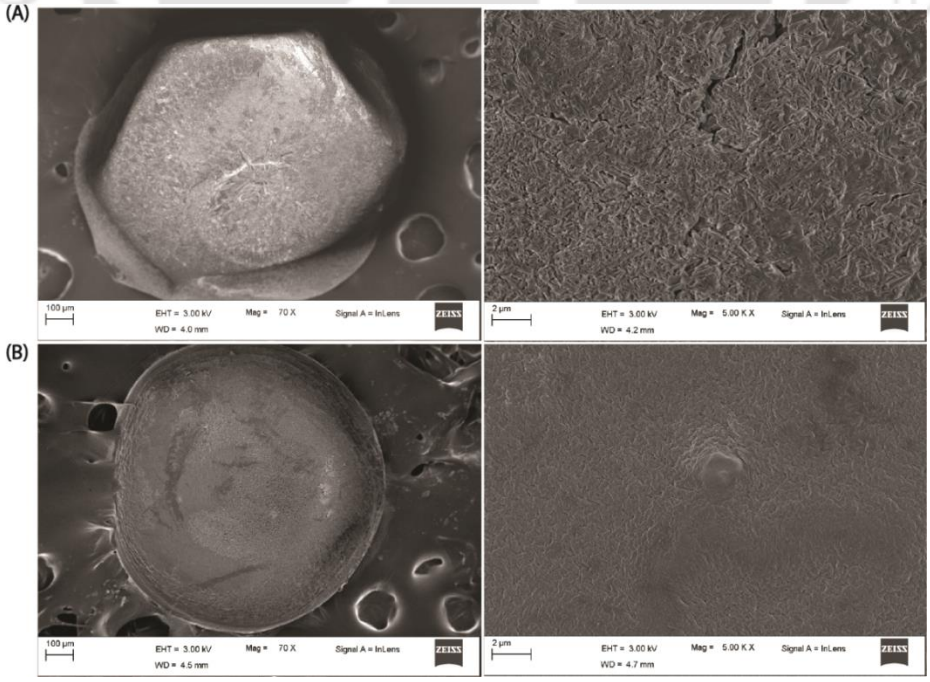

Figure 5.5 FESEM images of **(A)** uncoated beads; **(B)** coated beads.

5.3.8. Drug loading efficiency

The drug encapsulation efficiency in the beads was 87.45 %, which was determined indirectly from the concentration of leftover DOX in the TPP solution after the extraction of drug encapsulated beads. The following formula was used:

$$\textit{Encapsulation efficiency}\ (\%) = \left(\frac{\textit{Total drug taken initailly} - \textit{drug in TPP solution}}{\textit{Total drug taken initailly}}\right) * 100$$

5.3.9. *In vitro* drug release study

The plot of the percentage drug release vs. time of uncoated and coated nanoparticles is shown in **Figure 5.6 (A)** and **(B)**, respectively. It can be seen that the coated beads showed a slower release of DOX compared to uncoated ones, which is due to the diffusion barrier created by the SF coating. The uncoated beads showed an initial burst release of 40% in 4h. While, upon coating, it was reduced to 16%. The percentage drug release in uncoated and coated beads was found to be 90% and 64% respectively after 40 h.

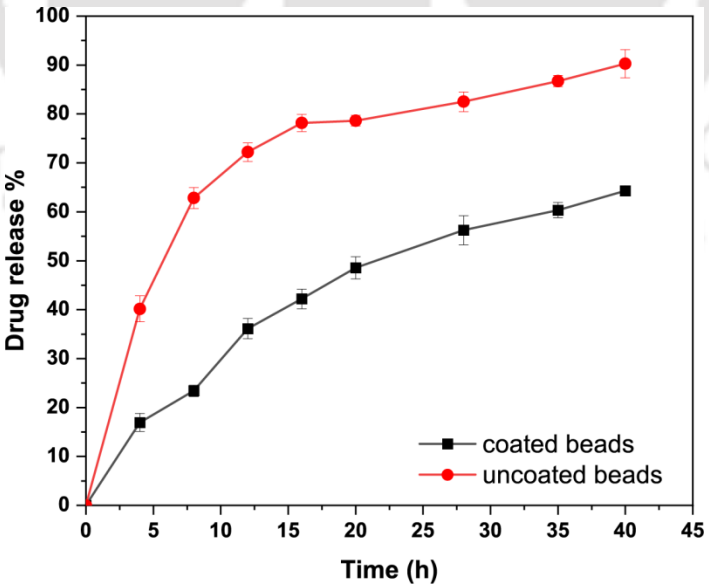

Figure 5.6 Percentage of drug release from **(A)** uncoated beads; **(B)** coated beads.

5.4. Conclusions

The Hydrogel beads, due to their high biocompatibility and drug loading capacity, can be an effective oral and depot drug delivery tool. Chitosan-based beads can be synthesized using TPP by ionic cross-linking techniques. TPP is non-toxic; thus, the process is a simple and environmentally friendly approach. The presence of gold nanoparticles makes it more effective in terms of cell-penetrating property and anticancer properties. The size of the beads, as obtained by optical microscopy, was 900-100 µm. The coating of the beads was successfully done by FL functionalized SF. The FL was used to detect the SF coating by fluorescence microscopy, which showed a uniform fluorescent layer upon excitation. Moreover, the coating provided a smoother and more spherical morphology to the beads. The drug release was fairly retarded by the coating, which can be useful for slow and sustained drug release. The FL conjugation can also be useful for cell imaging purposes.

5.5. Individual FTIR spectra

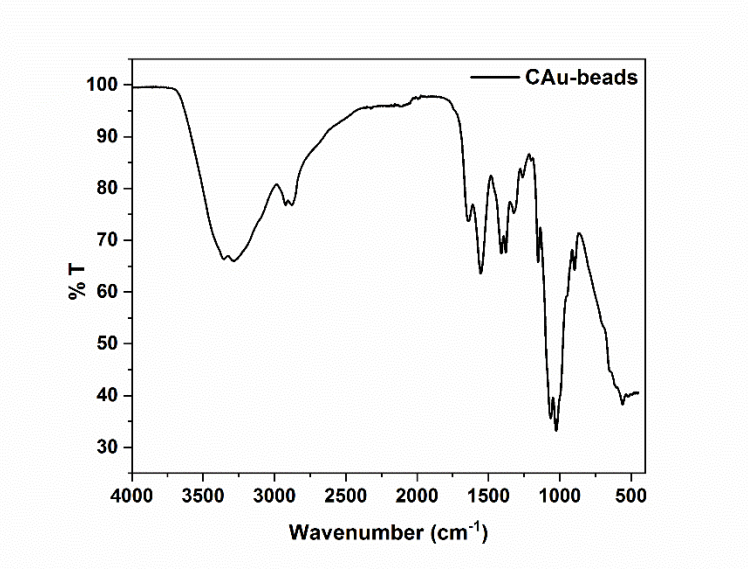

Figure 5.7 FTIR spectra of CAu beads.

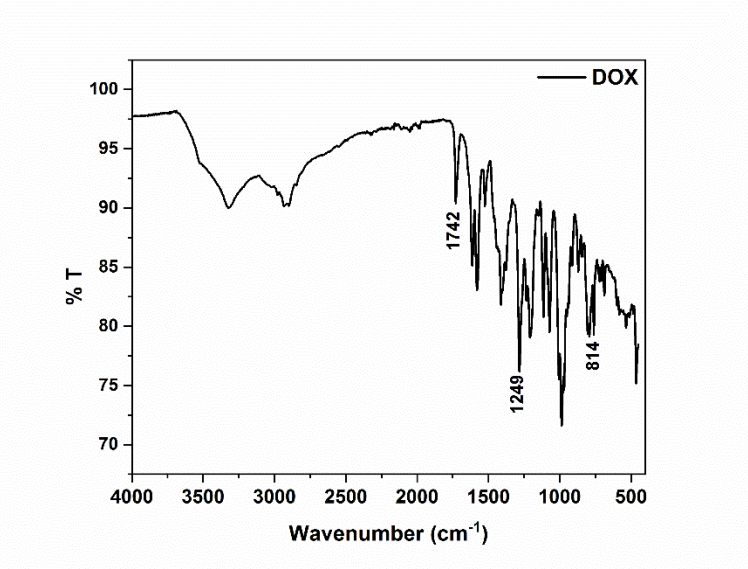

Figure 5.8 FTIR spectra of DOX.

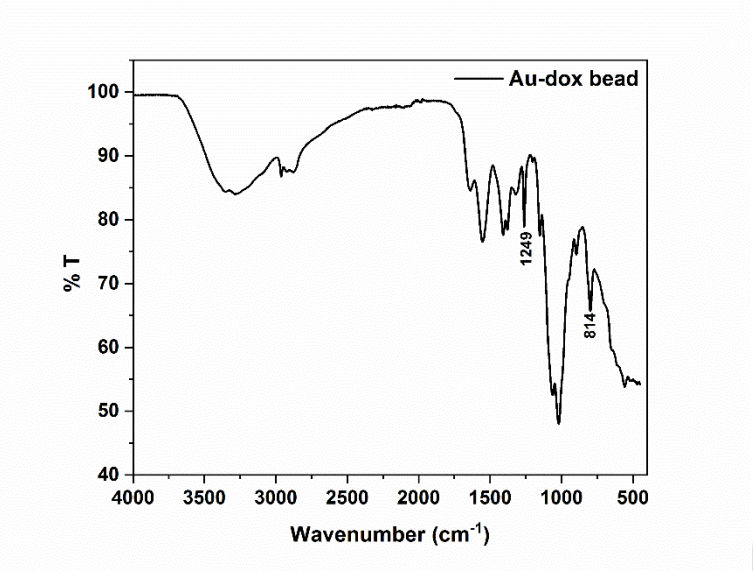

Figure 5.9 FTIR spectra of CAu-DOX.

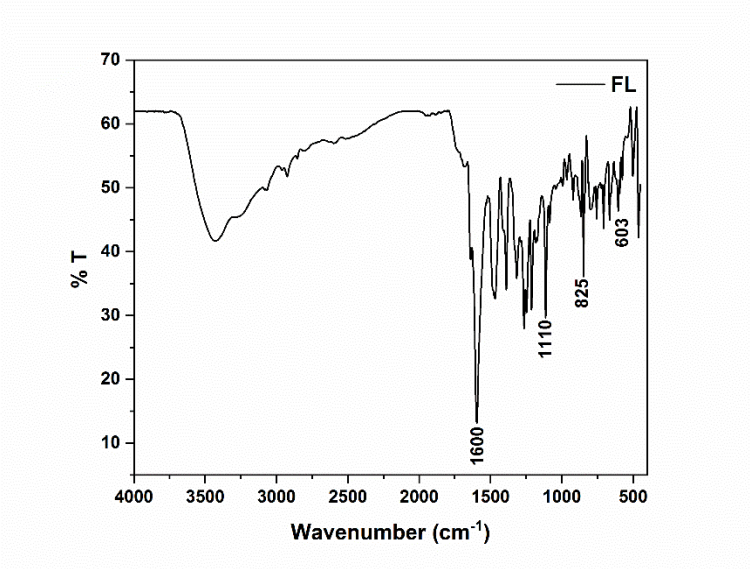

Figure 5.10 FTIR spectra of FL.

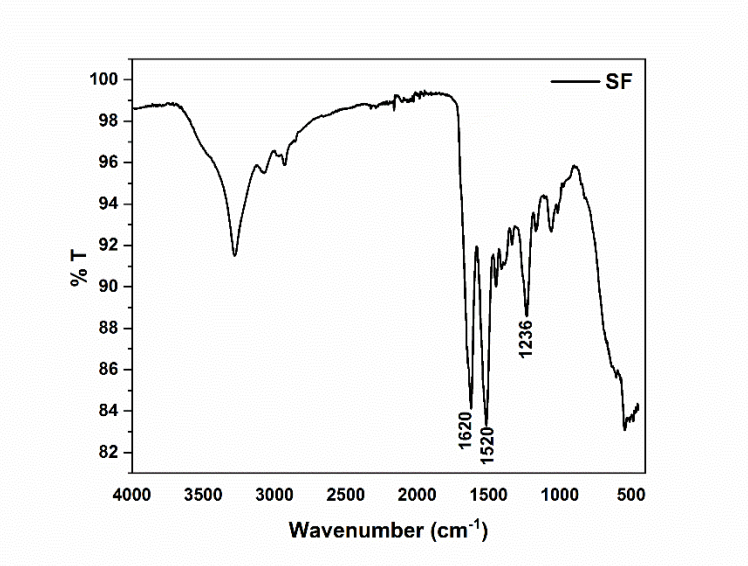

Figure 5.11 FTIR spectra of SF.

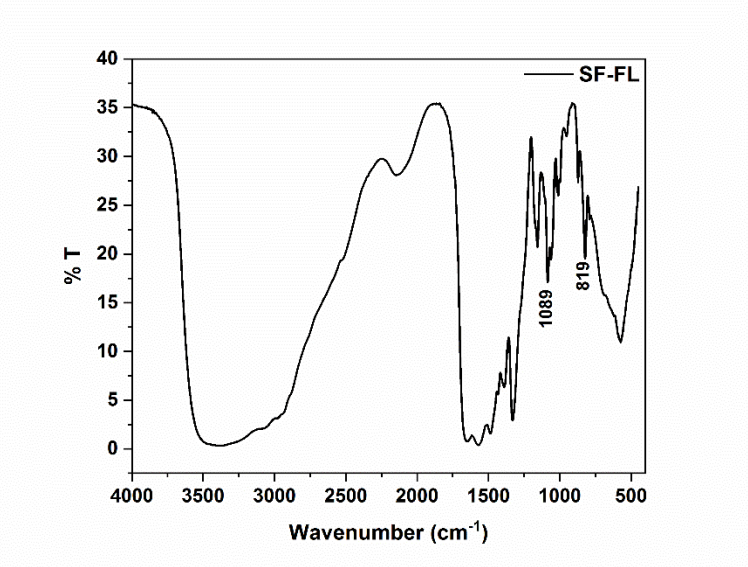

Figure 5.12 FTIR spectra of SF-FL.

Chapter 6 Fabrication of biotin conjugated LMWC/SF carbon dots for targeted drug delivery of 5-FU

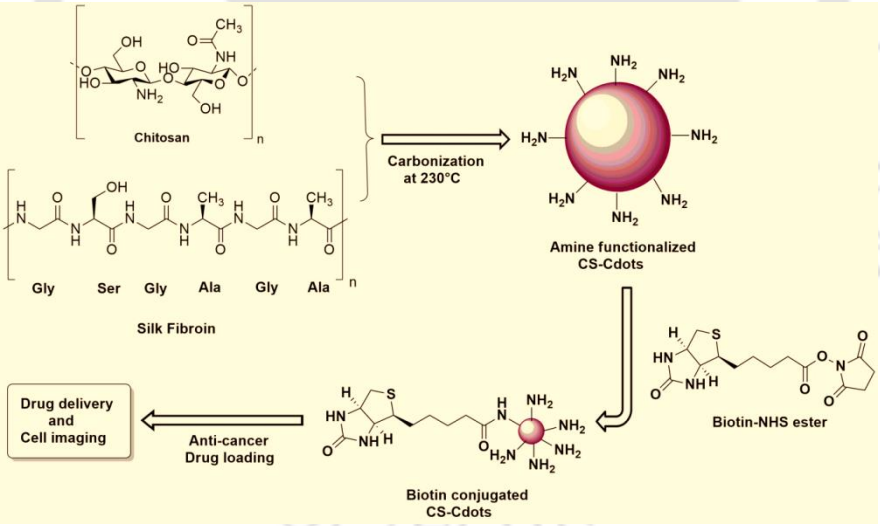

6.1. Overview

Cdots have gained massive attention in pharmaceutical fields due to high biocompatibility, water-solubility, low-cost, and tunable fluorescence property. They possess a quasi-spherical shape with a size below 10 nm. Because of their tunable fluorescence property, they can also be used for cell imaging and smart sensing systems. There are two general approaches for the synthesis of Cdots, "top-down" and "bottom-up". In the "top-down" approach, larger carbon materials are broken down by arc-discharge, laser ablation, electrochemical synthesis, and chemical oxidation. The functionalization and purification step in this approach is time-consuming and complex. Thus, it is not preferable mostly in scientific and commercial points of view. In the "bottom-up" approach, small carbon sources are used to build Cdots using pyrolysis, microwave, ultrasonication, hydrothermal, and plasma-treatment.

Depending on the types of precursor and synthesis route, various types of functional groups like amino, hydroxyl, and carboxyl functional groups appear on the surface of the Cdots. These functional groups can be used for covalent interactions with other molecules. Some cost-effective and environment-friendly processes have been adopted to synthesize Cdots in a green synthesis way using biopolymers, proteins, biomass, plant extracts, etc. Liu *et al*. have reported amine-functionalized Cdots using chitosan as the precursor[263], which can be explored for various functionalization.

Biotin has been one of the significant cell-targeting ligands that target the tumor cells, as biotin receptors are overexpressed in some of the cancer cells, even more than folate and vitamin B-12 receptors[264]. It can be easily attached covalently to other molecules with free amino groups by amide coupling due to the presence of the free carboxyl group. Biotin-NHS ester has been used for coupling with amines because of a large number of advantages such as (a) they are highly reactive; (b) gives high yield in amine coupling reaction[265]; (c) they are resistant to hydrolysis thus stable and can be stored for a more extended period[266].

Herein, we have synthesized Cdots using LMWC and SF mixture. Biotin was covalently conjugated to the amine-functionalized Cdots for cell targeting properties. A model drug 5-FU was loaded to it. The system is expected to possess cell targeting and cell imaging properties. The Cdots were synthesized by pyrolysis, a 'bottom-up' approach. Pyrolysis is a process that involves high-temperature thermal decomposition in the absence of oxygen. It is one of the simplest techniques of C-dot synthesis.

6.2. Experimental Procedures

6.2.1. Materials

LMWC (M_v =129 kDa; 94% deacetylation) and 5-FU were purchased from Sigma Aldrich. Biotin was procured from Tokyo Chemical Industry. NHS was purchased from Alfa Aesar. Lithium bromide and N,N′-Dicyclohexylcarbodiimide (DCC) was purchased from Spectrochem, and *Bombyx mori* silk cocoons were acquired from local suppliers. Sodium carbonate was purchased from Merck (India).

6.2.2. Extraction of silk fibroin and drying

The SF was extracted from *Bombyx mori* silk cocoons using the same protocol, as described in Section 4.2.3. The purified SF solution was lyophilized to obtain dried SF flakes, which were stored at 4°C for further steps.

6.2.3. Synthesis of LMWC and silk fibroin based carbon dots (CS-Cdots)

The Cdots were synthesized by the pyrolysis process in under nitrogen atmosphere. LMWC and dried SF powder were mixed in different ratios (LMWC: SF) of 1:0, 1:0.66, 1:1, and 1:1.5. The mixtures were heated at 230°C for 3 h, and then they were ground to fine powders using mortar and pestle. The powders were dissolved in distilled water using proper shaking and finally filtered. The Cdots dissolved in water were collected in the filtrate, and the

residue was discarded. The solutions were then dried using freeze-drying and stored at 4°C until further use.

6.2.4. Synthesis of biotin-NHS ester (BT-NHS)

The BT-NHS was synthesized using a reported protocol with minor modifications[267]. Briefly, biotin (100 mg, 0.5 mmol) was dissolved in hot DMF at 60°C until a clear solution is obtained. After cooling to room temperature, the NHS (57.52 mg, 0.6 mmol) and DCC (84.38 mg, 0.5 mmol) were added under stirring conditions. The solution was stirred overnight at room temperature. The precipitated solid byproduct (dicyclohexylurea) was filtered off, and the filtrate was concentrated using a rotary evaporator. The concentrated solution was precipitated using diethyl ether. The solid was recrystallized using 2-propanol and dried in a vacuum.

6.2.5. Synthesis of LMWC and silk fibroin based carbon dots and BT-NHS conjugate (BT-CS-Cdots)

CS-Cdots (80 mg) was dissolved in 16 ml of 100 mM sodium bicarbonate buffer of pH 9.0. Biotin-NHS (160 mg) was dissolved in 3 ml of DMSO until a clear solution was obtained. The CS-Cdots solution was dropwise added to the Biotin-NHS solution and reacted overnight at room temperature. The reaction mixture was dialyzed against distilled water using a dialysis membrane (MW 1kDa).

6.2.6. Loading of 5-FU on BT-CS-Cdots (FU- BT-CS-Cdots)

26 mg of 5-FU was stirred with 10 ml of BT-CS-Cdots at 37°C for 24 h for loading of 5-FU into it. The solution was centrifuged at 16,000 rpm to collect the drug loaded nanoparticle pellets, which were then stored at 4°C.

6.2.7. Drug loading efficiency

The drug loading efficiency on the nanoparticles was determined by measuring the amount of drug on supernatant of the centrifuged FU-BT-CS-Cdots. The UV-Visible absorbance of the supernatant was determined at a wavelength of 266 nm, and using the calibration curve of 5-FU, the amount of drug was determined.

6.2.8. *In vitro* drug release study

The *in vitro* release of 5-FU from FU- BT-CS-Cdots was done by dissolving a known amount of drug loaded nanoparticles in a PBS buffer of pH 7.4. The suspension was transferred to the dialysis membrane (MW cutoff 1 kDa) and immersed in 20 ml of PBS buffer maintained under constant stirring. At the chosen time interval, 500 µL aliquot of sample was taken out and replaced with the same quantity of fresh PBS buffer. The collected aliquots were analyzed spectrophotometrically at 266 nm, and the percentage of drug release was calculated using a standard calibration curve of pure 5-FU.

6.2.9. UV-Visible spectroscopy

The drug loading efficiency and drug release percentage was determined by UV-Visible spectroscopy at room temperature using Agilent Carry 100 UV-Visible spectrophotometer

6.2.10. Fluorescence spectroscopy

The fluorescence intensity of 1mg/ml concentration of all the ratios of CS-Cdots in water was analyzed by using Horiba Scientific Fluoromax-4 Spectrofluorometer.

6.2.11. FTIR spectroscopy

The FTIR spectra of CS-Cdots, BT-NHS, BT-CS-Cdots, and FU-BT-CS-Cdots were recorded on Perkin Elmer Spectrum 2 FTIR spectrometer at room temperature using KBr pellet, over a frequency range of 4000-400 cm^{-1}.

6.2.12. FETEM

The particle size of the CS-Cdots (1:1.5) was determined by Jeol 2100F Field Emission Transmission Electron Microscope. For the analysis, a droplet of dilute carbon dot solution was cast on a copper grid without being stained. The excess liquid was removed by touching the edge of the copper grid with a small piece of filter paper and further dried overnight in a desiccator.

6.2.13. Powder XRD

The crystallinity of the CS-Cdots (1:1.5) was determined by powder XRD using Rigaku SmartLab 9 kW X-ray diffractometer fitted with CuK_{α} radiation of λ=1.54 Å in a 2θ range of 5-60°.

6.3. Results and Discussions

6.3.1. Synthesis of BT-CS-Cdots

The Cdots were synthesized by pyrolysis and green synthesis method using LMWC and SF as the precursor and no other toxic chemicals. The amine-functionalized CS-Cdots were formed by the carbonization of the mixture for covalent attachment of carboxylic acid group-containing molecules. Biotin was covalently attached to the CS-Cdots using an amide coupling mechanism. The free carboxyl group of biotin was attached to the free amino group of CS-Cdots by forming biotin-NHS ester. In a typical NHS ester synthesis, one-pot DCC coupling is followed.

As shown in **Scheme 6.1**, biotin **(1)** reacts with DCC **(2)** to form an *O*-acylisourea intermediate **(3)** after a nucleophilic attack of the carboxyl group of biotin on the carbodiimide carbon of DCC. The NHS **(4)** reacts with the *O*-acylisourea intermediate to form biotin-NHS **(5)** and a byproduct dicyclohexylurea **(6)**, which is insoluble in DMF, so

can be easily separated by filtration. Then **(5)** reacts with the free amino group of CS-dots to form BT-CS-Cdots **(7).**

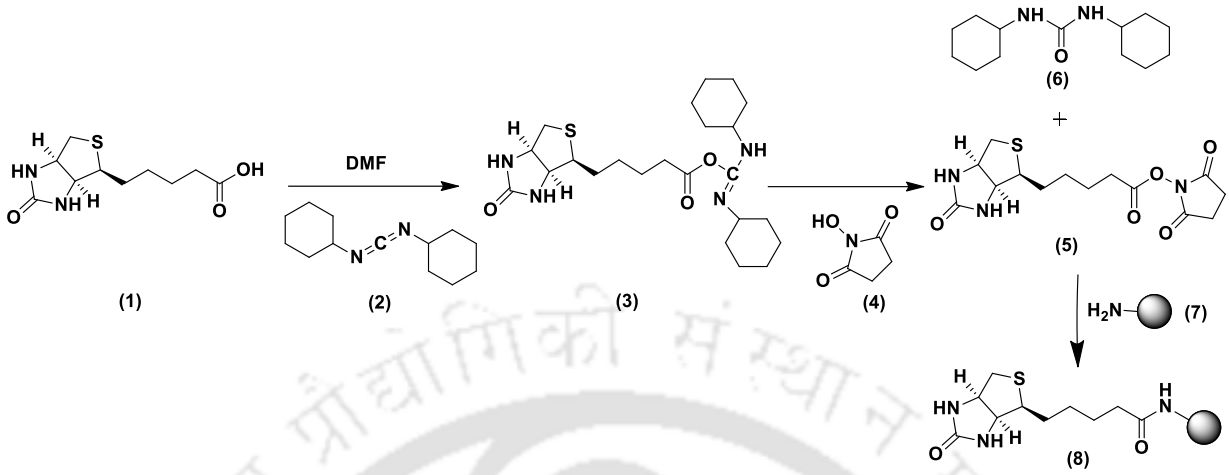

Scheme 6.1 Stepwise synthesis of biotin-NHS and BT-CS-Cdots.

6.3.2. Characterization of the CS-Cdots

(A) Optical Properties of the CS-Cdots

The CS-Cdots of different ratios were analyzed under daylight and UV-lamp of wavelength 365 nm. They were colorless to light yellow in daylight depending upon the ratios, as shown in **Figure 6.1 (A)**, while showed bright blue color after excitation by UV lamp shown in **Figure 6.1 (B)**.

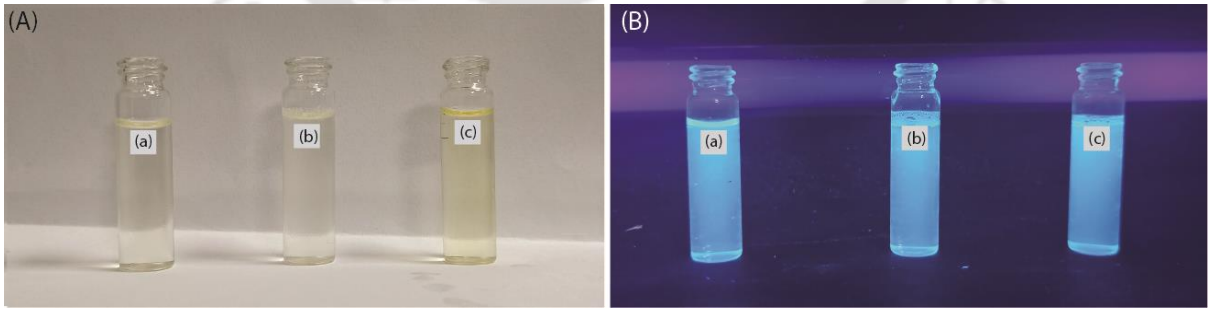

Figure 6.1 Image of CS-Cdots of different ratios (a) 1:0.66, 1:1, and 1:1.5 under **(A)** daylight; **(B)** 365 nm UV light.

The fluorescence spectra of different ratios of CS-Cdots, i.e., 1:0, 1:0.66, 1:1, and 1:1.5, were recorded at an excitation wavelength of 350 nm, and the emission was checked from

360-650. It was observed that upon increasing the SF content, there was an increase in the CS-Cdot's fluorescence intensity. **Figure 6.2** shows the fluorescence spectra of different ratios of CS-Cdots. Since the intensity corresponding to the ratio of 1:1.5 was maximum, we have taken CS-Cdots (1:1.5) for our further studies.

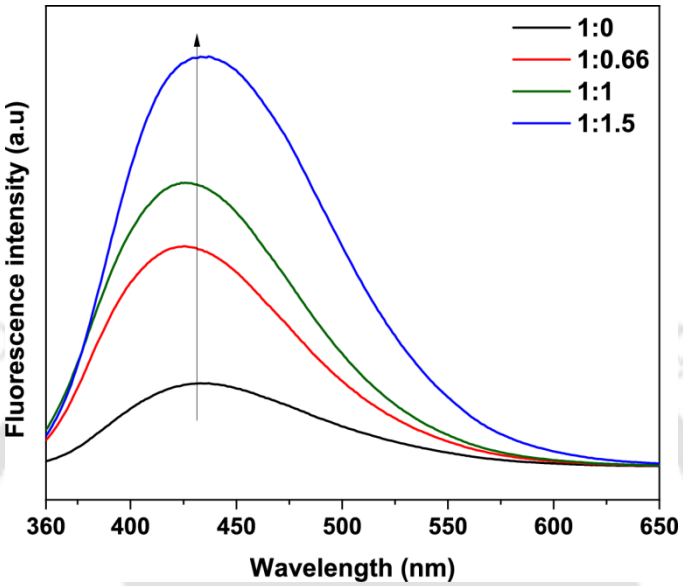

Figure 6.2 Plot of fluorescence intensity vs. emission wavelength of different ratios of CS-Cdots, showing an increase in the fluorescence intensity with SF content.

The quantum yield (φ) of the different ratios of CS-Cdots was determined with respect to fluorescein as the reference dye having φ value of 0.92 in 0.1N NaOH as reported by Magde *et al.* [268]. The Ψ was determined using the following formula in Eq. 6.1[269].

$$\boldsymbol{\varphi_x = \varphi_s\left(\frac{A_x}{A_s}\right)\left(\frac{E_s}{E_r}\right)\left(\frac{\eta_x}{\eta_{st}}\right)^2} \qquad \textbf{(Eq. 6.1)}$$

Where φ is the relative fluorescence quantum yield; A is the absorbance or optical density (OD) at the excitation wavelength; E is the integrated fluorescence intensity (calculated by trapezoidal rule using MATLAB); η is the refractive index of the solvent; Subscript 'x' and's' refers to the unknown and reference respectively.

The relative φ of the Cdots prepared from blank LMWC, and SF was obtained to be 15.67% and 43.88%, respectively. While the relative quantum yields of the Cdots from the mixtures

of various ratios of CS-Cdots, 1:0.66, 1:1, and 1:1.5 were 38.77%, 45.21%, and 65.69%. Thus, an increase in the value of relative φ can be seen in the Cdots formulated using the mixtures than Cdots prepared from the individual polymers. Moreover, there was an increase in the relative φ with SF content.

(B) Size of the CS-Cdots

The size of the CS-Cdots (1:1.5) was determined by FETEM analysis. From the FETEM micrograph in **Figure 6.3 (A)**, it's evident that the formed CS-Cdots were quasi-spherical in shape with a size of 3±1.5 nm. **Figure 6.3 (B)** shows the size distribution histogram (obtained using ImageJ software) of the carbon dots showing a very narrow particle size distribution.

(C) Powder XRD

The powder XRD pattern of the CS-Cdots (1:1.5) shown in **Figure 6.3 (C)** presents a broad amorphous peak at 2θ=22.14° attributed to highly disordered carbon atoms[263,270].

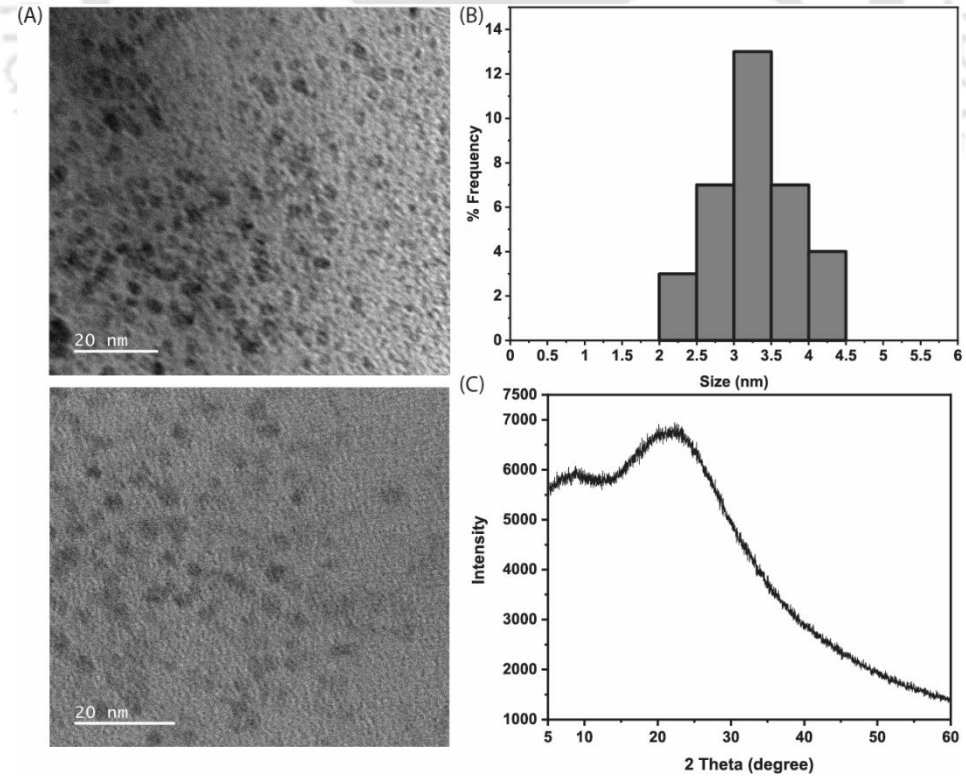

Figure 6.3 (A) FETEM micrographs of CS-Cdots (1:1.5); **(B)** Size distribution histogram; **(C)** XRD pattern of CS-Cdots (1:1.5).

6.3.3. Determination of formation of BT-CS-Cdots and drug loading

The FTIR spectrum of CS-Cdots (1:1.5) is shown in **Figure 6.4 (B)**. The peak at 3293 cm^{-1} is assigned to the stretching vibration of amine ($-NH_2$) and hydroxyl (O-H) group. The peak at 1654 cm^{-1} is due to amide I (C=O stretching), and 1534 due to amide II (N-H bending). Thus, showing the formation of amine-functionalized Cdots. The FTIR spectrum of BT-NHS is presented in **Figure 6.4 (A)**. The peak at 3246 cm^{-1} is for N-H stretching, 2925 cm^{-1} is for C-H stretching, 1831-1701 cm^{-1} is due to C=O stretching, 1475, and 1369 cm^{-1} is for C-H and N-H, 1202 cm^{-1} is for ester N-O and 1072 cm^{-1} for ester C-O[271]. In the FTIR spectrum of BT-CS-Cdots in **Figure 6.4 (C)**, the peak at 3246 cm^{-1} is due to N-H stretching, 2925 cm^{-1} is for C-H stretching of biotin, 1689 cm^{-1} is for C=O stretching, 1558 cm^{-1} is due to N-H bending vibration of the new amide bond formation and1024 cm^{-1} is for ester N-O of biotin. This presence of the peaks of biotin in BT-CS-Cdots confirms the conjugation. The FTIR spectrum of FU- BT-CS-Cdots is shown in **Figure 6.4 (D),** which shows peaks of CS-Cdots along with peaks of C-F stretching vibration of 5-FU, confirming the loading of the drug on it.

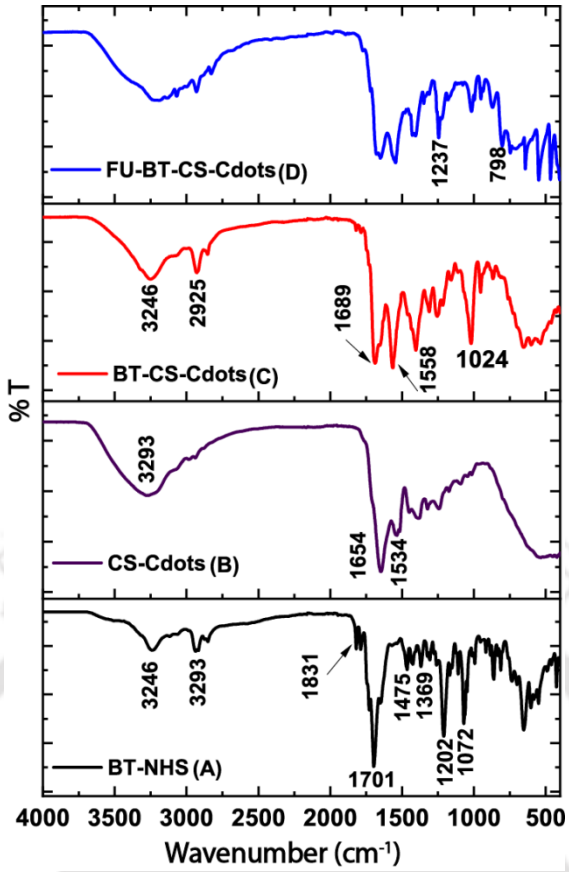

Figure 6.4 Stacked FTIR spectra of **(A)** BT-NHS; **(B)** CS-Cdots; **(C)** BT-CS-Cdots; **(D)** FU-BT-CS-Cdots.

6.3.4. Drug loading efficiency

The drug loading efficiency was calculated to be 97 %. The following equation was used to calculate the drug loading efficiency.

$$\boldsymbol{Drug\ loading\ efficiency}(\%) = \left(\frac{\boldsymbol{amount\ of\ drug\ fed\ initially - amount\ of\ drug\ in\ supernatant}}{\boldsymbol{amount\ of\ drug\ fed\ initially}}\right) \times \mathbf{100}$$

6.3.5. *In vitro* drug release study

The *in vitro* release curve of 5-FU from FU-BT-CS-Cdots is shown in **Figure 6.5.** The release of 5-FU from the Cdots was done in triplicates, and the error was estimated from the standard deviation using origin. A uniform release of drugs from the nanoparticles can be

seen. The percentage drug release was found to be 81% after 36 h. The equation used for calculation is as follows:

$$\textbf{\textit{Perecentage of Drug release}} = \frac{\textbf{\textit{Amount of drug released at time 't'}}}{\textbf{\textit{Total drug content}}} \times \mathbf{100\%}$$

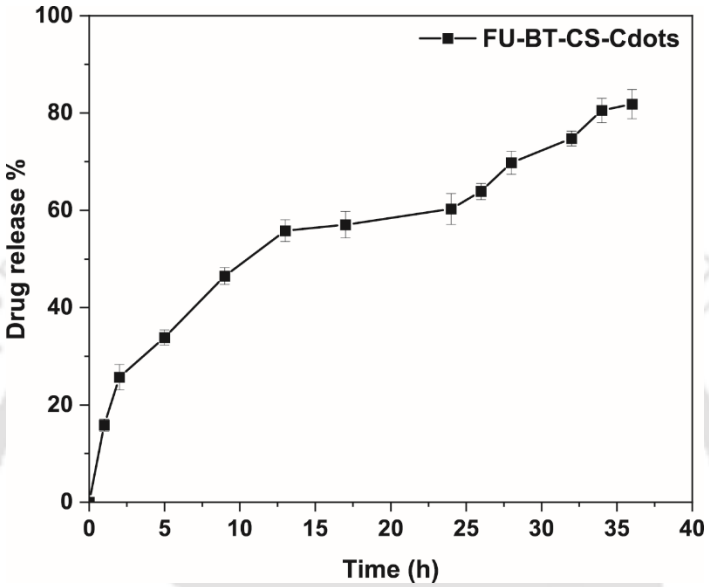

Figure 6.5 Percentage of drug release from FU-BT-CS-Cdots with time.

6.4. Conclusions

Cdots-based drug carriers can provide exceptional properties for drug delivery. They are highly biocompatible, easily functionalized, and possess tunable fluorescence properties that can be utilized for cell imaging. LMWC-SF based Cdots were successfully synthesized, which was confirmed by fluorescence spectroscopy. The size of the nanoparticles, as obtained by FETEM, was 3±1.5 nm. It was observed that the Cdots formulated using the LMWC and SF mixture possess high fluorescence intensity as well as relative quantum yield compared to the Cdots prepared from blank LMWC and SF. Upon increasing the SF content, there was an enhancement in fluorescence properties. The conjugation of biotin and loading of 5-FU to the Cdots was confirmed by FTIR spectroscopy. The biomaterial possess high

fluorescence properties with conjugated cell-targeting moiety, thus can be effective for targeted drug delivery of anti-cancer agents and cancer cell imaging.

6.5. Individual FTIR spectra

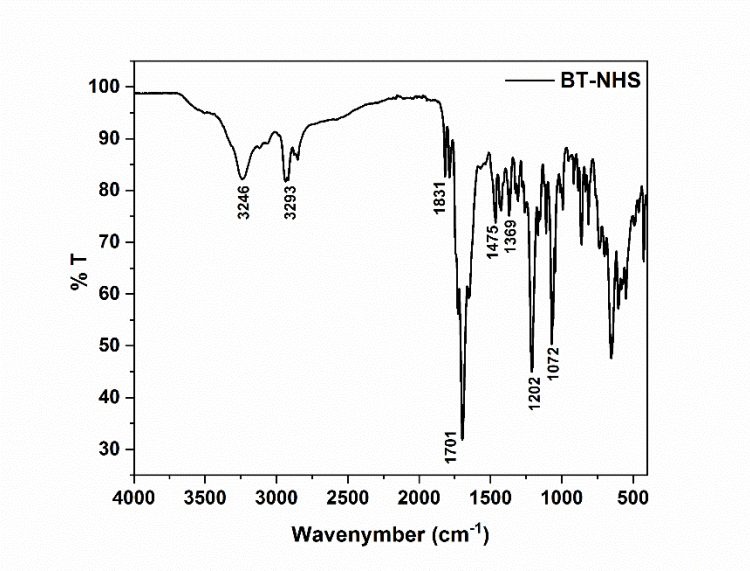

Figure 6.6 FTIR spectra of BT-NHS

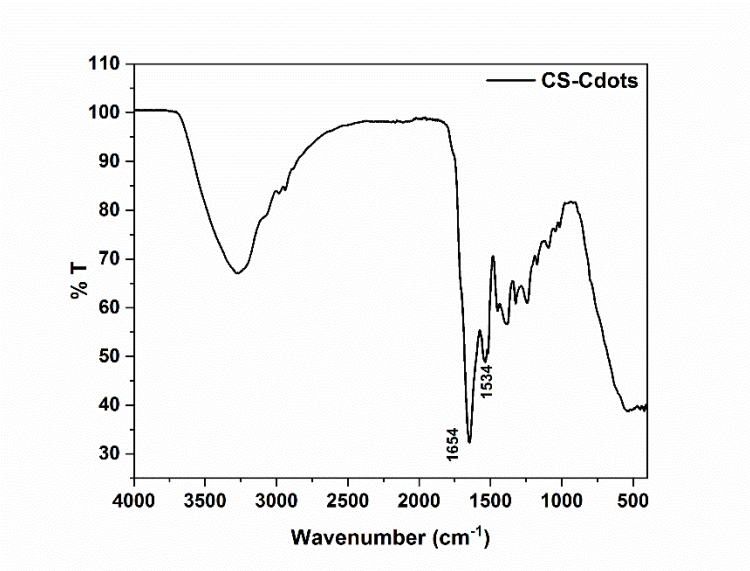

Figure 6.7 FTIR spectra of CS-Cdots

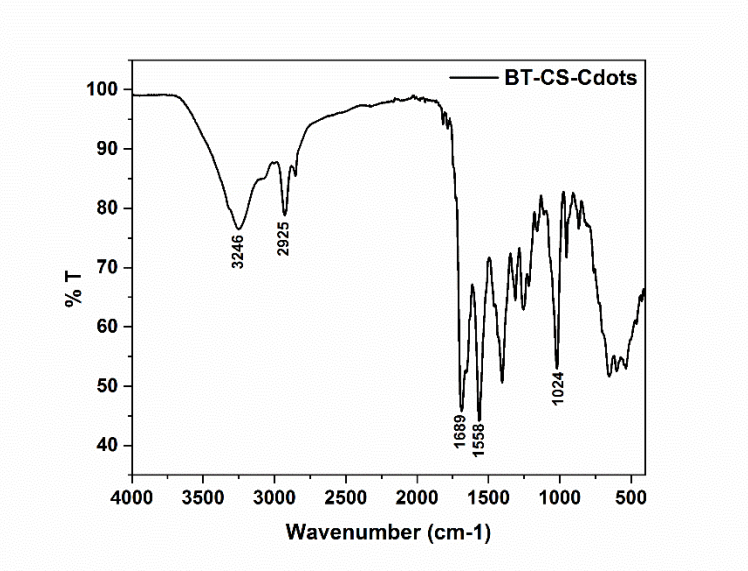

Figure 6.8 FTIR spectra of BT-CS-Cdots

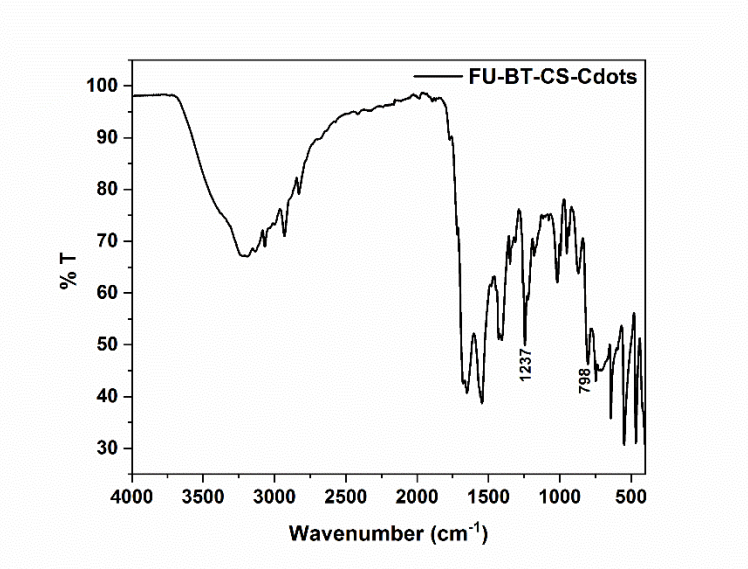

Figure 6.9 FTIR spectra of FU-BT-CS-Cdots

Chapter 7 Summary and Future prospects

7.1. Research Summary

In the field of design and development of drug delivery systems for anti-cancer drugs, nanomaterials mediated techniques have proved to be a very efficient approach. Mainly, the nanoparticles derived from biopolymers, using the polymer as the precursor, reducing agents, or coating agent, have been found to possess remarkable properties that are essential for a drug delivery tool. Without compromising the cost-effectiveness, various desirable properties like biocompatibility, cell penetrability, functionalization properties, drug loading capacities, etc., can be easily achieved.

We have developed different types of chitosan and SF based nanomaterials and coating materials for controlled and targeted delivery of anti-cancer drugs. We have synthesized a photo-controlled drug delivery nanocarrier that can deliver 5-FU only when it is exposed to the light of a particular wavelength. We have also synthesized an enzyme-prodrug combinatorial system of 5-FC and CD enzyme, where 5-FC acts as a prodrug that, upon the action of CD, gets converted to 5-FU, an active antitumor agent. Chitosan-based silver nanoparticles were used as the carrier of 5-FC for this study. Similarly, we have also developed chitosan-based gold nanoparticles and microparticles for targeted and sustained release of DOX. The SF coating proves to provide an effective diffusion barrier to the drugs, thus, helping in sustained and long-term drug release. Moreover, it provided a site for functionalization, which is helpful in attaching cell-targeting moieties. Biotin conjugated Cdots has been developed, where the Cdots with high fluorescence and quantum yield was obtained by chitosan and silk mixture. The percentage drug release profile from all the materials has been studied. The materials were also tested for their cell-cytotoxicity in cancer cell lines. Overall, our experimental results showed that the materials produced can be an effective therapeutic tool.

7.2. Future prospects

The investigations carried out in this thesis work include synthesis, characterization, and cell cytotoxicity study of chitosan and SF-derived nanomaterials. However, more modifications and studies can be done for their effective use as a chemotherapeutic tool. We would like to propose some points to be addressed in the next steps of research as delineated below.

(a) The 5-FU-linker-LMWC conjugate formed hydrogel and DMSO gel. The gel properties and drug release profile from the gel can be studied, which will be useful for photo-controlled delivery of anti-cancer drugs for skin cancers. Its film-forming properties can also be examined for the formulation of photo-controlled patches.

(b) 5-FC loaded silver nanoparticles can be made target specific by attaching some cell-targeting moieties like folic acid and biotin by chemical modifications. Other types of biopolymer derived nanomaterials can also be explored, substituting the silver nanoparticles.

(c) The swelling behavior or crosslinking densities can be studied for both the 5-FU-linker-LMWC conjugate hydrogel and CAu-DOX beads at different pH.

(d) The kinetics of aggregation can be studied for all the synthesized nanoparticles for analyzing their stability.

(e) A comparative study to analyze the effect of particle size on drug release kinetics can be done.

(f) The MTT assay and cell imaging studies of biotin-conjugated SF-LMWC can be done to check the efficiency of biotin as a targeting moiety.

(g) Animal model studies can be done for the synthesized materials.

Bibliography

(1) Cooper, Geoffrey M., and R. E. H. The Development and Causes of Cancer. In *The Cell: A Molecular Approach.*; 2000.

(2) Longley, D. B.; Harkin, D. P.; Johnston, P. G. 5-Fluorouracil: Mechanisms of Action and Clinical Strategies. *Nat. Rev. Cancer* **2003**, *3* (5), 330–338.

(3) Paolino, D.; Cosco, D.; Muzzalupo, R.; Trapasso, E.; Picci, N.; Fresta, M. Innovative Bola-Surfactant Niosomes as Topical Delivery Systems of 5-Fluorouracil for the Treatment of Skin Cancer. *pharmeceutical Nanotechnol.* **2008**, *353* (1–2), 233–242.

(4) Rocha, P. R. S.; Ph, D.; Rodrigues, M. A. G. Modified Therapy with 5-Fluorouracil , Doxorubicin , and Methotrexate in Advanced Gastric Cancer. *Cancer* **1993**, *72* (1), 37–41.

(5) Moertel, C. G., Frytak, S., Hahn, R. G., O'Connell, M. J., Reitemeier, R. J., Rubin, J.,& Lavin, P. T. Therapy of Locally Unresectable Pancreatic Carcinoma: A Randomized Comparison of High Dose (6000 Rads) Radiation Alone, Moderate Dose Radiation (4000 Rads + 5-Fluorouracil), and High Dose Radiation + 5-Fluorouracil. *Cancer* **1973**, *48* (8), 1705–1710.

(6) Prados, J.; Melguizo, C.; Ortiz, R.; Vélez, C.; Alvarez, P. J.; Arias, J. L.; Ruíz, M. A.; Gallardo, V.; Aranega, A. Doxorubicin-Loaded Nanoparticles : New Advances in Breast Cancer Therapy. *Anti-Cancer Agents Med. Chem. (Formerly Curr. Med. Chem. Agents)* **2012**, *12* (9), 1058–1070.

(7) Hong, Y.; Che, S.; Hui, B.; Yang, Y.; Wang, X.; Zhang, X. Biomedicine & Pharmacotherapy Lung Cancer Therapy Using Doxorubicin and Curcumin Combination : Targeted Prodrug Based , PH Sensitive Nanomedicine. *Biomed. Pharmacother.* **2019**, *112* (277), 108614.

(8) Green, A. E.; Rose, P. G. Pegylated Liposomal Doxorubicin in Ovarian Cancer. **2006**,

1 (3), 229–239.

(9) Lee, C. S.; Kim, H.; Yu, J.; Yu, S. H.; Ban, S.; Oh, S.; Jeong, D.; Im, J.; Baek, M. J.; Kim, T. H. Doxorubicin-Loaded Oligonucleotide Conjugated Gold Nanoparticles: A Promising in Vivo Drug Delivery System for Colorectal Cancer Therapy. *Eur. J. Med. Chem.* **2017**, *142*, 416–423.

(10) Kumari, A.; Yadav, S. K.; Yadav, S. C. Biodegradable Polymeric Nanoparticles Based Drug Delivery Systems. *Colloids Surfaces B Biointerfaces* **2010**, *75* (1), 1–18.

(11) Patel, A. G.; Kaufmann, S. H. Cancer: How Does Doxorubicin Work? *Elife* **2012**, *1*, 2011–2013.

(12) Tacar, O.; Sriamornsak, P.; Dass, C. R. Doxorubicin: An Update on Anticancer Molecular Action, Toxicity and Novel Drug Delivery Systems. *J. Pharm. Pharmacol.* **2012**, *65* (2), 157–170.

(13) Senter, P. D.; Su, P. C. D.; Katsuragi, T.; Sakai, T.; Cosand, W. L.; Hellstrom, I.; Hellstrom, K. E. Generation of 5-Fluorouracil from 5-Fluorocytosine by Monoclonal Antibody-Cytosine Deaminase Conjugates. *Bioconjugate Chem.* **1991**, *2* (6), 447–451.

(14) Doppalapudi, S.; Jain, A.; Domb, A. J.; Khan, W. Biodegradable Polymers for Targeted Delivery of Anti-Cancer Drugs. *Expert Opin. Drug Deliv.* **2016**, *13* (6), 1–19.

(15) Lin, R.; Ng, L. S.; Wang, C. H. In Vitro Study of Anticancer Drug Doxorubicin in PLGA-Based Microparticles. *Biomaterials* **2005**, *26* (21), 4476–4485.

(16) Chuen-Chang Lin & Chun-Hsien Fu. Controlled Release Study of 5-Fluorouracil-Loaded Chitosan/Polyethylene Glycol Microparticles. *Drug Deliv.* **2009**, *16* (5), 274–279.

(17) Wicki, A.; Witzigmann, D.; Balasubramanian, V.; Huwyler, J. Nanomedicine in Cancer Therapy: Challenges, Opportunities, and Clinical Applications. *J. Control. Release* **2015**, *200*, 138–157.

(18) Zeeshan, A.; Farhan, M.; Siddiqui, A. Nanomedicine and Drug Delivery : A Mini

Review. *Int. Nano Lett.* **2014**, *4* (1), 94.

(19) Joncour, V. Le; Laakkonen, P. Bioorganic & Medicinal Chemistry Seek & Destroy , Use of Targeting Peptides for Cancer Detection and Drug Delivery. *Bioorg. Med. Chem.* **2018**, *26* (10), 2797–2806.

(20) Zhang, X.; Eden, H. S.; Chen, X. Peptides in Cancer Nanomedicine : Drug Carriers , Targeting Ligands and Protease Substrates. *J. Control. Release* **2012**, *159* (1), 2–13.

(21) Park, J.; Cho, H.; Yeol, H.; Yoon, I.; Ko, S.; Shim, J.; Cho, J.; Hyung, J.; Kim, K.; Chan, I.; et al. Hyaluronic Acid Derivative-Coated Nanohybrid Liposomes for Cancer Imaging and Drug Delivery. *J. Control. Release* **2014**, *174*, 98–108.

(22) Patri, A. K.; Kukowska-latallo, J. F.; Jr, J. R. B. Targeted Drug Delivery with Dendrimers : Comparison of the Release Kinetics of Covalently Conjugated Drug and Non-Covalent Drug Inclusion Complex. *Adv. Drug Deliv. Rev.* **2005**, *57* (15), 2203–2214.

(23) Ranger, M.; Leroux, J. Micelles in Anticancer Drug Delivery. *Am. J. Drug Deliv.* **2004**, *2* (1), 15–42.

(24) Sadeghi-Varkani, Atina; Emam-Djomeh, Zahra; Askari, G. Physicochemical and Microstructural Properties of a Novel Edible Film Synthesized from Balangu Seed Mucilage. *Int. J. Biol. Macromol.* **2018**, *108*, 1110–1119.

(25) Quiñones, J. P.; Peniche, H.; Peniche, C. Chitosan Based Self-Assembled Nanoparticles in Drug Delivery. *Polymers (Basel).* **2018**, *10* (3), 235.

(26) Bhumkar, D. R.; Joshi, H. M.; Sastry, M.; Pokharkar, V. B. Chitosan Reduced Gold Nanoparticles as Novel Carriers for Transmucosal Delivery of Insulin. *Pharm. Res.* **2007**, *24* (8), 1415–1426.

(27) Zhao, Q. S.; Cheng, X. J.; Ji, Q. X.; Kang, C. Z.; Chen, X. G. Effect of Organic and Inorganic Acids on Chitosan/Glycerophosphate Thermosensitive Hydrogel. *J. sol-gel*

Sci. Technol. **2009**, *50* (1), 111–118.

(28) Bhattarai, N.; Gunn, J.; Zhang, M. Chitosan-Based Hydrogels for Controlled, Localized Drug Delivery. *Adv. Drug Deliv. Rev.* **2010**, *62* (1), 83–99.

(29) Nivethaa, E. A. K.; Dhanavel, S.; Rebekah, A.; Narayanan, V.; Stephen, A. A Comparative Study of 5-Fluorouracil Release from Chitosan/Silver and Chitosan/Silver/MWCNT Nanocomposites and Their Cytotoxicity towards MCF-7. *Mater. Sci. Eng. C* **2016**, *66*, 244–250.

(30) Annur, D.; Wang, Z.; Liao, J.; Kuo, C. Plasma-Synthesized Silver Nanoparticles on Electrospun Chitosan Nano Fi Ber Surfaces for Antibacterial Applications. *Biomacromolecules* **2015**, *16* (10), 3248–3255.

(31) Jaiswal, A.; Chattopadhyay, A.; Sankar, S. Functional Chitosan Nanocarriers for Potential Applications in Gene Therapy. *Mater. Lett.* **2012**, *68*, 261–264.

(32) Agnihotri, S. A.; Mallikarjuna, N. N.; Aminabhavi, T. M. Recent Advances on Chitosan-Based Micro- and Nanoparticles in Drug Delivery. *J. Control. Release* **2004**, *100* (1), 5–28.

(33) Cheng, L.; Ma, H.; Shao, M.; Fan, Q.; Lv, H.; Peng, J.; Hao, T.; Li, D.; Zhao, C.; Zong, X. Synthesis of Folate-Chitosan Nanoparticles Loaded with Ligustrazine to Target Folate Receptor Positive Cancer Cells. *Mol. Med. Rep.* **2017**, *16* (2), 1101–1108.

(34) Prabaharan, M.; Mano, J. F. Chitosan-Based Particles as Controlled Drug Delivery Systems. *Drug Deliv. J. Deliv. Target. Ther. Agents* **2005**, *12* (1), 41–57.

(35) Sinha, V. R.; Singla, A. K.; Wadhawan, S.; Kaushik, R.; Kumria, R.; Bansal, K.; Dhawan, S. Chitosan Microspheres as a Potential Carrier for Drugs. *Int. J. Pharm.* **2004**, *274* (1–2), 1–33.

(36) Science, B.; Edition, P.; Yallapu, M.; Technology, C.; Govt, B. Fabrication , Characterization of Chitosan / Nanosilver Film and Its Potential Antibacterial

Application. *J. Biomater. Sci. Polym. Ed.* **2009**, *20* (14), 2129–2144.

(37) Vimala, K.; Mohan, Y. M.; Sivudu, K. S.; Varaprasad, K.; Ravindra, S.; Reddy, N. N.; Padma, Y.; Sreedhar, B.; MohanaRaju, K. Fabrication of Porous Chitosan Films Impregnated with Silver Nanoparticles: A Facile Approach for Superior Antibacterial Application. *Colloids Surfaces B Biointerfaces* **2010**, *76* (1), 248–258.

(38) Ligler, F. S.; Lingerfelt, B. M.; Price, R. P.; Schoen, P. E. Development of Uniform Chitosan Thin-Film Layers on Silicon Chips. *Langmuir* **2001**, *17* (16), 5082–5084.

(39) Lei, L.; Liu, X.; Guo, S.; Tang, M.; Cheng, L.; Tian, L. 5-Fluorouracil-Loaded Multilayered Films for Drug Controlled Releasing Stent Application: Drug Release, Microstructure, and Ex Vivo Permeation Behaviors. *J. Control. Release* **2010**, *146* (1), 45–53.

(40) Reddy, A. B.; Manjula, B.; Jayaramudu, T.; Sadiku, E. R.; Anand Babu, P.; Periyar Selvam, S. 5-Fluorouracil Loaded Chitosan–PVA/Na+MMT Nanocomposite Films for Drug Release and Antimicrobial Activity. *Nano-Micro Lett.* **2016**, *8* (3), 260–269.

(41) Leceta, I.; Guerrero, P.; Caba, K. De. Functional Properties of Chitosan-Based Films. *Carbohydr. Polym.* **2013**, *93* (1), 339–346.

(42) Sun, J.; Perry, S. L.; Schi, J. D. Electrospinning Nano Fi Bers from Chitosan/Hyaluronic Acid Complex Coacervates. *Biomacromolecules* **2019**, *20* (11), 4191–4198.

(43) Ohkawa, K., Minato, K.I., Kumagai, G., Hayashi, S. and Yamamoto, H. Chitosan Nanofiber. *Biomacromolecules* **2006**, *7* (11), 3291–3294.

(44) Buranachai, T.; Praphairaksit, N.; Muangsin, N. Chitosan/Polyethylene Glycol Beads Crosslinked with Tripolyphosphate and Glutaraldehyde for Gastrointestinal Drug Delivery. *AAPS PharmSciTech* **2010**, *11* (3), 1128–1137.

(45) Fujiwara, K.; Ramesh, A.; Maki, T.; Hasegawa, H.; Ueda, K. Adsorption of Platinum

(IV), Palladium (II) and Gold (III) from Aqueous Solutions onto l-Lysine Modified Crosslinked Chitosan Resin. *J. Hazard. Mater.* **2007**, *146* (1–2), 39–50.

(46) Tsai, W. B.; Chen, Y. R.; Liu, H. L.; Lai, J. Y. Fabrication of UV-Crosslinked Chitosan Scaffolds with Conjugation of RGD Peptides for Bone Tissue Engineering. *Carbohydr. Polym.* **2011**, *85* (1), 129–137.

(47) Madhusudhan, A.; Reddy, G. B.; Venkatesham, M.; Veerabhadram, G.; Kumar, A. D.; Natarajan, S.; Yang, M. Y.; Hu, A.; Singh, S. S. Efficient Ph Dependent Drug Delivery to Target Cancer Cells by Gold Nanoparticles Capped with Carboxymethyl Chitosan. *Int. J. Mol. Sci.* **2014**, *15* (5), 8216–8234.

(48) Song, J.; Zhao, L.; Wang, Y.; Xue, Y.; Deng, Y.; Zhao, X. Carbon Quantum Dots Prepared with Chitosan for Synthesis of CQDs / AuNPs for Iodine Ions Detection. *Nanomaterials* **2018**, *8* (12), 1043.

(49) Wang, B.; Chen, K.; Jiang, S.; Reincke, F.; Tong, W.; Wang, D.; Gao, C. Chitosan-Mediated Synthesis of Gold Nanoparticles on Patterned Poly(Dimethylsiloxane) Surfaces. *Biomacromolecules* **2006**, *7* (4), 1203–1209.

(50) Twu, Y.-K.; Chen, Y.-W.; Shih, C.-M. Preparation of Silver Nanoparticles Using Chitosan Suspensions. *Powder Technol.* **2008**, *185* (3), 251–257.

(51) Zhang, C.; Cheng, Y.; Qu, G.; Wu, X.; Ding, Y.; Cheng, Z. Preparation and Characterization of Galactosylated Chitosan Coated BSA Microspheres Containing 5-Fluorouracil. *Carbohydr. Polym.* **2008**, *72* (3), 390–397.

(52) Nagarwal, R. C.; Kumar, R.; Pandit, J. K. European Journal of Pharmaceutical Sciences Chitosan Coated Sodium Alginate – Chitosan Nanoparticles Loaded with 5-FU for Ocular Delivery : In Vitro Characterization and in Vivo Study in Rabbit Eye. *Eur. J. Pharm. Sci.* **2012**, *47* (4), 678–685.

(53) Sutherland, T. D.; Young, J. H.; Weisman, S.; Hayashi, C. Y.; Merritt, D. J. Insect Silk : One Name , Many Materials. *Annu. Rev. Entomol.* **2010**, *55*, 171–188.

(54) Craig, C. L.; Hsu, M.; Kaplan, D.; Pierce, N. E. A Comparison of the Composition of Silk Proteins Produced by Spiders and Insects. *Int. J. Biol. Macromol.* **1999**, *24* (2–3), 109–118.

(55) Qi, Y.; Wang, H.; Wei, K.; Yang, Y.; Zheng, R.; Kim, I. S.; Zhang, K. A Review of Structure Construction of Silk Fibroin Biomaterials from Single Structures to Multi-Level Structures. *Int. J. Mol. Sci.* **2017**, *18* (3), 237.

(56) Amanda R. Murphya and David L. Kaplan. Biomedical Applications of Chemically-Modified Silk Fibroin. *J Mater Chem.* **2010**, *19* (36), 6443–6450.

(57) Rockwood, D. N.; Preda, R. C.; Yücel, T.; Wang, X.; Lovett, M. L.; Kaplan, D. L. Materials Fabrication from Bombyx Mori Silk Fibroin. *Nat Protoc.* **2013**, *6* (10), 1–43.

(58) Melke, J.; Midha, S.; Ghosh, S.; Ito, K.; Hofmann, S. Silk Fibroin as Biomaterial for Bone Tissue Engineering. *Acta Biomater.* **2016**, *31*, 1–16.

(59) Mao, B.; Liu, C.; Zheng, W.; Li, X.; Ge, R.; Shen, H.; Guo, X.; Lian, Q.; Shen, X.; Li, C. Cyclic CRGDfk Peptide and Chlorin E6 Functionalized Silk Fibroin Nanoparticles for Targeted Drug Delivery and Photodynamic Therapy. *Biomaterials* **2018**, *161*, 306–320.

(60) Nathwani, B. B.; Jaffari, M.; Juriani, A. R.; Mathur, A. B.; Meissner, K. E. Fabrication and Characterization of Silk-Fibroin-Coated Quantum Dots. *IEEE Trans. Nanobioscience* **2009**, *8* (1), 72–77.

(61) Kasoju, N.; Bora, U. Silk Fibroin in Tissue Engineering. *Adv. Healthc. Mater.* **2012**, *1* (4), 393–412.

(62) Zeng, D.; Cao, L. Enhanced Bone Regeneration of the Silk Fibroin Electrospun Scaffolds through the Modification of the Graphene Oxide Functionalized by BMP-2 Peptide. *Int. J. Nanomedicine* **2019**, *14*, 733–751.

(63) Weng, J.; Zhang, Z.; Sun, L.; An, J. Biosensors and Bioelectronics High Sensitive

Detection of Cancer Cell with a Folic Acid-Based Boron-Doped Diamond Electrode Using an AC Impedimetric Approach. *Biosens. Bioelectron.* **2011**, *26* (5), 1847–1852.

(64) Melo, B. A. G. De; Jodat, Y. A.; Mehrotra, S.; Calabrese, M. A.; Kamperman, T.; Mandal, B. B.; Santana, M. H. A.; Alsberg, E.; Leijten, J. 3D Printed Cartilage-Like Tissue Constructs with Spatially Controlled Mechanical Properties. *Adv. Funct. Mater.* **2019**, *29* (51), 1906330.

(65) Azharuddin, M.; Zhu, G. H.; Das, D.; Patra, H. K. ChemComm A Repertoire of Biomedical Applications of Noble Metal Nanoparticles. *Chem. Commun.* **2019**, *55* (49), 6964–6996.

(66) Horan, R. L.; Toponarski, I.; Boepple, H. E.; Weitzel, P. P.; Richmond, J. C.; Altman, G. H. Design and Characterization of a Scaffold for Anterior Cruciate Ligament Engineering. *J. Knee Surg.* **2009**, *22* (1), 82–92.

(67) Ryong, C.; Yeo, I.; Eun, K.; Hun, J.; Jin, S.; Ho, W.; Min, B. Effect of Chitin / Silk Fibroin Nanofibrous Bicomponent Structures on Interaction with Human Epidermal Keratinocytes. *Int. J. Biol. Macromol.* **2008**, *42* (4), 324–334.

(68) Barreiro-Iglesias, R.; Coronilla, R.; Concheiro, A.; Alvarez-Lorenzo, C. Preparation of Chitosan Beads by Simultaneous Cross-Linking/ Insolubilisation in Basic PH: Rheological Optimisation and Drug Loading/Release Behaviour. *Eur. J. Pharm. Sci.* **2005**, *24* (1), 77–84.

(69) Ren, Y.; Zhou, Z.; Liu, B.; Xu, Q.; Cui, F. Preparation and Characterization of Fibroin / Hyaluronic Acid Composite Scaffold. *Int. J. Biol. Macromol.* **2009**, *44* (4), 372–378.

(70) Yang, Y.; Chen, X.; Ding, F.; Zhang, P.; Liu, J.; Ã, X. G. Biocompatibility Evaluation of Silk Fibroin with Peripheral Nerve Tissues and Cells in Vitro. *Biomaterials* **2007**, *28* (9), 1643–1652.

(71) Yun, Y. H.; Lee, B. K.; Park, K.; Lafayette, W. Controlled Drug Delivery: Historical Perspective for the next Generation. *J. Control. Release* **2016**, *219*, 2–7.

(72) Palanikumar, L.; Al-hosani, S.; Kalmouni, M.; Nguyen, V. P.; Barrera, F. N.; Magzoub, M. PH-Responsive High Stability Polymeric Nanoparticles for Targeted Delivery of Anticancer Therapeutics. *Commun. Biol.* **2020**, *3* (1), 1–17.

(73) Zheng, Y.; Wang, L.; Lu, L.; Wang, Q.; Benicewicz, B. C. PH and Thermal Dual-Responsive Nanoparticles for Controlled Drug Delivery with High Loading Content. *ACS Omega* **2017**, *2* (7), 3399–3405.

(74) Vivek, R.; Nipun Babu, V.; Thangam, R.; Subramanian, K. S.; Kannan, S. PH-Responsive Drug Delivery of Chitosan Nanoparticles as Tamoxifen Carriers for Effective Anti-Tumor Activity in Breast Cancer Cells. *Colloids Surfaces B Biointerfaces* **2013**, *111*, 117–123.

(75) Woraphatphadung, T.; Sajomsang, W.; Rojanarata, T.; Ngawhirunpat, T.; Tonglairoum, P.; Opanasopit, P. Development of Chitosan-Based PH-Sensitive Polymeric Micelles Containing Curcumin for Colon-Targeted Drug Delivery. *AAPS PharmSciTech* **2017**, *19* (3), 991–1000.

(76) Wu, H.; Liu, S.; Xiao, L.; Dong, X.; Lu, Q.; Kaplan, D. L. Injectable and PH-Responsive Silk Nanofiber Hydrogels for Sustained Anticancer Drug Delivery. *ACS Appl. Mater. Interfaces* **2016**, *8* (27), 17118–17126.

(77) Pang, X.; Jiang, Y.; Xiao, Q.; Leung, A. W.; Hua, H.; Xu, C. PH-Responsive Polymer – Drug Conjugates : Design and Progress. *J. Control. Release* **2016**, *222*, 116–129.

(78) Dhara, D. Photoresponsive Block Copolymer Prodrug Nanoparticles as Delivery Vehicle for Single and Dual Anticancer Drugs. *ACS omega* **2017**, *2* (10), 6677–6690.

(79) Meng, L.; Huang, W.; Wang, D.; Huang, X.; Zhu, X.; Yan, D. Chitosan-Based Nanocarriers with PH and Light Dual Response for Anticancer Drug Delivery. *Biomacromolecules* **2013**, *14* (8), 2601–2610.

(80) Zhou, X.; Guo, L.; Shi, D.; Duan, S.; Li, J. Biocompatible Chitosan Nanobubbles for

Ultrasound-Mediated Targeted Delivery of Doxorubicin. *Nanoscale Res. Lett.* **2019**, *14* (1), 24.

(81) Fokong, S.; Theek, B.; Wu, Z.; Koczera, P.; Appold, L.; Jorge, S.; Resch-genger, U.; Zandvoort, M. Van; Storm, G.; Kiessling, F.; et al. Image-Guided , Targeted and Triggered Drug Delivery to Tumors Using Polymer-Based Microbubbles. *J. Control. Release* **2012**, *163* (1), 75–81.

(82) Min, H. S.; You, D. G.; Son, S.; Jeon, S.; Park, J. H.; Lee, S.; Chan, I.; Kim, K. Echogenic Glycol Chitosan Nanoparticles for Ultra- Sound-Triggered Cancer Theranostics. *Theranostics* **2015**, *5* (12), 1402.

(83) Gao, Z.; Fain, H. D.; Rapoport, N. Ultrasound-Enhanced Tumor Targeting of Polymeric Micellar Drug Carriers. *Mol. p* **2004**, *1* (4), 317–330.

(84) Patel, M. P.; Patel, R. R.; Patel, J. K. Chitosan Mediated Targeted Drug Delivery System: A Review. *J. Pharm. Pharm. Sci.* **2010**, *13* (4), 536–557.

(85) Van Vlerken, L. E.; Vyas, T. K.; Amiji, M. M. Poly(Ethylene Glycol)-Modified Nanocarriers for Tumor-Targeted and Intracellular Delivery. *Pharm. Res.* **2007**, *24* (8), 1405–1414.

(86) Yang, X.; Hong, H.; Grailer, J. J.; Rowland, I. J.; Javadi, A.; Hurley, S. A.; Xiao, Y.; Yang, Y.; Zhang, Y.; Nickles, R. J.; et al. Biomaterials Oxide Nanoparticles for Targeted Anticancer Drug Delivery and PET / MR Imaging. *Biomaterials* **2011**, *32* (17), 4151–4160.

(87) Shi, K.; Li, J.; Cao, Z.; Yang, P.; Qiu, Y.; Yang, B.; Wang, Y.; Long, Y.; Liu, Y.; Zhang, Q.; et al. A PH-Responsive Cell-Penetrating Peptide-Modi Fi Ed Liposomes with Active Recognizing of Integrin α v β 3 for the Treatment of Melanoma. *J. Control. Release* **2015**, *217*, 138–150.

(88) Wang, R.; Zhu, G.; Mei, L.; Xie, Y.; Ma, H.; Ye, M.; Qing, F. L.; Tan, W. Automated Modular Synthesis of Aptamer-Drug Conjugates for Targeted Drug Delivery. *J. Am.*

Chem. Soc. **2014**, *136* (7), 2731–2734.

(89) Emtiazi, G.; Zohrabi, T.; Lee, L. Y.; Habibi, N.; Zarrabi, A. Covalent Diphenylalanine Peptide Nanotube Conjugated to Folic Acid/Magnetic Nanoparticles for Anti-Cancer Drug Delivery. *J. Drug Deliv. Sci. Technol.* **2017**, *41*, 90–98.

(90) Nelson, E. E.; Guyer, A. E. Mechanism-Based Tumor-Targeting Drug Delivery System. Validation of Efficient Vitamin Receptor-Mediated Endocytosis and Drug Deliver. *Bioconjug. Chem.* **2012**, *1* (3), 233–245.

(91) Dash, T. K.; Konkimalla, V. B. Polymeric Modi Fi Cation and Its Implication in Drug Delivery : Poly- ε - Caprolactone (PCL) as a Model Polymer. *Mol. Pharm.* **2012**, *9* (9), 2365–2379.

(92) Arya, G.; Das, M.; Sahoo, S. K. Biomedicine & Pharmacotherapy Evaluation of Curcumin Loaded Chitosan / PEG Blended PLGA Nanoparticles for Effeective Treatment of Pancreatic Cancer. *Biomed. Pharmacother.* **2018**, *102*, 555–566.

(93) Parveen, S.; Sahoo, S. K. Long Circulating Chitosan/PEG Blended PLGA Nanoparticle for Tumor Drug Delivery. *Eur. J. Pharmacol.* **2011**, *670* (2–3), 372–383.

(94) Hadjianfar, Mehdi, Dariush Semnani, and J. V. Polycaprolactone/Chitosan Blend Nanofibers Loaded by 5-fluorouracil: An Approach to Anticancer Drug Delivery System. *Polym. Adv. Technol.* **2018**, *29* (12), 2972–2981.

(95) Alwaan, I.; Kadim, K. Starch-Chitosan Modified Blend as Long-Term Controlled Drug. *Pak. J. Biotechnol* **2018**, *15* (4), 947–955.

(96) Nivethaa, E. A. K.; Dhanavel, S.; Narayanan, V.; Vasu, C. A.; Stephen, A. An in Vitro Cytotoxicity Study of 5-Fluorouracil Encapsulated Chitosan/Gold Nanocomposites towards MCF-7 Cells. *RSC Adv.* **2015**, *5* (2), 1024–1032.

(97) Bothiraja, C.; Thorat, U. H.; Pawar, A. P.; Shaikh, K. S. Chitosan Coated Layered Clay Montmorillonite Nanocomposites Modulate Oral Delivery of Paclitaxel in

Colonic Cancer. *Mater. Technol.* **2014**, *29* (sup3), B120–B126.

(98) Jose L. Arias, L. H. R. and P. C. Fe3O4/Chitosan Nanocomposite for Magnetic Drug Targeting to Cancer. *J. Mater. Chem.* **2012**, *22* (15), 7622–7632.

(99) Zarouni, M., Salehi, R., Akbarzadeh, A., Samadi, N., Davaran, S., Ramezani, F., & Dariushnejad, H. Biocompatible Polymer Coated Paramagnetic Nanoparticles for Doxorubicin Delivery: Synthesis and Anticancer Effects Against Human Breast Cancer Cells. *Int. J. Polym. Mater. Biocompatible* **2015**, *64* (14), 718–726.

(100) Hazhir, N., Chekin, F., Raoof, J. B., & Fathi, S. A Porous Reduced Graphene Oxide/Chitosan-Based Nanocarrier as a Delivery System of Doxorubicin. *RSC Adv.* **2019**, *9* (53), 30729–30735.

(101) Salahuddin, N., Elbarbary, A. A., & Alkabes, H. A. Antibacterial and Anticancer Activity of Loaded Quinazolinone Polypyrrole/Chitosan Silver Chloride Nanocomposite. *Int. J. Polym. Mater. Polym. Biomater.* **2017**, *66* (6), 307–316.

(102) Hosseini, L.; Mahboobnia, K.; Irani, M. Fabrication of PLA / MWCNT / Fe3O4 Composite Nanofibers for Leukemia Cancer Cells. *Int. J. Polym. Mater. Polym. Biomater.* **2016**, *65* (4), 176–182.

(103) Taleb, M. F. A.; Kahtani, A. Al; Mohamed, S. Radiation Synthesis and Characterization of Sodium Alginate / Chitosan / Hydroxyapatite Nanocomposite Hydrogels : A Drug Delivery System for Liver Cancer. *Polym. Bull.* **2015**, *72* (4), 725–742.

(104) Fried, J. R. *POLYMER SCIENCE AND TECHNOLOGY Third Edition*; 2014.

(105) Raval, N.; Kalyane, D.; Maheshwari, R.; Tekade, R. K. *Copolymers and Block Copolymers in Drug Delivery and Therapy*; Elsevier Inc., 2019.

(106) Wang, Y.; Luo, Q.; Sun, R.; Zha, G.; Li, X.; Shen, Z.; Zhu, W. Acid-Triggered Drug Release from Micelles Based on Amphiphilic Oligo(Ethylene Glycol)–Doxorubicin Alternative Copolymers. *J. Mater. Chem. B Mater. Biol. Med.* **2014**, *2* (43), 7612–

7619.

(107) Guragain, S.; Torad, N. L.; Alghamdi, Y. G. Synthesis of Nanoporous Calcium Carbonate Spheres Using Double Hydrophilic Block Copolymer Poly (Acrylic Acid-b -N-Isopropylacrylamide). *Mater. Lett.* **2018**, *230*, 143–147.

(108) Popa, M.; Delaite, C.; Costuleanu, M. Chitosan Grafted-Poly (Ethylene Glycol) Methacrylate Nanoparticles as Carrier for Controlled Release of Bevacizumab. *Mater. Sci. Eng. C* **2019**, *98*, 843–860.

(109) Avgoustakis, K.; Beletsi, A.; Panagi, Z.; Klepetsanis, P.; Karydas, A. G. PLGA – MPEG Nanoparticles of Cisplatin : In Vitro Nanoparticle Degradation , in Vitro Drug Release and in Vivo Drug Residence in Blood Properties. *J. Control. release* **2002**, *79* (1–3), 123–135.

(110) Zhang, Y.; Chen, J.; Zhang, Y.; Pan, Y.; Zhao, J.; Ren, L.; Liao, M.; Hu, Z.; Kong, L.; Wang, J. A Novel PEGylation of Chitosan Nanoparticles for Gene Delivery. *Biotechnol. Appl. Biochem.* **2007**, *46* (4), 197–204.

(111) Nag, M.; Gajbhiye, V.; Kesharwani, P.; Jain, N. K. Transferrin Functionalized Chitosan-PEG Nanoparticles for Targeted Delivery of Paclitaxel to Cancer Cells. *Colloids Surfaces B Biointerfaces* **2016**, *148*, 363–370.

(112) Chan, P.; Kurisawa, M.; Chung, J. E.; Ã, Y. Y. Synthesis and Characterization of Chitosan-g-Poly (Ethylene Glycol)-Folate as a Non-Viral Carrier for Tumor-Targeted Gene Delivery. *Biomaterials* **2007**, *28* (3), 540–549.

(113) Babu, A.; Ramesh, R. Multifaceted Applications of Chitosan in Cancer Drug Delivery and Therapy. *Mar. Drugs* **2017**, *15* (4), 96.

(114) Khan, S; Anwar, N. Highly Porous PH-Responsive Carboxymethyl Chitosan- Grafted -Poly (Acrylic Acid) Based Smart Hydrogels for 5-Fluorouracil Controlled Delivery and Colon Targeting. *Int. J. Polym. Sci.* **2019**, *2019*, 1–15.

(115) Yang, C.; Gao, S.; Kjems, J. Folic Acid Conjugated Chitosan for Targeted Delivery of SiRNA to Activated Macrophages in Vitro and in Vivo. *J. Mater. Chem. B* **2014**, *2* (48), 8608–8615.

(116) Wang, H.; Zhao, P.; Liang, X.; Gong, X.; Song, T.; Niu, R.; Chang, J. Folate-PEG Coated Cationic Modified Chitosan - Cholesterol Liposomes for Tumor-Targeted Drug Delivery. *Biomaterials* **2010**, *31* (14), 4129–4138.

(117) Jin, H. Folate-Chitosan Nanoparticles Loaded with Ursolic Acid Confer Anti-Breast Cancer Activities in Vitro and in Vivo. *Sci. Rep.* **2016**, *6*, 30782.

(118) Akinyelu, J.; Singh, M. Folic Acid-Conjugated Chitosan Functionalized Gold Nanoparticles for Targeted Delivery of 5-Fluorouracil in Breast Cancer. *Proc. 3rd World Congr. Rec. Adv. Nanotechnol* **2018**.

(119) Subia, B.; Dey, T.; Sharma, S.; Kundu, S. C. Target Specific Delivery of Anti-Cancer Drug in Silk Fibroin Based 3D Distribution Model of Bone-Breast Cancer Cells. *ACS Appl. Mater. Interfaces* **2015**, *7* (4), 2269–2279.

(120) Sun, N.; Lei, R.; Xu, J.; Kundu, S. C. Fabricated Porous Silk Fibroin Particles for PH-Responsive Drug Delivery and Targeting of Tumor Cells. *J. Mater. Sci.* **2018**, *54* (4), 3319-3330.

(121) Subia, B.; Chandra, S.; Talukdar, S.; Kundu, S. C. Folate Conjugated Silk Fibroin Nanocarriers for Targeted Drug Delivery. *Integr. Biol.* **2014**, *6* (2), 203–214.

(122) Zhao, H.; Yue, L.; Yung, L. Selectivity of Folate Conjugated Polymer Micelles against Different Tumor Cells. *Int. J. Pharm.* **2008**, *349* (1–2), 256–268.

(123) Bittleman, K. R.; Dong, S.; Roman, M.; Lee, Y. W. Folic Acid-Conjugated Cellulose Nanocrystals Show High Folate-Receptor Binding Affinity and Uptake by KB and Breast Cancer Cells. *ACS Omega* **2018**, *3* (10), 13952–13959.

(124) Aswathy, R. G.; Sivakumar, B.; Brahatheeswaran, D. Multifunctional Biocompatible Fluorescent Carboxymethyl Cellulose Nanoparticles. *J. Biomater. Nanobiotechnol.*

2012, *3*, 254–261.

(125) Priya, P.; Raj, R. M.; Vasanthakumar, V.; Raj, V. Curcumin-Loaded Layer-by-Layer Folic Acid and Casein Coated Carboxymethyl Cellulose / Casein Nanogels for Treatment of Skin Cancer. *Arab. J. Chem.* **2020**, *13* (1), 694–708.

(126) Phuong, H.; Hoai, N.; Thuc, B.; Anh, H. In Vitro and in Vivo Targeting Effect of Folate Decorated Paclitaxel Loaded PLA – TPGS Nanoparticles. *Saudi Pharm. Journal*, *23(6), 683-688.* **2015**, *23* (6), 683–688.

(127) Tian, X.; Yin, H.; Zhang, S.; Luo, Y.; Xu, K.; Ma, P.; Sui, C.; Meng, F.; Liu, Y.; Jiang, Y.; et al. Bufalin Loaded Biotinylated Chitosan Nanoparticles : An Efficient Drug Delivery System for Targeted Chemotherapy against Breast Carcinoma. *Eur. J. Pharm. Biopharm.* **2014**, *87* (3), 445–453.

(128) Poudel, I.; Ahiwale, R.; Pawar, A.; Mahadik, K. Development of Novel Biotinylated Chitosan- Decorated Docetaxel-Loaded Nanocochleates for Breast Cancer Targeting. *Artif. Cells, Nanomedicine, Biotechnol.* **2018**, *46* (Sup 2), 1–12.

(129) Physiology, C. Synthesis of Biotin-Modified Galactosylated Chitosan Nanoparticles and Their Characteristics in Vitro and in Vivo. *Cell. Physiol. Biochem.* **2018**, *5* (2), 569–584.

(130) Cheng, M.; Zhu, W.; Li, Q.; Dai, D.; Hou, Y. Anti-Cancer Efficacy of Biotinylated Chitosan Nanoparticles in Liver Cancer. *Oncotarget* **2017**, *8* (35), 59068–59085.

(131) Donaldson, O.; Huang, Z. J.; Comolli, N. An Integrated Experimental and Modeling Approach to Propose Biotinylated PLGA Microparticles as Versatile Targeting Vehicles for Drug Delivery. *Prog. Biomater.* **2013**, *2* (1), 3.

(132) Journal, A. I.; Mehdizadeh, M.; Rouhani, H.; Sepehri, N.; Ghahremani, M. H.; Amini, M.; Ostad, S. N.; Atyabi, F.; Baharian, A. Biotin Decorated PLGA Nanoparticles Containing SN-38 Designed for Cancer Therapy. *Artif. cells, nanomedicine,*

Biotechnol. **2017**, *45* (3), 495–504.

(133) Pulkkinen, M.; Pikkarainen, J.; Wirth, T.; Tarvainen, T.; Haapa-aho, V.; Korhonen, H.; Seppa, J. Three-Step Tumor Targeting of Paclitaxel Using Biotinylated PLA-PEG Nanoparticles and Avidin – Biotin Technology : Formulation Development and in Vitro Anticancer Activity. *Eur. J. Pharm. Biopharm.* **2008**, *70* (1), 66–74.

(134) Journal, A. I.; Nosrati, H.; Barzegari, P.; Danafar, H.; Kheiri, H.; Group, F. Biotin-Functionalized Copolymeric PEG-PCL Micelles for in Vivo Tumour-Targeted Delivery of Artemisinin. *Artif. Cells, Nanomedicine, Biotechnol.* **2019**, *47* (1), 104–114.

(135) Alizadeh, L.; Alizadeh, E.; Zarebkohan, A. AS1411 Aptamer-Functionalized Chitosan-Silica Nanoparticles for Targeted Delivery of Epigallocatechin Gallate to the SKOV-3 Ovarian Cancer Cell Lines. *J. Nanoparticle Res.* **2020**, *22* (1), 1–14.

(136) Sadat, F.; Tekie, M.; Soleimani, M.; Zakerian, A.; Dinarvand, M. Glutathione Responsive Chitosan-Thiolated Dextran Conjugated MiR-145 Nanoparticles Targeted with AS1411 Aptamer for Cancer Treatment. *Carbohydr. Polym.* **2018**, *201*, 131–140.

(137) Yousefi, M.; Jadidi-niaragh, F.; Aghebati-maleki, L.; Shanehbandi, D. Anti-Mucin1 Aptamer-Conjugated Chitosan Nanoparticles for Targeted Co-Delivery of Docetaxel and IGF-1R SiRNA to SKBR3 Metastatic Breast Cancer Cells. *Iran. Biomed. J.* **2019**, *23* (1), 21–33.

(138) Kaur, J.; Tikoo, K. Ets1 Identified as a Novel Molecular Target of RNA Aptamer Selected against Metastatic Cells for Targeted Delivery of Nano-Formulation. *Oncogene* **2015**, *34* (41), 5216–5228.

(139) Das, M.; Duan, W.; Sahoo, S. K. Multifunctional Nanoparticle – EpCAM Aptamer Bioconjugates : A Paradigm for Targeted Drug Delivery and Imaging in Cancer Therapy. *Nanomedicine Nanotechnology, Biol. Med.* **2015**, *11* (2), 379–389.

(140) Wu, M.; Wang, Y.; Wang, Y.; Tang, J.; Wang, Z.; Wang, D.; Wang, D. Paclitaxel-

Loaded and A10-3.2 Aptamer-Targeted Poly(Lactide-Co-Glycolic Acid) Nanobubbles for Ultrasound Imaging and Therapy of Prostate Cancer. *Int. J. Nanomedicine* **2017**, *12*, 5313–5330.

(141) Taghavi, S.; Ramezani, M.; Alibolandi, M.; Abnous, K.; Mohammad, S. Chitosan-Modi Fi Ed PLGA Nanoparticles Tagged with 5TR1 Aptamer for in Vivo Tumor-Targeted Drug Delivery. *Cancer Lett.* **2017**, *400*, 1–8.

(142) Alibolandi, M.; Ramezani, M.; Abnous, K.; Hadizadeh, F. AS1411 Aptamer-Decorated Biodegradable Polyethylene Glycol e Poly (Lactic-Co-Glycolic Acid) Nanopolymersomes for the Targeted Delivery of Gemcitabine to Nonsmall Cell Lung Cancer In Vitro. *J. Pharm. Sci.* **2016**, *105* (5), 1741–1750.

(143) Jiao, J.; Zou, Q.; Zou, M. H.; Guo, R. M.; Zhu, S.; Zhang, Y. Aptamer-Modified PLGA Nanoparticle Delivery of Triplex Forming Oligonucleotide for Targeted Prostate Cancer Therapy. *Neoplasma* **2016**, *63* (4), 569–575.

(144) Powell, D.; Chandra, S.; Dodson, K.; Shaheen, F.; Wiltz, K.; Ireland, S.; Syed, M.; Dash, S.; Wiese, T.; Mandal, T.; et al. Aptamer-Functionalized Hybrid Nanoparticle for the Treatment of Breast Cancer. *Eur. J. Pharm. Biopharm.* **2017**, *114*, 108–118.

(145) Farokhzad, O. C.; Cheng, J.; Teply, B. A.; Sherifi, I.; Jon, S.; Kantoff, P. W.; Richie, J. P.; Langer, R. Targeted Nanoparticle-Aptamer Bioconjugates for Cancer Chemotherapy in Vivo. *Proc. Natl. Acad. Sci.* **2006**, *103* (16), 6315–6320.

(146) Pan, M.; Li, W.; Yang, J.; Li, Z.; Zhao, J.; Xiao, Y.; Xing, Y.; Zhang, X.; Ju, W. Plumbagin-Loaded Aptamer-Targeted Poly D,L- Lactic-Co-Glycolic Acid-b-Polyethylene Glycol Nanoparticles for Prostate Cancer Therapy. *Medicine (Baltimore).* **2017**, *96* (30), 1–7.

(147) Alibolandi, M.; Ramezani, M.; Sadeghi, F.; Abnous, K.; Hadizadeh, F.; Plga, P. E. G. Epithelial Cell Adhesion Molecule Aptamer Conjugated PEG – PLGA

Nanopolymersomes for Targeted Delivery of Doxorubicin to Human Breast Adenocarcinoma Cell Line in Vitro. *Int. J. Pharm.* **2015**, *479* (1), 241–251.

(148) Gao, J.; Wang, H.; Fan, W.; Wang, X. Second-Generation Aptamer-Conjugated PsMA-Targeted Delivery System for Prostate Cancer Therapy. *nternational J. nanomedicine* **2011**, *6*, 1747–1756.

(149) Yousefpour, P.; Atyabi, F.; Vasheghani-, E.; Mousavi, A.; Dinarvand, R. Targeted Delivery of Doxorubicin-Utilizing Chitosan Nanoparticles Surface-Functionalized with Anti-Her2 Trastuzumab. *Int. J. Nanomedicine* **2011**, *6*, 1977.

(150) Zhu, R.; Zhang, C.; Liu, Y.; Yuan, Z.; Chen, W.; Yang, S. CD147 Monoclonal Antibody Mediated by Chitosan Nanoparticles Loaded with α -Hederin Enhances Antineoplastic Activity and Cellular Uptake in Liver Cancer Cells. *Sci. Rep.* **2015**, *5* (march), 17904.

(151) Naruphontjirakul, P.; Viravaidya-, K. Development of Anti-HER2-Targeted Doxorubicin – Core-Shell Chitosan Nanoparticles for the Treatment of Human Breast Cancer. *Int. J. Nanomedicine* **2019**, *14*, 4105.

(152) Vongchan, P.; Wutti-in, Y.; Sajomsang, W.; Gonil, P.; Kothan, S.; Linhardt, R. J. N , N , N -Trimethyl Chitosan Nanoparticles for the Delivery of Monoclonal Antibodies against Hepatocellular Carcinoma Cells. *Carbohydr. Polym.* **2011**, *85* (1), 215–220.

(153) Sousa, F.; Cruz, A.; Fonte, P.; Pinto, I. M.; Neves-, M. T. A New Paradigm for Antiangiogenic Therapy through Controlled Release of Bevacizumab from PLGA Nanoparticles. *Sci. Rep.* **2017**, *7* (1), 1–13.

(154) Jitendrakumar, P.; Jitendra, A.; Priyanka, B.; Ankit, J.; Mukul, J.; Ambikanandan, M. Targeted Delivery of Monoclonal Antibody Conjugated Docetaxel Loaded PLGA Nanoparticles into EGFR Overexpressed Lung Tumor Cells. *J. Microencapsul.* **2018**, *35* (2), 204–217.

(155) Kocbek, P.; Cegnar, M.; Kos, J.; Kristl, J. Targeting Cancer Cells Using PLGA

Nanoparticles Surface Modified with Monoclonal Antibody. *J. Control. release* **2007**, *120* (1–2), 18–26.

(156) Ornell, K. J.; Shimada, H.; Taylor, J. S.; Coburn, J. M.; Zeki, J.; Chiu, B. Local Delivery of Dinutuximab from Lyophilized Silk Fibroin Foams for Treatment of an Orthotopic Neuroblastoma Model. *Cancer Med.* **2020**, *9* (8), 2891-2903.

(157) Wang, P. Photolabile Protecting Groups : Structure and Reactivity. *Asian J. Org. Chem.* **2013**, *2* (6), 452–464.

(158) Kim, M. S.; Diamond, S. L. Photocleavage of o -Nitrobenzyl Ether Derivatives for Rapid Biomedical Release Applications. *Bioorg. Med. Chem. Lett.* **2006**, *16* (15), 4007–4010.

(159) Zhang, Z.; Hatta, H.; Ito, T.; Nishimoto, S. Synthesis and Photochemical Properties of Photoactivated Antitumor Prodrugs Releasing 5-Fluorouracil. *Org. Biomol. Chem.* **2005**, *3* (4), 592–596.

(160) Li, Y.; Shen, Y.; Wang, S.; Zhu, D.; Jiang, J. Disulfide Cross-Linked Cholic-Acid Modified PEG–Poly(Amino Acid) Block Copolymer Micelles for Controlled Drug Delivery of Doxorubicin†. *RSC Adv.* **2015**, *5* (38), 30380–30388.

(161) Duan, X., Bai, T., Du, J., & Kong, J. One-Pot Synthesis of Glutathione-Responsive Amphiphilic Drug Self-Delivery Micelle of Doxorubicin-Disulfide-Methoxy Polyethylene Glycol for Tumor Therapy. *J. Mater. Chem. B* **2018**, *6* (1), 39–43.

(162) Lee, E.; Lee, J.; Lee, I. H.; Yu, M.; Kim, H.; Chae, S. Y.; Jon, S. Conjugated Chitosan as a Novel Platform for Oral Delivery of Paclitaxel. *J. Med. Chem.* **2008**, *51* (20), 6442–6449.

(163) Lee, R.; Choi, Y. J.; Jeong, M. S.; Park, Y. Il; Motoyama, K.; Kim, M. W.; Kwon, S.; Choi, J. H. Hyaluronic Acid-Decorated Glycol Chitosan Nanoparticles for PH-Sensitive Controlled Release of Doxorubicin and Celecoxib in Nonsmall Cell Lung

Cancer. *bioconjuagate Chem.* **2020**, *31* (3), 923–932.

(164) Shumatbaeva, A. M.; Morozova, J. E.; Syakaev, V. V; Shalaeva, Y. V; Sapunova, A. S.; Voloshina, A. D.; Gubaidullin, A. T.; Bazanova, O. B.; Babaev, V. M.; Nizameev, I. R.; et al. The PH-Responsive Calix [4] Resorcinarene-MPEG Conjugates Bearing Acylhydrazone Bonds : Synthesis and Study of the Potential as Supramolecular Drug Delivery Systems. *Colloids Surfaces A* **2020**, *589* (January), 124453.

(165) Gillies, E. R.; Goodwin, A. P.; Fre, J. M. J. Acetals as PH-Sensitive Linkages for Drug Delivery. *Bioconjugate Chem. 2004*, **2004**, *15* (6), 1254–1263.

(166) Gao, Y.; Yang, C.; Liu, X.; Ma, R.; Kong, D.; Shi, L. A Multifunctional Nanocarrier Based on Nanogated Mesoporous Silica for Enhanced Tumor-Specific Uptake and Intracellular Delivery. *Macromol. Biosci.* **2012**, *12* (2), 251–259.

(167) Gawali, S. L.; Barick, K. C.; Shetake, N. G.; Rajan, V.; Pandey, B. N.; Kumar, N. N.; Priyadarsini, K. I.; Hassan, P. A. PH-Labile Magnetic Nanocarriers for Intracellular Drug Delivery to Tumor Cells. *ACS Omega* **2019**, *4* (7), 11728–11736.

(168) Ko, J.; Park, K.; Kim, Y.; Sang, M.; Kwon, J.; Kim, K.; Park, R.; Kim, I.; Kyu, H.; Sung, D.; et al. Tumoral Acidic Extracellular PH Targeting of PH-Responsive MPEG-Poly (β -Amino Ester) Block Copolymer Micelles for Cancer Therapy. *J. Control. Release* **2007**, *123* (2), 109–115.

(169) Wang, Y.; Li, P.; Chen, F.; Jia, L.; Xu, Q.; Gai, X.; Yu, Y. A Novel PH-Sensitive Carrier for the Delivery of Antitumor Drugs : Histidine-Modified Auricularia Auricular Polysaccharide Nano- Micelles. *Sci. Rep.* **2017**, *7* (1), 1–10.

(170) Zhong, Y.; Shao, L.; Li, Y. A. N. Cathepsin B-Cleavable Doxorubicin Prodrugs for Targeted Cancer Therapy (Review). *Int. J. Oncol.* **2013**, *42* (2), 373–383.

(171) Dong, H., Pang, L., Cong, H., Shen, Y., & Yu, B. Application and Design of Esterase-Responsive Nanoparticles for Cancer Therapy. *Drug Deliv.* **2019**, *26* (1), 416–432.

(172) Guo, X.; Cheng, Y.; Zhao, X.; Luo, Y.; Chen, J.; Yuan, W. E. Advances in Redox -

Responsive Drug Delivery Systems of Tumor Microenvironment. *J. Nanobiotechnology* **2018**, *16* (1), 1–10.

(173) Li, P.; Wang, Y.; Peng, Z.; She, F.; Kong, L. Development of Chitosan Nanoparticles as Drug Delivery Systems for 5-Fluorouracil and Leucovorin Blends. *Carbohydr. Polym.* **2011**, *85* (3), 698–704.

(174) Tiğli Aydin, R. S.; Pulat, M. 5-Fluorouracil Encapsulated Chitosan Nanoparticles for PH-Stimulated Drug Delivery: Evaluation of Controlled Release Kinetics. *J. Nanomater.* **2012**, *2012*.

(175) Risbud, M. V; Hardikar, A. A.; Bhat, S. V; Bhonde, R. R. Hydrogels As Controlled Release System for Antibiotic Delivery. *J. Control. Release* **2000**, *68* (1), 23–30.

(176) Shaima, C.; Moorthi, P. V.; Kutty, S. N. In Vitro Anticancer Activity of 5-Fluorouracil Coated Chitosan Nanoparticle. *Int J Curr Pharm Res*, **2016**, *8* (4), 6–8.

(177) Janes, K. A.; Fresneau, M. P.; Marazuela, A.; Fabra, A. Chitosan Nanoparticles as Delivery Systems for Doxorubicin. **2001**, *73*, 255–267.

(178) Abdel-hakeem, M. A.; Abdel-haseb, O. M.; Abdel-ghany, S. E.; Cevik, E.; Sabit, H. Doxorubicin Loaded on Chitosan-Protamine Nanoparticles Triggers Apoptosis via Downregulating Bcl-2 in Breast Cancer Cells. *J. Drug Deliv. Sci. Technol.* **2020**, *55*, 101423.

(179) Akbucat, J.; Bergisadis, N. 5-Fluorouracil-Loaded Chitosan Microspheres : Preparation and Release Characteristics. **1996**, *13* (2), 161–168.

(180) Sun, Y.; Gu, L.; Gao, Y.; Gao, F. Preparation and Characterization of 5-Fluorouracil Loaded Chitosan Microspheres by a Two-Step Solidification Method. *Chem. Pharm. Bull. (Tokyo).* **2010**, *58* (July), 891–895.

(181) Patel, N.; Desai, J.; Kumar, P.; Thakkar, H. P. Development and in Vitro Characterization of Capecitabine-Loaded Alginate-Pectinate-Chitosan Beads for Colon

Targeting. *J. Macromol. Sci. Part B Phys.* **2016**, *55* (1), 33–54.

(182) Costa da Silva, M.; Leite, M. D. R.; Lima Oliveira, S. S.; Fideles, T. B.; Fook, M. V. L. Morphological Evaluation of Chitosan/Curcumin Beads and Powder: Effect of the Methanol as a Solvent. *Mater. Sci. Forum* **2016**, *869*, 854–858.

(183) Kim, H.; Lee, G.; Kuh, H.; Kwak, B. K.; Lee, J. Liposomal Doxorubicin-Loaded Chitosan Microspheres Capable of Controlling Release of Doxorubicin for Anti-Cancer Chemoembolization : In Vitro Characteristics. *J. Drug Deliv. Sci. Technol.* **2013**, *23* (3), 283–286.

(184) Guptha, A. Nano Drug Delivery System - a Mini Review. *Res. Rev. J. Pharm. Nanotechnol.* **2015**, *3* (2), 126–144.

(185) Jena, P.; Mohanty, S.; Mallick, R.; Jacob, B.; Sonawane, A. Toxicity and Antibacterial Assessment of Chitosancoated Silver Nanoparticles on Human Pathogens and Macrophage Cells. *Int. J. Nanomedicine* **2012**, *7*, 1805–1818.

(186) Sharma, V. K. Stability and Toxicity of Silver Nanoparticles in Aquatic Environment: A Review. *ACS Symp. Ser.* **2013**, *1124*, 165–179.

(187) Manivasagan, P.; Bharathiraja, S.; Quang, N. Paclitaxel-Loaded Chitosan Oligosaccharide-Stabilized Gold Nanoparticles as Novel Agents for Drug Delivery and Photoacoustic Imaging of Cancer Cells. *Int. J. Pharm.* **2016**, *511* (1), 367–379.

(188) Mahmoud, M.; Elshemey, W. M. Physica Medica Multifunctional Chitosan-Capped Gold Nanoparticles for Enhanced Cancer Chemo-Radiotherapy : An Invitro Study. *Phys. Medica* **2018**, *48* (November), 76–83.

(189) Mohamed, N. Synthesis of Hybrid Chitosan Silver Nanoparticles Loaded with Doxorubicin with Promising Anti-Cancer Activity. *Bionanoscience* **2020**, *10*, 758–765.

(190) Qu, Y.; Kang, M.; Cheng, X.; Zhao, J. Chitosan-Coated Titanium Dioxide-Embedded Paclitaxel Nanoparticles Enhance Anti-Tumor Efficacy Against Osteosarcoma. **2020**,

10 (September), 1–13.

(191) Anitha, J.; Selvakumar, R.; Murugan, K. Chitosan Capped ZnO Nanoparticles with Cell Specific Apoptosis Induction through P53 Activation and G2 / M Arrest in Breast Cancer Cells – In Vitro Approaches International Journal of Biological Macromolecules Chitosan Capped ZnO Nanoparticles with Cell. *Int. J. Biol. Macromol.* **2019**, *136* (June), 686–696.

(192) Webster, T. J.; Rajagopal, G. ROS-Responsive Chitosan Coated Magnetic Iron Oxide Nanoparticles as Potential Vehicles for Targeted Drug Delivery in Cancer Therapy. *Int. J. Nanomedicine* **2020**, *15*, 3333–3346.

(193) Wang, X.; Hu, X.; Daley, A.; Rabotyagova, O.; Cebe, P.; Kaplan, D. L. Nanolayer Biomaterial Coatings of Silk Fibroin for Controlled Release. *J. Control. Release* **2007**, *121* (3), 190–199.

(194) Gobin, A. S.; Rhea, R.; Newman, R. A.; Mathur, A. B. Silk-Fibroin-Coated Liposomes for Long-Term and Targeted Drug Delivery. *Int. J. Nanomedicine* **2006**, *1* (1), 81–87.

(195) Zhou, J.; Fang, T. L.; Wen, J.; Shao, Z.; Dong, J. Silk Coating on Poly(ε-Caprolactone) Microspheres for the Delayed Release of Vancomycin. *J. Microencapsul.* **2011**, *28* (2), 99–107.

(196) Kwan, T.; Bin, K.; Kim, J. Solid Lipid Nanoparticles Coated with Silk Fibroin. *J. Ind. Eng. Chem.* **2011**, *17* (1), 10–13.

(197) Wu, F.; Yang, M.; Qian, X.; Yu, L.; Jiang, X.; Liu, B. Facile Preparation of Paclitaxel Loaded Silk Fibroin Nanoparticles for Enhanced Antitumor E Ffi Cacy by Locoregional Drug Delivery. *ACS Appl. Mater. Interfaces* **2013**, *5* (23), 12638−12645.

(198) Rahmani, H.; Id, A. F.; Id, K. S.; Id, S. K.; Shokoohinia, Y. Preparation and Characterization of Silk Fibroin Nanoparticles as a Potential Drug Delivery System for 5-Fluorouracil. *Tabriz Univ. Med. Sci.* **2019**, *9* (4), 601–608.

(199) Li, H., Tian, J., Wu, A., Wang, J., Ge, C., & Sun, Z. Self-Assembled Silk Fibroin Nanoparticles Loaded with Binary Drugs in the Treatment of Breast Carcinoma. *Int. J. Nanomedicine* **2016**, *11*, 4373–4380.

(200) Tian, Y.; Jiang, X.; Chen, X.; Shao, Z.; Yang, W. Doxorubicin-Loaded Magnetic Silk Fibroin Nanoparticles for Targeted Therapy of Multidrug-Resistant Cancer. *Adv. Mater.* **2014**, *26* (43), 7393–7398.

(201) Sonia, T. A.; Sharma, C. P. An Overview of Natural Polymers for Oral Insulin Delivery. *Drug Discov. Today* **2012**, *17* (13–14), 784–792.

(202) Ikada, Y.; Tsuji, H. Biodegradable Polyesters for Medical and Ecological Applications. *Macromol. Rapid Commun.* **2000**, *132*, 117–132.

(203) Mi, F.; Tan, Y.; Liang, H.; Sung, H. In Vivo Biocompatibility and Degradability of a Novel Injectable-Chitosan-Based Implant. *Biomaterials* **2002**, *23*, 181–191.

(204) Yin, H.; Du, Y.; Zhang, J. Low Molecular Weight and Oligomeric Chitosans and Their Bioactivities. *Curr. Top. Med. Chem.* **2009**, *9*, 1546–1559.

(205) Zolfagharian, H.; Heydari, M. Preparation of Chitosan Nanoparticles Containing Naja Naja Oxiana Snake Venom. *Nanomedicine Nanotechnology, Biol. Med.* **2010**, *6* (1), 137–143.

(206) Rampino, A.; Borgogna, M.; Blasi, P.; Bellich, B.; Cesàro, A. Chitosan Nanoparticles : Preparation , Size Evolution and Stability. *Int. J. Pharm.* **2013**, *455* (1–2), 219–228.

(207) Huang, X.; Brazel, C. S. On the Importance and Mechanisms of Burst Release in Matrix-Controlled Drug Delivery Systems. **2001**, *73*, 121–136.

(208) Agasti, S. S.; Chompoosor, A.; You, C.; Ghosh, P.; Kim, C. K.; Rotello, V. M. Photoregulated Release of Caged Anticancer Drugs from Gold Nanoparticles to Regulate Drug Release , Minimizing Side Effects and Improving. *J. Am. Chem. Soc.* **2009**, *131* (16), 5728–5729.

(209) Yuan, Y.; Chesnutt, B. M.; Haggard, W. O.; Bumgardner, J. D. Deacetylation of

Chitosan: Material Characterization and in Vitro Evaluation via Albumin Adsorption and Pre-Osteoblastic Cell Cultures. *Materials (Basel).* **2011**, *4* (8), 1399–1416.

(210) Pourjavadi, A.; Mahdavinia, G. R.; Zohuriaan-Mehr, M. J.; Omidian, H. Modified Chitosan. I. Optimized Cerium Ammonium Nitrate-Induced Synthesis of Chitosan-Graft-Polyacrylonitrile. *J. Appl. Polym. Sci.* **2003**, *88* (8), 2048–2054.

(211) Jia, Z.; Shen, D. Effect of Reaction Temperature and Reaction Time on the Preparation of Low-Molecular-Weight Chitosan Using Phosphoric Acid. *Carbohydr. Polym.* **2002**, *49*, 2–5.

(212) Sreekumar, S.; Goycoolea, F. M.; Moerschbacher, B. M.; Rivera-rodriguez, G. R. Parameters Influencing the Size of Chitosan-TPP Nano- and Microparticles. *Sci. Rep.* **2018**, *8* (1), 1–11.

(213) Czechowska-biskup, R.; Rokita, B.; Rosiak, J. M. Determination of Degree of Deacetylation of Chitosan - Comparision of Methods. *Prog. Chem. Appl. Chitin its Deriv.* **2012**, *17*, 5–20.

(214) Tomoiaga, A. M.; Ochiuz, L.; Vasile, A. Sonochemical Development of Magnetic Nanoporous Therapeutic Systems as Carriers for 5-Fluorouracil. *J. Nanotechnol. Diagnosis Treat.* **2013**, *1*, 26–35.

(215) Zheng, Z.; Zhang, L.; Kong, L.; Wang, A.; Gong, Y.; Zhang, X. The Behavior of MC3T3-E1 Cells on Chitosan/Poly-L-Lysine Composite Films: Effect of Nanotopography, Surface Chemistry, and Wettability. *J. Biomed. Mater. Res. - Part A* **2009**, *89* (2), 453–465.

(216) Jirawutthiwongchai, J.; Klaharn, I.; Hobang, N. Chitosan-Phenylalanine-MPEG Nanoparticles : From a Single Step Water-Based Conjugation to the Potential Allergen Delivery System. *Carbohydr. Polym.* **2016**, *141*, 41–53.

(217) Duan, W.; Chen, C.; Jiang, L.; Li, G. H. Preparation and Characterization of the Graft

Copolymer of Chitosan with Poly [Rosin- (2-Acryloyloxy) Ethyl Ester]. *Carbohydr. Polym.* **2008**, *73*, 582–586.

(218) Agrawal, S.; Narula, A. K. Synthesis and Characterization of Heat-Resistant and Soluble Poly (Amide-Imide) s from Unsymmetrical Dicarboxylic Acid Containing 2-(Triphenyl Phosphoranylidene) Moiety and Various Aromatic Diamines. *J. Chem. Sci.* **2015**, *127* (4), 737–749.

(219) Thomas, V.; Yallapu, M. M.; Sreedhar, B.; Bajpai, S. K. Fabrication, Characterization of Chitosan/Nanosilver Film and Its Potential Antibacterial Application. *J. Biomater. Sci. Polym. Ed.* **2009**, *20* (14), 2129–2144.

(220) Kalva, N.; Parekh, N.; Ambade, A. V. Controlled Micellar Disassembly of Photo- and PH-Cleavable Linear-Dendritic Block Copolymers. *Polym. Chem.* **2015**, *6*, 6826–6835.

(221) Xie, M.; Zhang, F.; Liu, L.; Zhang, Y.; Li, Y.; Li, H.; Xie, J. Surface Modification of Graphene Oxide Nanosheets by Protamine Sulfate/Sodium Alginate for Anti-Cancer Drug Delivery Application. *Appl. Surf. Sci.* **2018**, *440*, 853–860.

(222) Perfézou, M.; Turner, A.; Merkoçi, A. Cancer Detection Using Nanoparticle-Based Sensors. *Chem. Soc. Rev.* **2012**, *41* (7), 2606–2622.

(223) Qiu, L.; Li, J. W.; Hong, C. Y.; Pan, C. Y. Silver Nanoparticles Covered with PH-Sensitive Camptothecin-Loaded Polymer Prodrugs: Switchable Fluorescence “off” or “on” and Drug Delivery Dynamics in Living Cells. *ACS Appl. Mater. Interfaces* **2017**, *9* (46), 40887–40897.

(224) He, Y.; Du, Z.; Ma, S.; Liu, Y.; Li, D.; Huang, H.; Jiang, S.; Cheng, S.; Wu, W.; Zhang, K.; et al. Effects of Green-Synthesized Silver Nanoparticles on Lung Cancer Cells in Vitro and Grown as Xenograft Tumors in Vivo. *Int. J. Nanomedicine* **2016**, *11*, 1879–1887.

(225) Matai, I.; Sachdev, A.; Gopinath, P. Multicomponent 5-Fluorouracil Loaded PAMAM

Stabilized-Silver Nanocomposites Synergistically Induce Apoptosis in Human Cancer Cells. *Biomater. Sci.* **2015**, *3* (3), 457–468.

(226) Vazquez-Muñoz, R.; Borrego, B.; Juárez-Moreno, K.; García-García, M.; Mota Morales, J. D.; Bogdanchikova, N.; Huerta-Saquero, A. Toxicity of Silver Nanoparticles in Biological Systems: Does the Complexity of Biological Systems Matter? *Toxicol. Lett.* **2017**, *276*, 11–20.

(227) Regiel-Futyra, A.; Kus-Liśkiewicz, M.; Sebastian, V.; Irusta, S.; Arruebo, M.; Kyzioł, A.; Stochel, G. Development of Noncytotoxic Silver-Chitosan Nanocomposites for Efficient Control of Biofilm Forming Microbes. *RSC Adv.* **2017**, *7* (83), 52398–52413.

(228) Stensberg, M. C.; Wei, Q.; Mclamore, E. S.; Marshall, D. Toxicological Studies on Silver Nanoparticles: Challenges and Oopportunities in Assessment, Monitoring and Imaging. *Nanomedicine* **2011**, *6* (5), 879–898.

(229) Venkatesham, M.; Ayodhya, D.; Madhusudhan, A.; Veera Babu, N.; Veerabhadram, G. A Novel Green One-Step Synthesis of Silver Nanoparticles Using Chitosan: Catalytic Activity and Antimicrobial Studies. *Appl. Nanosci.* **2012**, *4* (1), 113–119.

(230) Wang, Z.; Xu, C.; Zhao, M.; Zhao, C. One-Pot Synthesis of Narrowly Distributed Silver Nanoparticles Using Phenolic-Hydroxyl Modified Chitosan and Their Antimicrobial Activity. *RSC Adv.* **2014**, *4*, 47021–47030.

(231) Cheng, W.; Cheng, H.; Wan, S.; Zhang, X.; Yin, M. Dual-Stimulus-Responsive Fluorescent Supramolecular Prodrug for Antitumor Drug Delivery. **2017**.

(232) Saha, B.; Haldar, U.; De, P. Polymer-Chlorambucil Drug Conjugates : A Dynamic Platform of Anticancer Drug Delivery. *Macromol. Rapid Commun.* **2016**, *37*, 1015.

(233) Saha, B.; Bhattacharyya, S.; Mete, S.; Mukherjee, A.; De, P. Redox-Driven Disassembly of Polymer–Chlorambucil Polyprodrug: Delivery of Anticancer Nitrogen Mustard and DNA Alkylation. *ACS Appl. Polym. Mater.* **2019**, *1*, 2503–2515.

(234) Ren, W. X.; Kim, J. S. Binary Drug Reinforced First Small-Molecule-Based Prodrug for Synergistic Anticancer E Ff Ects. *ACS Appl. Bio Mater.* **2019**, *2* (8), 3532-3539.

(235) Yata, V. K.; Gopinath, P. Emerging Implications of Nonmammalian Cytosine Deaminases on Cancer Therapeutics. *Appl. Biochem. Biotechnol.* **2012**, *167* (7), 2103–2116.

(236) Kumar, V.; Siddhartha, Y.; Ghosh, S. Synthesis and Characterization of a Novel Chitosan Based E . Coli Cytosine Deaminase Nanocomposite for Potential Application in Prodrug Enzyme Therapy. *Biotechnol Lett* **2011**, *31* (1), 153–157.

(237) Kalaivani, R.; Maruthupandy, M.; Muneeswaran, T.; Beevi, A. H.; Anand, M.; Ramakritinan, C. M.; Kumaraguru, A. K. Frontiers in Laboratory Medicine Synthesis of Chitosan Mediated Silver Nanoparticles (Ag NPs) for Potential Antimicrobial Applications. *Front. Lab. Med.* **2018**, *2* (1), 30–35.

(238) Caraway, T. Colorimetric Determination Guanase Activity of Serum. *Clin. Chem.* **1966**, *12* (4), 187–193.

(239) Gaded, V.; Anand, R. Selective Deamination of Mutagens by a Mycobacterial Enzyme. *J. Am. Chem. Soc.* **2017**, *139* (31), 10762–10768.

(240) Bitra, A.; Hussain, B.; Tanwar, A. S.; Anand, R. Identification of Function and Mechanistic Insights of Guanine Deaminase from Nitrosomonas Europaea : Role of the C- Terminal Loop in Catalysis. *Biochemistry* **2013**, *52* (20), 3512–3522.

(241) Lee, Y. J.; Ahn, E.; Park, Y. Shape-Dependent Cytotoxicity and Cellular Uptake of Gold Nanoparticles Synthesized Using Green Tea Extract. *Nanoscale Res. Lett.* **2019**, *14* (129), 1–14.

(242) Jin, L.; Liu, Q.; Sun, Z.; Ni, X.; Wei, M. Preparation of 5-Fluorouracil / -Cyclodextrin Complex Intercalated in Layered Double Hydroxide and the Controlled Drug Release Properties. *Ind. Eng. Chem. Res.* **2010**, *49*, 11176–11181.

(243) Pai, M. P.; Bruce, H.; Felton, L. A. Clinical Pharmacokinetics of Oral Controlled-

Release. *Antimicrob. Agents Chemother.* **2010**, *54* (3), 1237–1241.

(244) Olukman, M. Release of Anticancer Drug 5-Fluorouracil from Different Ionically Crosslinked Alginate Beads. *J. Biomater. Nanobiotechnol.* **2012**, *03* (04), 469–479.

(245) Hall, R. S.; Fedorov, A. A.; Xu, C.; Fedorov, E. V; Almo, S. C.; Raushel, F. M. Three-Dimensional Structure and Catalytic Mechanism of Cytosine Deaminase. *Biochemistry* **2011**, *50* (22), 5077–5085.

(246) Mahan, S. D.; Ireton, G. C.; Knoeber, C.; Stoddard, B. L.; Black, M. E. Random Mutagenesis and Selection of Escherichia Coli Cytosine Deaminase for Cancer Gene Therapy. **2004**, *17* (8), 625–633.

(247) Li, J.; Chang, S.; Liau, I.; Chan, P.; Liu, R.; Yen, S. Targeted Antitumor Prodrug Therapy Using CNGRC-YCD Fusion Protein in Combination with 5-Fluorocytosine. *J. Biomed. Sci.* **2016**, *23* (1), 15.

(248) Huang, H.; Yang, X. Synthesis of Chitosan-Stabilized Gold Nanoparticles in the Absence/Presence of Tripolyphosphate. *Biomacromolecules* **2004**, *5* (6), 2340–2346.

(249) Chandran, P. R.; Thomas, R. T. *Gold Nanoparticles in Cancer Drug Delivery*; Elsevier Inc., 2015.

(250) Ghosh, P.; Han, G.; De, M.; Kim, C. K.; Rotello, V. M. Gold Nanoparticles in Delivery Applications. *Adv. Drug Deliv. Rev. J.* **2008**, *60* (11), 1307–1315.

(251) Wang, X.; Wenk, E.; Hu, X.; Castro, G. R.; Meinel, L.; Wang, X.; Li, C.; Merkle, H.; Kaplan, D. L. Silk Coatings on PLGA and Alginate Microspheres for Protein Delivery. *Biomaterials* **2007**, *28* (28), 4161–4169.

(252) Chiani, M.; Norouzian, D.; Shokrgozar, M. A.; Azadmanesh, K.; Najmafshar, A.; Mehrabi, M. R.; Akbarzadeh, A. Folic Acid Conjugated Nanoliposomes as Promising Carriers for Targeted Delivery of Bleomycin. *Artif. Cells, Nanomedicine Biotechnol.* **2018**, *46* (4), 757–763.

(253) Rockwood, D. N.; Preda, R. C.; Yücel, T.; Wang, X.; Lovett, M. L.; Kaplan, D. L. Materials Fabrication from Bombyx Mori Silk Fibroin. *Nat. Protoc.* **2011**, *6* (10), 1612–1631.

(254) Wang, X.; Kim, H. J.; Xu, P.; Matsumoto, A.; Kaplan, D. L. Biomaterial Coatings by Stepwise Deposition of Silk Fibroin. *Langmuir* **2005**, *21* (24), 11335–11341.

(255) Hyun, S.; Johnson, S. B.; Bakken, S. Shaping the Future of Nanomedicine: Anisotropy in Polymeric Nanoparticle Design. *Wiley Interdiscip. Rev. Nanomedicine Nanobiotechnology* **2016**, *8* (2), 191–207.

(256) Das, J.; Choi, Y. J.; Han, J. W.; Reza, A. M. M. T.; Kim, J. H. Nanoceria-Mediated Delivery of Doxorubicin Enhances the Anti-Tumour Efficiency in Ovarian Cancer Cells via Apoptosis. *Materials (Basel).* **2017**, *7* (1), 1–12.

(257) Al-kadhemy, M. F. H. FTIR Spectrum Of Laser Dye Fluorescein Doped Polymer PMMA Films. *RRPL* **2012**, *3* (3), 102–106.

(258) Huang, H.; Yuan, Q.; Shah, J. S.; Misra, R. D. K. A New Family of Folate-Decorated and Carbon Nanotube-Mediated Drug Delivery System: Synthesis and Drug Delivery Response. *Adv. Drug Deliv. Rev.* **2011**, *63* (14–15), 1332–1339.

(259) Rani, M.; Agarwal, A.; Negi, Y. S. Review: Chitosan Based Hydrogel Polymeric Beads - as Drug Delivery System. *BioResources* **2010**, *5* (4), 2765–2807.

(260) Donnelly, L.; Hardy, J. G.; Gorman, S. P.; Jones, D. S.; Irwin, N. J.; McCoy, C. P. Photochemically Controlled Drug Dosing from a Polymeric Scaffold. *Pharm. Res.* **2017**, *34* (7), 1469–1476.

(261) Wu, S.; Zhao, X.; Li, Y.; Du, Q.; Sun, J.; Wang, Y.; Wang, X.; Xia, Y.; Wang, Z.; Xia, L. Adsorption Properties of Doxorubicin Hydrochloride onto Graphene Oxide: Equilibrium, Kinetic and Thermodynamic Studies. *Materials (Basel).* **2013**, *6* (5), 2026–2042.

(262) Rana, S.; Gallo, A.; Srivastava, R. S.; Misra, R. D. K. On the Suitability of

Nanocrystalline Ferrites as a Magnetic Carrier for Drug Delivery: Functionalization, Conjugation and Drug Release Kinetics. *Acta Biomater.* **2007**, *3* (2), 233–242.

(263) Liu, X.; Pang, J.; Xu, F.; Zhang, X. Simple Approach to Synthesize Amino-Functionalized Carbon Dots by Carbonization of Chitosan. *Sci. Rep.* **2016**, *6*, 31100.

(264) Zhao, X.; Chen, J.; Chen, J.; Kuznetsova, L.; Wong, S. S.; Ojima, IwaoChen, S. Mechanism-Based Tumor-Targeting Drug Delivery System. Validation of Efficient Vitamin Receptor-Mediated Endocytosis and Drug Release. *Bioconjug. Chem.* **2010**, *21* (5), 979–987.

(265) Anderson, G. W., Zimmerman, J. E., & Callahan, F. M. N-Hydroxysuccinimide Esters in Peptide Synthesis. *J. Am. Chem. Soc.* **1963**, *85* (19), 3039-3039.

(266) Klykov, O.; Weller, M. G. Quantification of N -Hydroxysuccinimide and N -Hydroxysulfosuccinimide by Hydrophilic Interaction. *Anal. Methods* **2015**, *7* (15), 6443–6448.

(267) Buller, Jens, André Laschewsky, Jean-François Lutz, and E. W. Polymer Chemistry Tuning the Lower Critical Solution Temperature of Thermoresponsive Polymers by Biospecific Recognition. *Polym. Chem.* **2011**, *2* (7), 1486–1489.

(268) Magde, D.; Wong, R.; Seybold, P. G. Fluorescence Quantum Yields and Their Relation to Lifetimes of Rhodamine 6G and Fluorescein in Nine Solvents: Improved Absolute Standards for Quantum Yields. *Photochem. Photobiol.* **2002**, *75* (4), 327–334.

(269) Radwan-pragłowska, J.; Bogdał, D. Chitosan-Based Carbon Quantum Dots for Biomedical Applications : Synthesis and Characterization. *Nanomaterials* **2019**, *9* (274), 1–13.

(270) Pawar, Shweta, Uday Kumar Togiti, Anupam Bhattacharya, and A. N. Functionalized Chitosan–Carbon Dots: A Fluorescent Probe for Detecting Trace Amount of Water in

Organic Solvents. *ACS omega* **2019**, *4* (6), 11301–11311.

(271) Chauhan, R. P.; Singh, G. Biotinylated Magnetic Nanoparticles for Pretargeting : Synthesis and Characterization Study. *cancer nano* **2011**, *2* (1–6), 111–120.

List of Publications

Horo, H.; Mandal, B.; Kundu, L. M*. "Biotin conjugated amine functionalized carbon dots for targeted delivery of 5-fluorouracil" (manuscript under preparation)

Horo, H.; Bhattacharya, S.; Mandal, B.; Kundu, L. M*. "Synthesis of functionalized silk-coated chitosan-gold nanoparticles and microparticles for target-directed delivery of antitumor agents" *Carbohydrate polymers*. 2021, 117659.

Horo, H.; Porathoor, S.; Anand, R.; Kundu, L. M*. "A combinatorial approach involving E. coli cytosine deaminase and 5-fluorocytosine-nanoparticles as an enzyme-prodrug therapeutic method for highly substrate selective in situ generation of 5-fluorouracil" *Journal of Drug Delivery Science and Technology*. **2020**, *58*, 101799.

Horo, H.; Das, S.; Mandal, B.; Kundu, L. M*. "Development of a photoresponsive chitosan conjugated prodrug nano-carrier for controlled delivery of antitumor drug 5-fluorouracil" *Int.J.Biol.Macromol.* **2019**, *121*, 1070-1076.

Das, S.; **Horo**, **H.**; Goswami, U.; Kundu, L. M*. "Synthesis of a peptide conjugated 5-Fluorouracil gelator prodrug for photo-controlled release of the antitumor agent" *ChemistrySelect.* **2019**, *4*, 6778 –6783.

Das, S.; **Horo**, **H.**; Kundu, L. M*. "Biopolymers and peptide based materials for targeted antitumor drug delivery: an overview" *Nov Appro Drug Des Dev*. **2018**, *4*(4),555643.

List of Conference Presentations

Himali Horo, Lal Mohan Kundu, Bishnupada Mandal. *International Conference on Functional Materials (*ICFM-2020*)*, IIT Kharagpur, West Bengal, India, 6-8th January, 2020. (Oral)

Himali Horo, Sini Porathoor, Ruchi Anand, Lal Mohan Kundu. *Issues & Challenges In Water Treatment And Allied Research For Sustainable Environment (WATER 2020*), IIT Guwahati, Assam, India. 23-25th January, 2020. (Poster)

Himali Horo, Bishnupada Mandal, Lal Mohan Kundu. *Research Conclave*, IIT Guwahati, Assam, India, 14-17th March, 2019. (Poster)

Himali Horo, Lal Mohan Kundu. *Second International Conference On Nano Science & Engineering Applications (ICONSEA - 2018)*, JNTU, Hyderabad, Andhra Pradesh, India, 4-6th October, 2018. (Poster)

Himali Horo, Bishnupada Mandal, Lal Mohan Kundu. *Fourth International Symposium on Advances in Sustainable Polymer* (ASP-17), IIT Guwahati, Assam, India, 8-11th January, 2018. (Poster)

Himali Horo, Lal Mohan Kundu. *Research Conclave*, IIT Guwahati, Assam, India, 16-19th March, 2016. (Poster)

A1.Buffers and solutions

A1.1. MES buffer for 5-FU-linker and LMWC conjugation (100 ml, 50 mM, pH 6.0)

- For 100 ml buffer solution, 0.9762 g MES buffer powder dissolved in dH_2O.
- pH adjusted to 6.0 using 10 N NaOH before makeup.

A1.2. PBS buffer saline for drug deloading studies (100 ml, pH 7.4)

- For 100 ml buffer solution, 0.8 g NaCl, 0.02 g KCl, 0.144 g $NaHPO_4$ and 0.024 g KH_2PO_4 dissolved in dH_2O.

A1.3. Sodium acetate and acetic acid buffer for Mv determination of LMWC (0.1 M CH_3COONa/ 0.2 M CH_3COOH)

- For 100 ml buffer solution, 1.64 g CH_3COONa and 1.72 ml CH_3COOH dissolved in dH_2O.

A1.4. Sodium bicarbonate buffer (100 mM, pH 9.0)

- For 100 ml buffer solution, 0.286 g Na_2CO_3 and 0.756 g $NaHCO_3$ dissolved in dH_2O.
- pH adjusted to 9.0 using 10 N NaOH before makeup.

A1.5. $AgNO_3$ solution preparation for CAg synthesis (54 mM)

- For 10 ml solution, 0.0913 g dissolved in dH_2O.

A1.6. $AuHCl_4$ solution preparation for CAu synthesis (125 mM)

- For 10 ml solution, 0.42 g dissolved in dH_2O.

A1.7. Na_2CO_3 solution preparation for SF extraction (0.02 M)

- For 1000 ml solution, 2.12 g dissolved in dH_2O.

A1.8. LiBr solution preparation for CAu synthesis (9.3 M)

- For 10 ml solution, 80.77 g dissolved in dH_2O.

A1.9. NaOH (10 N)

- For 100 ml solution, 40 g dissolved in dH_2O.

B1. Bacterial Strain used for CD extraction.

Strain		Genotype
Escherichia coli	Rosetta(DE3)pLysS	F^- ompT $hsdS_B$ (rB^- mB^-) gal dcm (DE3)pRARE (Cam^R)

C1. Culture medium for bacteria

Medium	Composition
Luria Bertani (LB) broth (1 L)	10 g Casein enzymic hydrolysate, 5g Yeast extract , 10 g NaCl, pH 7.5±0.2
Luria Bertani (LB) Agar (1 L)	10 g Casein enzymic hydrolysate, 5g Yeast extract , 10 g NaCl, Agar 15 g, pH 7.5±0.2

D1. Activation of dialysis membrane

- Washed in tape water for 3 h for the removal of glycerol that is added in the membrane as a humectant.
- Treated with 0.3 % (w/v) solution of sodium sulfide at 80°C for 1 min for the removal of sulfur compounds.
- Washed with hot water at 60°C for 2min
- Acidification with 0.2 %(v/v) of H_2SO_4 solution
- Rinsed with hot water for the removal of the acid.
- Stored in 10% ethanol at 4°C.